

Mesoporous SiCN Materials and their Modification for Catalytic and Electrochemical Applications

DISSERTATION

zur Erlangung des akademischen Grades eines
Doktors der Naturwissenschaften (Dr. rer. Nat.)
an der Bayreuther Graduiertenschule für Mathematik und
Naturwissenschaften (BayNAT) der Universität Bayreuth

vorgelegt von

M.Sc. Julia-Katharina Ewert

geboren in Braunschweig

Bayreuth, 2015

Die vorliegende Arbeit wurde in der Zeit von November 2012 bis November 2015 in Bayreuth am Lehrstuhl Anorganische Chemie II unter Betreuung von Herrn Prof. Dr. Rhett Kempe angefertigt.

Dissertation eingereicht am:	24.11.2015
Zulassung durch das Leitungsgremium:	25.11.2015
Wissenschaftliches Kolloquium:	21.04.2016

Amtierender Direktor:	Prof. Dr. Stephan Kümmel
-----------------------	--------------------------

Prüfungsausschuss:

Prof. Dr. Rhett Kempe	(Erstgutachter)
Prof. Dr. Josef Breu	(Zweitgutachter)
Prof. Dr. Matthias Breuning	(Vorsitz)
Prof. Dr. Georg Papastavrou	

Meiner Familie und meinem Domi in Dankbarkeit und Liebe gewidmet

Abbreviations

ACN	acetonitrile
Ap ^{TMA} H	(4-Methyl-pyridin-2-yl)-(2,4,6-trimethyl-phenyl)-amine
BET	Brunauer Emmett Teller
BMIM-BF ₄	1-butyl-3-methylimidazolium tetrafluoroborate
CCTP	coordinative chain transfer polymerization
CDC	carbide-derived carbon
CMC	critical micelle concentration
CMK-3	ordered mesoporous carbon template
CMK-8	ordered mesoporous carbon template
cod	cis-1,5-cyclooctadien
CTAB	(1-hexadecyl)trimethylammonium bromide
CV	cyclic voltammogram
DCP	dicumylperoxide
DVB	divinylbenzene
EDX	energy dispersive X-ray spectroscopy
EMIM-BF ₄	1-ethyl-3-methylimidazolium tetrafluoroborate
EMIM-TFSI	1-ethyl-3-methylimidazolium bis(trifluoromethyl-sulfonyl)imide
FWHM	full-width half maximum
FT-IR	fourier transform infrared spectroscopy
GC	gas chromatography
GC/MS	gas chromatography coupled with mass spectroscopy
GCPL	galvanostatic cycling with potential limitation
HRTEM	high resolution transmission electron microscopy
HTT-1800	commercially available polysilazane precursor
ICP-OES	inductively coupled plasma optical emission spectrometry
Ir/Al ₂ O ₃	aluminium oxide supported iridium
[IrAp ^{TMA} (cod)]	iridium[(4-methyl-pyridin-2-yl)-(2,4,6-trimethyl-phenyl)amine-(cyclooctadiene)]
Ir/C	carbon supported iridium
Ir/CaCO ₃	calcium carbonate supported iridium
Ir@SiCN	silicon carbonitride supported iridium
Ir@PS ₆₀ SiCN	silicon carbonitride supported iridium structured with PS ₆₀

M@SiCN	silicon carbonitride supported metal
M _w	molecular weight
NLDFT	non linear density functional theory
NMR	nuclear magnetic resonance
PC	propylene carbonate
PCS	photon correlation spectroscopy
PD-SiCN	polymer derived silicon carbonitride
PE	polyethylene
PEEK	polyether ether ketone
PEOH	hydroxy terminated polyethylene
PI- <i>b</i> -PDMAEMA	poly(isoprene- <i>block</i> -dimethylaminoethylmethacrylate)
PS	polystyrene
PS _x	polystyrene with x nm diameter
PSD	pore size distribution
PS ₆₀ SiCN _y	silicon carbonitride ceramic structured with PS ₆₀ template and pyrolysed at y °C
PS ₅₀ SiCN ₉₀₀ Cl _{2-z}	ceramic derived N-doped carbon material chlorinated at z °C
PTFE	polytetrafluoroethylene
PVSZ	poly(vinyl)silazane
ppm	parts per million
QSDFT	quenched-solid density functional theory
rpm	round per minute
SI	supporting information
SiCN	silicon carbonitride
SEM	scanning electron microscopy
SSA	specific surface area
TEA-BF ₄	tetraethylammonium tetrafluoroborate
TEM	transmission electron microscopy
TGA	thermal gravimetric analysis
XPS	X-ray photoelectron spectroscopy
XRD	X-ray diffraction

Table of Contents

Abbreviations.....	VII
1 Summary / Zusammenfassung	11
1.1 Summary.....	11
1.2 Zusammenfassung	13
2 Introduction	17
3 Overview of Thesis Results	25
3.1 Synopsis.....	25
3.2 Individual Contribution to Joint Publications.....	38
4 Meso-Structuring of SiCN Ceramics by Polystyrene Templates	41
4.1 Introduction	41
4.2 Results and Discussion	43
4.3 Experimental Section.....	47
4.4 Conclusions	49
4.5 Acknowledgments	50
4.6 References	50
5 Enhanced Capacitance of Nitrogen-Doped Hierarchical Porous Carbide-Derived Carbon in Matched Ionic Liquids.....	55
5.1 Introduction.....	56
5.2 Results and Discussion	57
5.3 Conclusion.....	63
5.4 Experimental Section.....	64
5.5 Acknowledgements	67
5.6 Notes and References	68
5.7 Supporting Information	71

6 A Hierarchical Structured Reusable Iridium Catalyst for the Sustainable Synthesis of Pyrroles, Pyridines, and Quinolines.....	75
6.1 Introduction	75
6.2 Results and Discussion	76
6.3 Conclusion.....	82
6.4 Experimental Section.....	82
6.5 Acknowledgements	83
6.6 References	83
6.7 Supporting Information	84
6.8 References	97
 7 Coating of an Ir@SiCN Nanocomposite on a Hierarchically Porous (Micro/Meso) SiCN Support.....	 99
7.1 Introduction	99
7.2 Results and Discussion	100
7.3 Conclusion.....	103
7.4 Experimental Section.....	104
7.5 Acknowledgements	105
7.6 References	105
 8 List of Publications	 109
 9 Acknowledgements / Danksagung.....	 111
9.1 Acknowledgements	111
9.2 Danksagung	112
 10 Declaration / Erklärung.....	 115

1 Summary / Zusammenfassung

1.1 Summary

The primary aim of this thesis was the design of mesoporous polymer derived (PD) silicon carbonitride (SiCN) materials. Therefore, a polystyrene (PS) particle based innovative synthesis route was developed. Diverse modifications of the obtained SiCN material enabled applications in the fields of electrochemistry and heterogeneous catalysis. (**Figure 1.1**).

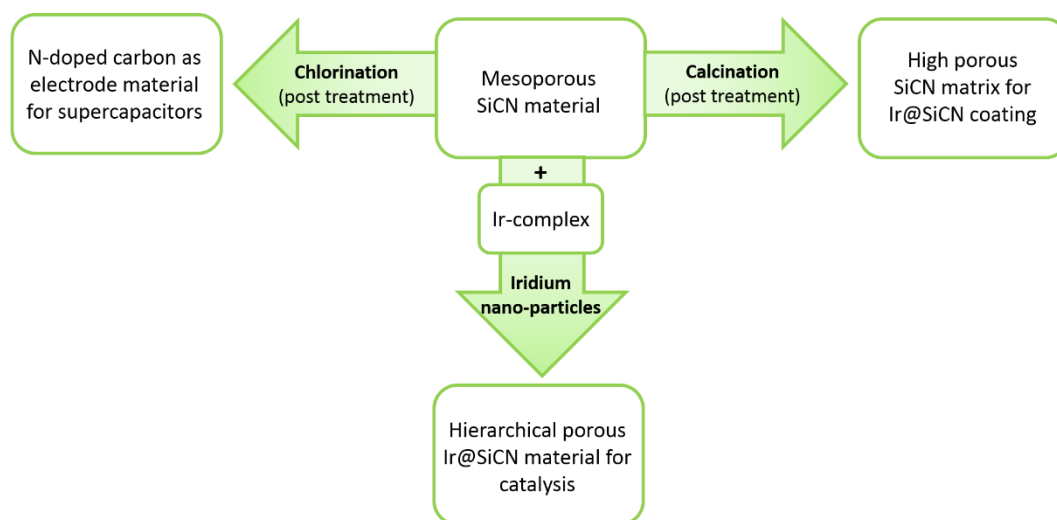


Figure 1.1 Modification of the mesoporous SiCN material by iridium nanoparticles as well as by post synthetic treatments like chlorination or calcination.

In general, PD-SiCN ceramics exhibit a low specific surface area (SSA). The here introduced simple and novel structuring method based on cross-linked PS particles is an elegant technique to approach this problem. PS particles with a diameter of 60 nm and a positive partial charge were synthesized by emulsion polymerization. The positive partial charge and the high cross-linking degree of the PS particles enabled a homogenous and stable suspension with the commercial available ceramic precursor HTT-1800 in organic solvents. The cross-linked and dried nanocomposite (green body) was converted into a mesoporous SiCN material using a tailored pyrolysis program under nitrogen atmosphere. Three SiCN materials were synthesized at temperatures between 900 °C and 1100 °C in order to investigate the influence of the pyrolysis temperature regarding the SSA and the pore stability. Increasing the pyrolysis temperature caused an enhanced collapse of the pores leading to a lower SSA. Decreasing the pyrolysis temperature to 900 °C enabled a higher stability of the mesopores and a larger SSA.

Furthermore, the mesoporous SiCN material was purposive modified in order to address electrochemical applications. Chlorine gas treatment enabled the release of the containing silicon as silicon tetrachloride and generated a highly porous N-doped carbon material. This compound was used as electrode material in supercapacitors. Two hierarchical porous N-doped carbon materials with different pore size distribution and nitrogen amount were obtained. Thereby, the N-richer material was more suitable as electrode material due to the higher cell capacitance and the twice as long stability over time. A significant increase of the specific capacitance was observed for the electrolyte 1-ethyl-3-methylimidazolium tetrafluoroborate (EMIM-BF₄) compared to standard electrolytes. In-situ resistivity measurements supported this result analyzing the electric properties independent of the electrolyte. Only the combination of the N-doped carbon electrode with EMIM-BF₄ led to a nearly constant normalized resistance. This indicated the capacitance enhancement because of the ideal match of electrode material and electrolyte.

The stabilization of iridium nanoparticles using the PS structured SiCN material led to a hierarchical porous Ir@PS₆₀SiCN composite. Therefore, an iridium aminopyridinato complex was used as metal precursor. This material showed good to excellent yields in the sustainable synthesis of N-heterocycles like pyrroles, pyridines, and quinolines using the concept of acceptorless dehydrogenative condensation. The innovative heterogeneous catalyst exhibits an excellent accessibility of very small, homogeneously distributed iridium nanoparticles. The accessibility is caused by the surface structuring resulting in a high SSA and open porosity. The activity and reusability of the catalyst was investigated in comparison to other heterogeneous Ir-catalyst (Ir/C, Ir/Al₂O₃, Ir/CaCO₃) as well as an unstructured Ir@SiCN catalyst. The structured Ir@PS₆₀SiCN system showed a good reusability and a significant higher activity.

An Ir@SiCN-SiCN core-shell material was generated in order to improve the metal accessibility and the metal content. Therefore, the incorporated carbon of the structured SiCN material was partial removed as carbon dioxide by calcination. The ideal calcination temperature was determined using a fixed-bed reactor with coupled online GC. The obtained material exhibits an appreciable enhanced SSA. The calcinated material was coated with a thin Ir@SiCN layer using a wetting technique. This way, metal nanoparticles were imbedded onto the porous surface of the SiCN support.

1.2 Zusammenfassung

Das primäre Ziel dieser Arbeit war die Entwicklung mesoporöser, polymerbasierter Siliziumcarbonitrid-(SiCN)-Materialien. Dafür wurde eine auf Polystyrol-(PS)-Partikeln basierte innovative Syntheseroute entwickelt. Diverse Modifizierungen des resultierenden SiCN-Materials ermöglichten Anwendungen im Bereich der Elektrochemie und der heterogenen Katalyse. (**Abbildung 1.1**).

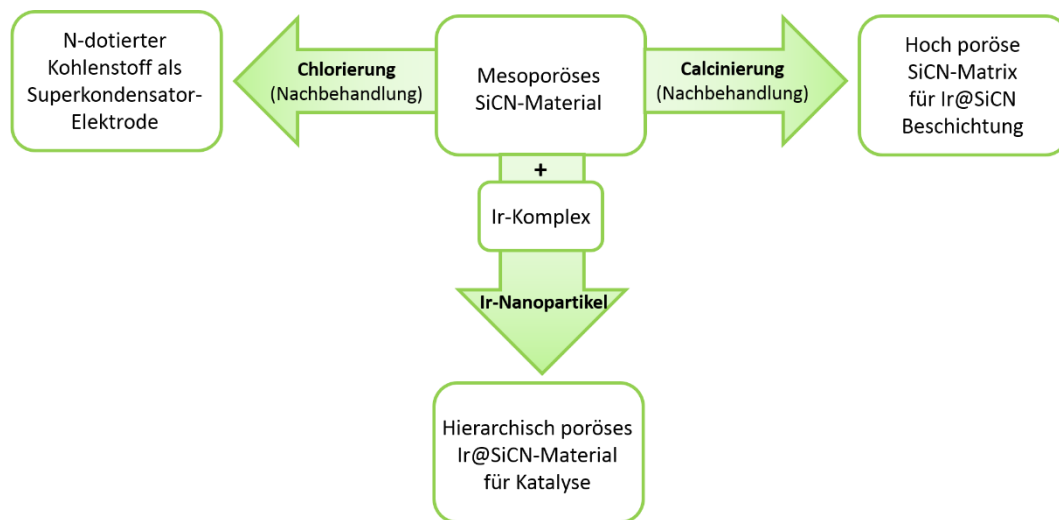


Abbildung 1.1 Modifizierung des mesoporösen SiCN-Materials durch Iridium-Nanopartikel sowie durch nachfolgende Chlorierung oder Calcinierung.

Polymerbasierte SiCN-Keramiken besitzen im Allgemeinen eine geringe spezifische Oberfläche. Die hier vorgestellte, innovative Strukturierungsmethode mit quervernetzten PS-Partikeln stellt eine elegante Methode dar, um dieses Problem anzugehen. Die PS-Partikel mit einem Durchmesser von 60 nm und einer positiven Partialladung wurden mittels Emulsionspolymerisation hergestellt. Die positive Partialladung und der hohe Vernetzungsgrad der PS-Partikel ermöglichten eine homogene und stabile Suspension mit dem kommerziell erhältlichen Keramik-Precursor HTT-1800 in organischen Lösungsmitteln. Das vernetzte und getrocknete Material (Grünkörper) wurde mittels eines maßgeschneiderten Pyrolyseprogramms unter Stickstoffatmosphäre in ein mesoporöses SiCN-Material umgewandelt. Die Herstellung von drei SiCN-Materialien im Temperaturbereich zwischen 900 °C und 1100 °C diente der Untersuchung des Einflusses der Pyrolysetemperatur auf die spezifische Oberfläche und die Porenstabilität. Mit zunehmender Pyrolysetemperatur kam es vermehrt zum Kollaps der Poren, was ein Einbrechen der spezifischen Oberfläche zur Folge hatte. Das Herabsetzen der

Pyrolysetemperatur auf 900 °C bewirke eine Erhöhung der Porenstabilität sowie der spezifischen Oberfläche.

Des Weiteren wurde das mesoporöse SiCN-Material zielgerichtet modifiziert, um Anwendungen im Bereich der Elektrochemie zu adressieren. Die Behandlung mit Chlorgas bewirkte die Freisetzung des enthaltenen Siliziums als Siliziumtetrachlorid und generierte ein hochporöses N-dotiertes Kohlenstoffmaterial. Dieses Material wurde als Elektrode in Superkondensatoren eingesetzt. Zu diesem Zweck wurden zwei hierarchisch poröse N-dotierte Kohlenstoffmaterialien hergestellt, die sich in ihrer Porenverteilung und ihrem Stickstoffgehalt unterschieden. Dabei zeigte sich das N-reichere Material als geeigneter, da es eine höhere Kapazität und eine Verdopplung der Langzeitstabilität aufwies. Es kam zu einem signifikanten Anstieg der spezifischen Kapazität für den Elektrolyt 1-Ethyl-3-methylimidazolium-tetrafluoroborat (EMIM-BF₄) im Vergleich zu gängigen Standardelektrolyten. In-situ Widerstandsmessungen stützten dieses Ergebnis, da auf diese Weise die elektrischen Eigenschaften unabhängig vom Elektrolyt betrachtet werden konnten. Ausschließlich die Kombination der N-dotierten Kohlenstoffelektrode mit EMIM-BF₄ führte zu einem nahezu konstanten normierten Widerstand. Dies spricht für die Kapazitätssteigerung durch die ideale Kompatibilität des Elektrodenmaterials und des Elektrolyts.

Die Stabilisierung von Iridium-Nanopartikeln durch die PS-strukturierte SiCN-Matrix führte zu einem hierarchisch strukturierten Ir@PS₆₀SiCN Kompositmaterial. Ein Iridium-Aminopyridinato Komplex diente als Metall-Precursor. Dieses Material zeigte gute bis hervorragende Ausbeuten bei der nachhaltigen Synthese von N-Heterocyclen wie Pyrrolen, Pyridinen und Quinolinen, wobei das Konzept der akzeptorlosen dehydrierenden Kondensation herangezogen wurde. Der innovative heterogene Katalysator zeichnete sich durch eine hervorragende Zugänglichkeit der sehr kleinen, homogen verteilten Iridium-Nanopartikeln aus. Die Zugänglichkeit ist in der Oberflächenstrukturierung und der daraus resultierenden hohen Oberfläche sowie der offenen Porosität begründet. Des Weiteren wurden die Aktivität und die Wiederverwendbarkeit des Katalysators im Vergleich zu anderen heterogenen Ir-Katalysatoren (Ir/C, Ir/Al₂O₃, Ir/CaCO₃) sowie einem unstrukturierten Ir@SiCN Katalysator untersucht. Es zeigte sich eine gute Wiederverwendbarkeit und eine signifikant höhere Aktivität für den Ir@PS₆₀SiCN Katalysator.

Außerdem wurde ein Ir@SiCN-SiCN Kern-Schale-Material hergestellt, um die Metallzugänglichkeit und den Metallgehalt zu optimieren. Hierfür wurde der in dem SiCN-Material enthaltende Kohlenstoff partiell durch einen Calcinierungsprozess als

Kohlenstoffdioxid entfernt. Unter Verwendung eines Festbett-Reaktors mit gekoppelter online-GC-Analyse wurde die ideale Calcinierungstemperatur bestimmt. Das erhaltene Material wies eine erhöhte spezifische Oberfläche auf. Eine Benetzungstechnik ermöglichte die dünne Beschichtung des calcinierten Materials mit Ir@SiCN. Auf diese Weise konnten Metall-Nanopartikel auf der porösen Oberfläche des SiCN-Trägermaterials eingebettet werden.

2 Introduction

In the last decades, polymer derived ceramics (PDC) gained a wide interest due to their high thermal stability and chemical resistance.¹ In contrast to traditional preparation techniques, ceramics based on polymer precursors have two main advantages. First, they can be produced at significantly lower processing temperatures. Second, their easy shaping character allows the fabrication of diverse structures like fibers, coatings and films.^{1h,m,2} PDCs consisting of organosilicon polymers are divided into oxide and non-oxide ceramics. In particular, PD-SiCN non-oxide ceramics are of great importance regarding the covalent bonded nitrogen in the ceramic network. The nitrogen enables the stabilization of metal nanoparticles by the ceramic support leading to robust heterogeneous catalysts.^{2,3} Our group established a molecular approach transferring transition metals from aminopyridinato complexes⁴ to the commercially available polysilazane HTT-1800. The resulting metallo polysilazane is subsequently converted into a SiCN-transitionmetal nanocomposite (M@SiCN) after cross-linking and pyrolysis under inert atmosphere (**Figure 2.1**). The nonporous M@SiCN materials exhibit very small metal nanoparticles and are versatile used in catalysis.⁵

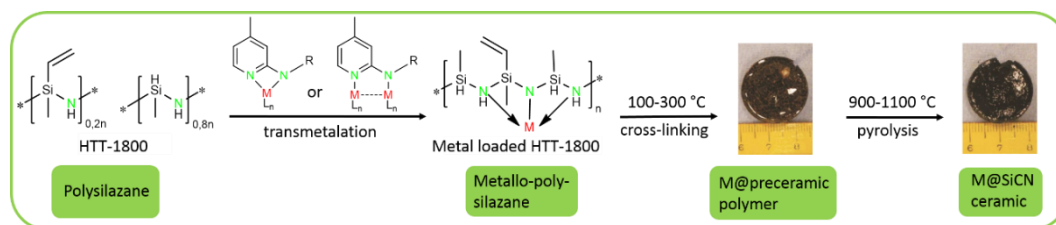


Figure 2.1 Synthesis of metal containing PD-SiCN ceramics by a molecular approach (image source of the M@preceramic polymer and the M@SiCN ceramic⁶).

Beside the excellent results in catalysis so far, such M@SiCN catalysts feature only a small specific surface area (SSA) and a low accessibility of the metal nanoparticles. Nanostructuring methods were recently developed by several research groups in order to rise the SSA of PD-SiCN ceramics. However, structuring is sophisticated due to the hydrolysis sensitivity of the ceramic polymer precursor. As seen in **Figure 2.2**, nanostructuring of PD-SiCN ceramics can be accomplished by a) block copolymers utilized as structure-directing agent (SDA) or exploiting their self-assembly behavior, b) the hard-templating method, and c) the self-sacrificial template method.⁷

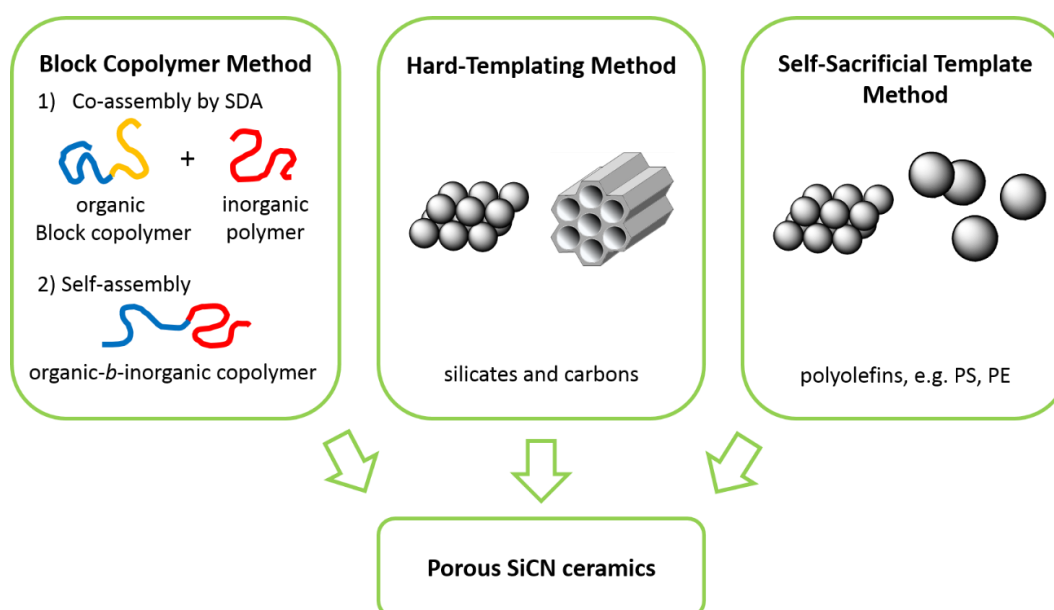


Figure 2.2 Nanostructuring methods leading to porous PD-SiCN ceramics.

The self-assembly of block copolymers leads to ordered meso structures by microphase separation. Block copolymers enable a direct synthesis route for meso structured SiCN ceramics.⁷ There are two pathways known in literature.⁷ The first method uses an organic block-copolymer as SDA and an inorganic polymer as ceramic precursor. The compatibility of the inorganic polymer with one block of the SDA is necessary for a successful microphase separation. The shape of the generated meso structured nanocomposite is conserved by cross-linking of the inorganic domain. The inorganic network is converted into a SiCN material under inert atmosphere. The organic domain is thermally removed by pyrolysis obtaining mesopores.⁷ This method was successfully developed by the group of Wiesner.⁸ They used poly(isoprene-*block*-dimethylaminoethylmethacrylate) (PI-*b*-PDMAEMA) as SDA and polyureamethylvinyl-silazane (commonly known as Ceraset) as ceramic precursor. A nanocomposite with a PI and a PDMAEMA/Ceraset domain was generated due to interaction of hydrogen bonds of the PDMAEMA block with Ceraset. Pyrolysis of the hybrid material led to a 2D hexagonal meso structured SiCN ceramic with a SSA of 51 m²/g. The group of Wan also used Ceraset as preceramic polymer and polybutadiene-*block*-poly(ethylene oxide) (PB-*b*-PEO) as SDA.⁹ They observed morphologies ranging from hexagonal to lamellar as well as to cylindrical structures. The main problem of this structuring method is a possible macrophase separation. They choose PB-*b*-PEO regarding its good miscibility with the ceramic precursor in order to avoid this problem. Moreover, crystallization of the PEO domain was handled using a high molecular weight of the SDA.

The second block-copolymer based structuring method avoids the matter of macrophase separation.⁷ An inorganic polymer serving as ceramic precursor and an organic polymer responsible for later mesopores are connected by covalent bonds. This method is based on the self-assembly character of the received block copolymer. Due to microphase separation of the two blocks, a meso structured nanocomposite is achieved. This compound is in situ transformed into a porous ceramic by pyrolysis.⁷ The group of Kim generated poly(vinyl)silazane-*block*-polystyrene (PVSZ-*b*-PS), which was subsequently converted into an ordered mesoporous SiCN ceramic.¹⁰ Our group developed a block-copolymer using the commercially available polysilazane HTT-1800 as inorganic block and hydroxyl terminated polyethylene (PEOH) as organic block. PEOH was synthesized via coordinative chain transfer polymerization (CCTP).¹¹ Ultrathin SiCN fibers as well as lamellar morphologies remained by a one pot self-assembly of PE-*b*-HTT-1800.¹² The block copolymer based methods have certain limitations. Oxygen is introduced using acrylic monomers and sophisticated synthesis routes are required.

A different pathway is the hard-templating method using mesoporous solids, for instance silicates and carbons as templates. A distinction is made between spherical templates, which are arranged in a hexagonal closed package bed and mesoporous templates. In both cases, the ceramic precursor is infiltrated into the voids of the template material. A nano structured SiCN material is received after pyrolysis and removal of the template.⁷ The groups of Kim and Kenis used SiO₂ spheres in order to obtain macro structured SiCN ceramics with SSAs up to 455 m²/g.¹³ Moreover, the group of Kim used the mesoporous carbon templates CMK-3 and CMK-8 generating mesoporous SiCN ceramics as negative replica of the templates.¹⁴ The group of Zhao fabricated ordered mesoporous SiCN ceramics with open and continuous frameworks combining a casting-by-casting method with an atmosphere-assisted in situ transformation process.¹⁵ This route led to SSAs between 200-400 m²/g. In general, the hard templates were removed using strong etching reagents like hydrofluoric acid (HF). This harsh procedure is a great disadvantage affecting not only the template but the porous SiCN ceramic as well. Thus, a possible stabilization of in situ generated metal particles is impeded.

The self-sacrificial template method was established by the groups of Kim and Kenis.^{13b,16} They used polyolefin based templates, in particular, spherical PS particles in order to avoid strong etching reagents. The thermal removal of the template was enabled during pyrolysis. A packed bed of PS spheres inside the microfluidic channels of a polydimethylsiloxane (PDMS) mold was formed by evaporation-driven self-assembly. Macroporous SiCN monoliths with SSAs up to 185 m²/g were obtained after infiltrating the template by a polymeric precursor and subsequent

pyrolysis. Furthermore, they were able to generate a PS bed by sedimentation of macro spherical PS particles. A macroporous SiCN material was achieved.¹⁷ Jones and Lodge introduced a microphase-separated polymer blend and used it for the generation of a mesoporous polyethylene (PE) template.¹⁸ They utilized Ceraset as ceramic polymer. The synthesis led to a disordered 3D continuous porous SiCN ceramic with macropores. The group of Motz used PE as sacrificial filler in a simple mixing and pressing route producing macroporous SiCN materials with an open porosity.¹⁹ Following this example, the group of Konegger also established a simple mixing and pressing route using ultrahigh molecular weight polyethylene (UHMW-PE) as template.²⁰ They produced structured SiCN ceramics with pores in the macro scale range ($> 10 \mu\text{m}$). The group of Colombo showed among others a structuring method of partially cross-linked HTT-1800 using poly(methylmethacrylate) microbeads as sacrificial filler and generated a porous SiCN ceramic.²¹ The groups of Li and Xu generated an opal template using poly(styrene-methylmethacrylate-acrylic acid).²² They infiltrated the template with a polysilazane and obtained a crack-free photonic crystal with ordered macropores after pyrolysis at 500°C . The self-sacrificial template approach has been restricted to macro structuring so far except the work of Jones and Lodge.¹⁸ Moreover, the infiltration of the preceramic polymer into the voids of the PS bed is subjected to diffusion control regarding the PDMS mold.

The first approach in the generation of porous M@SiCN catalysts was accomplished by the group of Wiesner.²³ They introduced a highly porous SiCN catalyst supporting platinum nanoparticles. A five component systems was established using PI-*b*-PDMAEMA as SDA, Ceraset as ceramic precursor, PS particles as macropore source, a PDMS mold as micro-channel generator, and a platinum-complex as Pt-source. The Pt@SiCN material was tested in the total methane oxidation with high activity and thermal inertness up to 600°C . Furthermore, our group developed a microporous Ni@SiCN catalyst, a hierarchically porous Pd@SiCN catalyst and a mesoporous Au@SiCN catalyst for several catalytic applications.^{6,24}

Beside catalytic reactions, high surface area materials find application for electrochemical performances. For instance, nanoporous carbon materials are used as electrode materials in electrochemical capacitors, also known as supercapacitors. The high specific surface area of these materials is necessary with regard to high efficiency. The performed capacitance depends on the amount and speed of the electrosorption reaction of the electrolyte ions at the charged interface of the electrode material. Thus, a high specific surface area and high pore volumes are required.²⁵ The groups of Colombo and Gogotsi demonstrated a chlorination treatment of a

SiCN template generating a carbide-derived carbon material.²⁶ This method seems very promising in order to establish a SiCN-derived N-doped carbon material. The influence of N-doped polymer derived carbons on the improved electrical conductivity was first investigated by the group of Frackowiak.²⁷ Several carbon materials with N-doping were developed.²⁸ A very efficient way of introducing nitrogen into carbon materials is the utilization of N-containing precursor materials, for instance, bio-materials and ionic liquids.^{28b,29} Nitrogen amounts up to 21 mass% are possible.³⁰

The nanostructuring of PD-SiCN ceramics is a challenging research field, which exhibits a great potential for catalytic and electrochemical applications. A continuous development of such porous materials is a desirable goal.

This thesis comprises:

- 1) The generation of mesoporous PD-SiCN materials utilizing a novel PS particle based one-pot synthesis route.
- 2) The transformation of the mesoporous SiCN material into a high porous N-doped carbon material for electrochemical performances in supercapacitors.
- 3) The stabilization of iridium nanoparticles by the mesoporous SiCN support leading to a hierarchical porous Ir@SiCN catalyst with a high metal accessibility for sustainable heterogeneous catalysis.
- 4) An Ir@SiCN coating of a micro and mesoporous SiCN material, which SSA was increased by a calcination treatment.

References

- 1 a) R. Riedel, H.-J. Kleebe, H. Schönfelder, F. Aldinger, *Nature* **1995**, 374, 526-528; b) W. Weibelzahl, G. Motz, D. Suttor, G. Ziegler, *Key Eng. Mater.* **1999**, 161-163, 111-114; c) E. Kroke, Y.-L. Li, C. Konetschny, E. Lecomte, C. Fasel, R. Riedel, *Mater. Sci. Eng. R* **2000**, 26, 97-199; d) P. Greil, *Adv. Eng. Mat.* **2000**, 2, 339-348; e) H. J. Kleebe, H. Störmer, S. Trassl, G. Ziegler, *Appl. Organomet. Chem.* **2001**, 15, 858-866; f) R. Riedel, G. Mera, R. Hauser, A. Klonczynski, *J. Ceram. Soc. Jpn.* **2006**, 114, 425-444; g) A. R. Studart, U. T. Gonzenbach, E. Tervoort, L. J. Gauckler, *J. Am. Ceram. Soc.* **2006**, 89, 1771-1789; h) P. Colombo, G. Mera, R. Riedel, G. D. Sorarù, *J. Am. Ceram. Soc.* **2010**, 93, 1805-1837; i) P. Colombo, R. Riedel, G. D. Soraru, H.-J. Kleebe, *Polymer Derived Ceramics - From Nanostructure to Applications*, DEStech

- Publications, Inc. Pennsylvania, **2010**; j) E. Kroke, Y.-L. Li, C. Konetschny, E. Lecomte, C. Fasel, and R. Riedel, *Mater. Sci. Eng. R*, **2000**, *26*, 97–199; k) E. E. Ionescu, H. J. Kleebe, R. Riedel, *Chem. Soc. Rev.* **2012**, *41*, 5032–5052; l) G. Mera, A. Navrotsky, S. Sen, H.-J. Kleebe, R. Riedel, *J. Mat. Chem. A* **2013**, *1*, 3826; m) *Ceramics Science and Technology: Volume 4: Applications*, (Eds: Ralf Riedel and I-Wei Chen), Wiley-VCH Verlag GmbH & Co. KGaA, **2013**; n). E. Bernardo, L. Fiocco, G. Parcianello, E. Storti, P. Colombo, *Materials* **2014**, *7*, 1927–1956.
- 2 M. Zaheer, *Design of Robust Heterogeneous Catalysts for Sustainable Chemistry*, **2013**, University of Bayreuth.
- 3 M. Zaheer, T. Schmalz, G. Motz, R. Kempe, *Chem. Soc. Rev.* **2012**, *41*, 5102–5116.
- 4 a) S. Deeken, S. Proch, E. Casini, H. F. Braun, C. Mechtler, C. Marschner, G. Motz, R. Kempe, *Inorg. Chem.* **2006**, *45*, 1871–1879; b) S. Deeken, G. Motz, R. Kempe, *Z. Anorg. Allg. Chem.* **2007**, *633*, 320–325; c) G. Glatz, G. Motz, R. Kempe, *Z. Anorg. Allg. Chem.* **2008**, *634*, 2897–2902.
- 5 a) G. Glatz, T. Schmalz, T. Kraus, F. Haarmann, G. Motz, R. Kempe, *Chem. Eur. J.* **2010**, *16*, 4231–4238; b) M. Zaheer, G. Motz, R. Kempe, *J. Mater. Chem.* **2011**, *21*, 18825; c) D. Forberg, J. Obenauf, M. Friedrich, S.-M. Hühne, W. Mader, G. Motz, R. Kempe, *Catal. Sci. Technol.* **2014**, *4*, 4188–4192.
- 6 M. Zaheer, C. D. Keenan, J. Hermannsdörfer, E. Roessler, G. Motz, J. Senker, R. Kempe, *Chem. Mater.* **2012**, *24*, 3952–3963.
- 7 Y. Shi, Y. Wan, D. Zhao, *Chem. Soc. Rev.* **2011**, *40*, 3854–3878.
- 8 M. Kamperman, C. B. Garcia, P. Du, H. Ow, U. Wiesner, *J. Am. Chem. Soc.* **2004**, *126*, 14708–14709.
- 9 a) J. Wan, A. Alizadeh, S. T. Taylor, P. R. L. Malenfant, M. Manoharan, S. M. Loureiro, *Chem. Mater.* **2005**, *17*, 5613–5617; b) J. Wan, P. R. L. Malenfant, S. T. Taylor, S. M. Loureiro, M. Manoharan, *Mater. Sci. Eng. A* **2007**, *463*, 78–88.
- 10 a) Q. D. Nghiem, D. J. Kim, D. P. Kim, *Adv. Mater.* **2007**, *19*, 2351–2354; b) C. T. Nguyen, P. H. Hoang, J. Perumal, D. P. Kim, *Chem. Commun.* **2011**, *47*, 3484–3486.
- 11 S. K. Pillai, W. P. Kretschmer, M. Trebbin, S. Forster, R. Kempe, *Chem. Eur. J.* **2012**, *18*, 13974–13978.
- 12 S. K. Pillai, W. P. Kretschmer, C. Denner, G. Motz, M. Hund, A. Fery, M. Trebbin, S. Forster, R. Kempe, *Small* **2013**, *9*, 984–989.

- 13 a) H. Wang, S.-Y. Zheng, X.-D. Lia, D.-P. Kim, *Microporous Mesoporous Mater.* **2005**, *80*, 357–362; b) I.-K. Sung, Christian, M. Mitchell, D.-P. Kim, P. J. A. Kenis, *Adv. Funct. Mater.* **2005**, *15*, 1336-1342.
- 14 J. Yan, A. Wang, D.-P. Kim, *Microporous Mesoporous Mater.* **2007**, *100*, 128–133.
- 15 Y. Shi, Y. Wan, Y. Zhai, R. Liu, Y. Meng, B. Tu, D. Zhao, *Chem. Mater.* **2007**, *19*, 1761-1771.
- 16 a) Christian, M. Mitchell, D. Kim, P. Kenis, *J. Catal.* **2006**, *241*, 235-242; b) Z. Xiao, A. Wang, D.-P. Kim, *J. Mater. Chem.* **2010**, *20*, 2853-2857.
- 17 J. Yan, L. Y. Hong, A. J. Wang, D. P. Kim, *Solid State Phenom.* **2007**, *124-126*, 727-730.
- 18 B. H. Jones, T. P. Lodge, *J. Am. Chem. Soc.* **2009**, *131*, 1676-1677.
- 19 T. Schmalz, J. M. Hausherr, W. Müller, T. Kraus, W. Krenkel, R. Kempe, G. Motz, *J. Ceram. Soc. Jpn.* **2011**, *119*, 477-482.
- 20 T. Konegger, L. F. Williams, R. K. Bordia, *J. Am. Ceram. Soc.* **2015**, *98*, 3047-3053.
- 21 C. Vakifahmetoglu, I. Menapace, A. Hirsch, L. Biasetto, R. Hauser, R. Riedel, P. Colombo, *Ceram. Inter.* **2009**, *35*, 3281-3290.
- 22 Z. Zhang, W. Shen, C. Ye, Y. Luo, S. Li, M. Li, C. Xu, Y. Song, *J. Mater. Chem.* **2012**, *22*, 5300-5303.
- 23 M. Kamperman, A. Burns, R. Weissgraeber, N. van Vegten, S. C. Warren, S. M. Gruner, A. Baiker, U. Wiesner, *Nano Lett.* **2009**, *9*, 2756-2762.
- 24 a) S. Schwarz, M. Friedrich, G. Motz, R. Kempe, *ZAAC*, **2015**, *641*, 2266-2271; b) S. K. Pillai, *Mesostructuring of SiCN Materials and Catalysts via Microphase Separation Technique utilizing High-Density Polyethylene Blocks*, **2013**, University of Bayreuth.
- 25 a) P. Simon, Y. Gogotsi, *Nat. Mater.* **2008**, *7*, 845-854; b) J. Segalini, E. Iwama, P.-L. Taberna, Y. Gogotsi, P. Simon, *Electrochem. Commun.* **2012**, *1*, 63-65; c) M. Beidaghi, Y. Gogotsi, *Energy Environ. Sci.* **2014**, *7*, 867-884; d). F. Beguin, V. Presser, A. Balducci, E. Frackowiak, *Adv. Mater.* **2014**, *26*, 2219-2251.
- 26 S.-H. Yeon, P. Reddington, Y. Gogotsi, J. E. Fischer, C. Vakifahmetoglu, P. Colombo, *Carbon* **2010**, *48*, 201-210.
- 27 G. Lota, B. Grzyb, H. Machnikowska, J. Machnikowski, E. Frackowiak, *Chem. Phys. Lett.* **2005**, *404*, 53-58.
- 28 a) J. D. Wiggins-Camacho, K. J. Stevenson, *J. Phys. Chem. C* **2009**, *113*, 19082-19090; b) R. J. White, M. Antonietti, M.-M. Titirici, *J. Mater. Chem.* **2009**, *19*, 8645-8650; c)

- L. G. Bulusheva, E. O. Fedorovskaya, A. G. Kurennya, A. V. Okotrub, *Phys. Status Solidi. B* **2013**, 250, 2586-2591. d) N. L. Torad, R. R. Salunkhe, Y. Li, H. Hamoudi, M. Imura, Y. Sakka, C.-C. Hu, Y. Yamauchi, *Chem. Eur. J.* **2014**, 20, 7895-7900; e) X. Fan, C. Yu, J. Yang, Z. Ling, J. Qiu, *Carbon* **2014**, 70, 130-141; f) J. Tang, J. Liu, C. Li, Y. Li, M. O. Tade, S. Dai, Y. Yamauchi, *Angew. Chem. Int. Ed.* **2015**, 54, 588-593; g) J. Tang, R. Salunkhe, J. Liu, N. L. Torad, M. Imura, S. Furukawa, Y. Yamauchi, *J. Am. Chem. Soc.* **2015**, 137, 1572-1580; h) R. R. Salunkhe, J. Tang, Y. Kamachi, T. Nakato, J. H. Kim, Y. Yamauchi, *ACS Nano*, **2015**, 9, 6288-6296.
- 29 a) N. Fechler, T.-P. Fellingner, M. Antonietti, *Adv. Mater.* **2013**, 25, 75-79; b) S. Zhang, K. Dokko, M. Watanabe, *Chem. Mater.* **2014**, 26, 2915-2926; c). M. Wahid, G. Parte, D. Phase, S. Ogale, *J. Mat. Chem. A* **2015**, 3, 1208-1215.
- 30 S. Zhang, S. Tsuzuki, K. Ueno, K. Dokko, M. Watanabe, *Angew. Chem. Int. Ed.* **2015**, 54, 1302-1306.

3 Overview of Thesis Results

The thesis is composed of four publications, which are presented in the chapters 4 to 7. The theme of the publications is summarized in chapter 3.1. In chapter 3.2, the individual contributions to joint publications are pointed out.

3.1 Synopsis

The primary aim of this thesis was the design of mesoporous polymer derived silicon carbonitride (PD-SiCN) materials. Therefore, a novel polystyrene (PS) particle based synthesis route was developed. These materials were used for further modifications addressing electrochemical and catalytic applications.

In general, PD-SiCN ceramics only feature low specific surface areas (SSA) and porosity. This problem was approached by an innovative synthesis route leading to mesoporous SiCN materials. The details are pointed out in the first manuscript mentioned in chapter 4. PS latex particles seem to be a suitable structuring template regarding the controlled thermal decomposition behavior. Thus, strong etching reagents can be avoided. Only macro spherical PS particles were used as templates in the literature so far. The first goal was the preparation of small PS latex particles for structuring at meso scale. The synthesis of PS particles with an average diameter of 60 nm (PS₆₀) was successfully realized by emulsion polymerization. It was important to work highly above the critical micelle concentration (CMC) of the surfactant (1-hexadecyl)trimethylammonium bromide (CTAB). The strong cross-linking of the PS latex particles with divinylbenzene (DVB) led to a small particle size. Moreover, the use of a small amount of the styrene monomer as well as the initiator [2,2'-azobis(2-methylpropionamidine)dihydrochloride] was necessary. A positive partial charge of the PS particles was caused by the cationic groups of the radical initiator. Shape and size of the PS template were determined by scanning electron microscopy (SEM, **Figure 3.1A**) and photon correlation spectroscopy (PCS, **Figure 3.1B**).

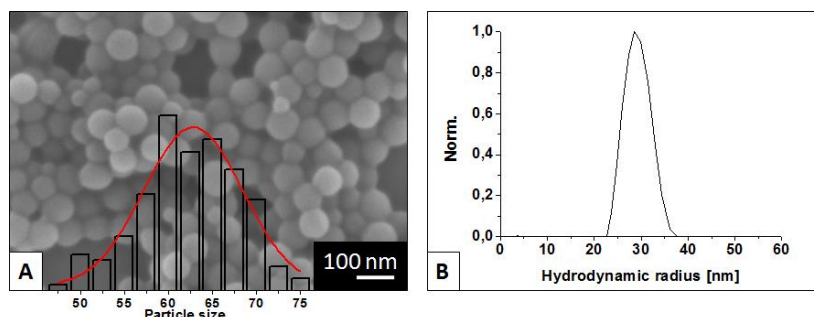


Figure 3.1 PS particle size determined by SEM (A) and PCS (B) measurements.

The decomposition temperature of the PS spheres at 470 °C with only one decomposition step was determined by thermal gravimetric analysis (TGA, **Figure 3.2**).

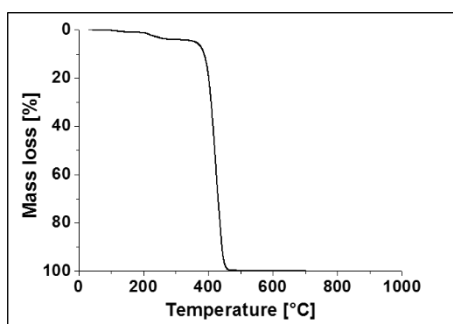


Figure 3.2 TGA measurement of the PS₆₀ template.

The PS₆₀ particles were the major key for the new synthesis development for structuring SiCN materials. The synthesis route had to be carried out in dry organic solvents because of the hydrolysis sensitivity of the ceramic precursor HTT-1800. The stability of the PS particles in organic solvents and the homogeneous miscibility with HTT-1800 were achieved by the positive partial charge of the PS spheres and the strong cross-linking degree respectively.

All these facts in mind, a simple one-pot synthesis route was designed (**Figure 3.3**). Cross-linking of the ceramic precursor occurred at 110 °C sealing the ordered PS spheres. The mixing ratio of 2 : 1 (PS : HTT-1800) was essential providing a comprehensive structuring. A meso structured SiCN material was obtained after the removal of the solvent and subsequent pyrolysis under nitrogen atmosphere. To guarantee the complete removal of the PS template, it was important to use a small heating rate between 400 °C and 500 °C because of the decomposition temperature of the PS particles.

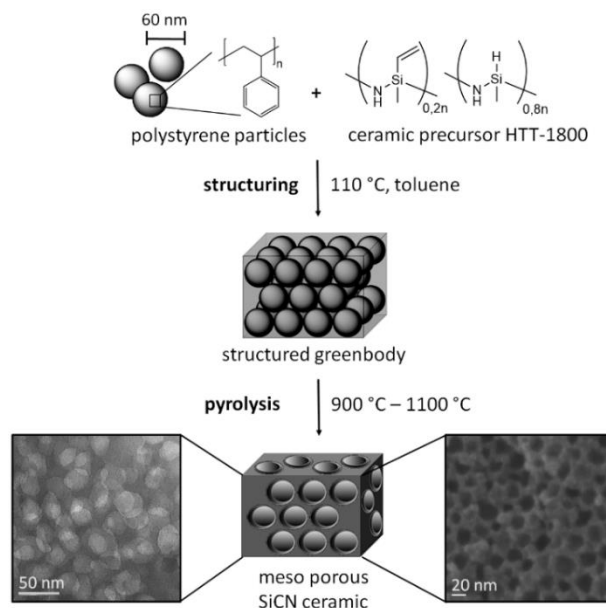


Figure 3.3 Synthesis route leading to meso structured SiCN materials: 1) Structuring: Dispersion of PS₆₀ in silazane-toluene mixture; crosslinking at 110 °C and removal of solvent leading to structured green bodies; 2) Pyrolysis with a tailored pyrolysis program at 900, 1000, or 1100 °C obtaining PS₆₀SiCN₉₀₀, PS₆₀SiCN₁₀₀₀, and PS₆₀SiCN₁₁₀₀.

The influence of the pyrolysis temperature was investigated between 900 °C and 1100 °C (PS₆₀SiCN₉₀₀, PS₆₀SiCN₁₀₀₀, and PS₆₀SiCN₁₁₀₀) regarding the resulting SSA and the pore stability. PS₆₀SiCN₉₀₀ exhibits a honey-combed pore structure with mesopores analyzed by SEM (**Figure 3.4A**). The mesopores were achieved because of the shrinking process of the PS₆₀ spheres during the pyrolysis. Increasing the pyrolysis temperature to 1000 °C or 1100 °C caused a collapse of the pores determined by SEM (**Figure 3.4B and C**).

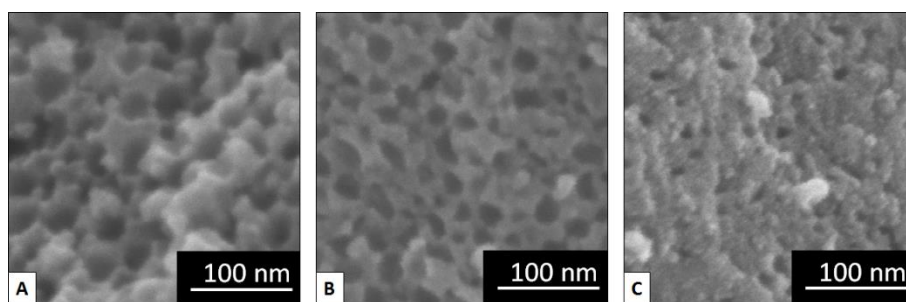


Figure 3.4 SEM images of PS₆₀SiCN₉₀₀ (A), PS₆₀SiCN₁₀₀₀ (B), and PS₆₀SiCN₁₁₀₀ (C).

Nitrogen sorption measurements show isotherms with hysteresis characteristic for mesoporous materials (**Figure 3.5A**). The highest SSA of 110 m²/g was verified for PS₆₀SiCN₉₀₀. The increase of the SSA as well as the mesopore volume correlates with the reduction of the pyrolysis temperature (**Figure 3.5B**), which is in agreement with the SEM measurements.

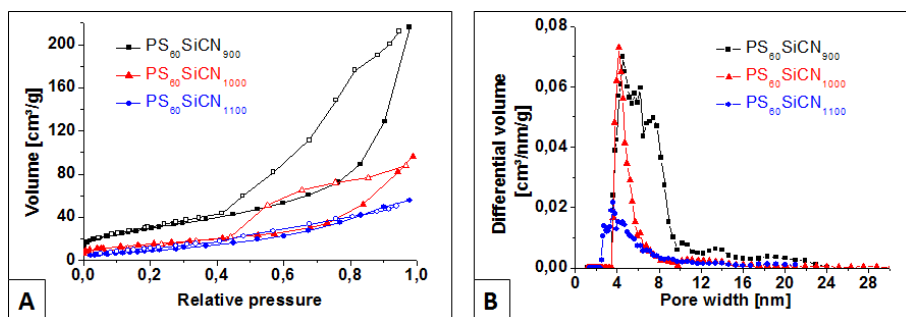


Figure 3.5 Nitrogen sorption measurements with isotherms (A) and pore size distributions (B) of PS₆₀SiCN₉₀₀, PS₆₀SiCN₁₀₀₀, and PS₆₀SiCN₁₁₀₀.

In the second manuscript in chapter 5, the well-structured, mesoporous PD-SiCN material was further modified in order to obtain a N-doped carbon material for electrochemical applications. The PS structured material was treated with chlorine gas removing the silicon as silicon tetrachloride, which leads to a high surface N-doped carbon compound. Therefore, the SiCN material was structured with PS₅₀ particles in order to maintain smaller mesopores and higher SSA of the chlorinated materials. The obtained PS₅₀SiCN₉₀₀ ceramic was chlorinated at 800 °C and 1000 °C investigating the influence of the chlorination temperature. The received N-doped carbon materials were characterized with nitrogen sorption analysis regarding the SSA and the pore size distribution (**Figure 3.6**). Both materials exhibited a SSA of about 1800 m²/g, which is an enormous increase compared to the untreated SiCN template (106 m²/g). A different temperature depending distribution of micro- and mesopores was also determined. The lower chlorination temperature of 800 °C led to an increased mesopore amount of 70 %.

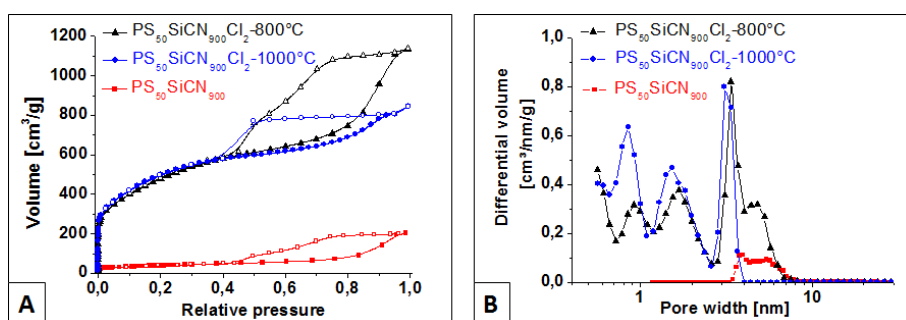


Figure 3.6 Nitrogen sorption measurements with isotherms (A) and pore size distributions (B) of PS₅₀SiCN₉₀₀, PS₅₀SiCN₉₀₀Cl₂-800°C, and PS₅₀SiCN₉₀₀Cl₂-1000°C.

As seen in the SEM images, the honey-combed pore structure of the PS₅₀SiCN₉₀₀ template was preserved after the chlorine treatment independent of the chlorination temperature (**Figure 3.7**).

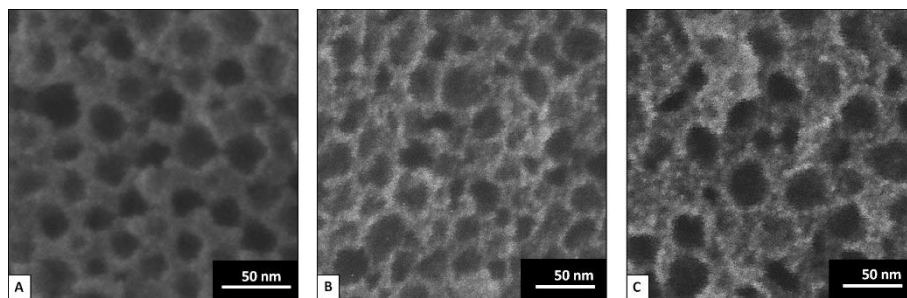


Figure 3.7 SEM images of $\text{PS}_{50}\text{SiCN}_{900}$ (A), $\text{PS}_{50}\text{SiCN}_{900}\text{Cl}_2\text{-}800^\circ\text{C}$ (B), and $\text{PS}_{50}\text{SiCN}_{900}\text{Cl}_2\text{-}1000^\circ\text{C}$ (C).

TEM measurements of the $\text{PS}_{50}\text{SiCN}_{900}$ template show homogeneously distributed pores of the material (**Figure 3.8A**). The pores remained after the chlorination treatment, which is in good agreement with the SEM measurements. The obtained N-doped carbon materials exhibited a less dense matrix structure caused by the removal of the originally containing silicon (**Figure 3.8B and C**).

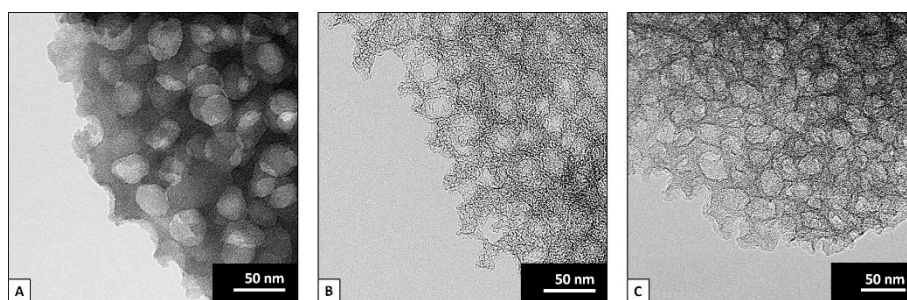


Figure 3.8 TEM images of $\text{PS}_{50}\text{SiCN}_{900}$ (A), $\text{PS}_{50}\text{SiCN}_{900}\text{Cl}_2\text{-}800^\circ\text{C}$ (B), and $\text{PS}_{50}\text{SiCN}_{900}\text{Cl}_2\text{-}1000^\circ\text{C}$ (C).

Raman spectroscopy shows the pronounced D- and G-peaks (1350 cm^{-1} and 1590 cm^{-1}) as result of an incomplete graphitized carbon material for both compounds (**Figure 3.9A**). Elemental analysis and X-ray photoelectron emission spectroscopy (XPS) were carried out investigating the nitrogen amount of the materials (**Figure 3.9B**). The decrease of the chlorination temperature causes a lower removal of nitrogen. Thus, a higher nitrogen amount remains in the material chlorinated at 800°C (elemental analysis: 5.5 wt% for 800°C and 1.6 % for 1000°C).

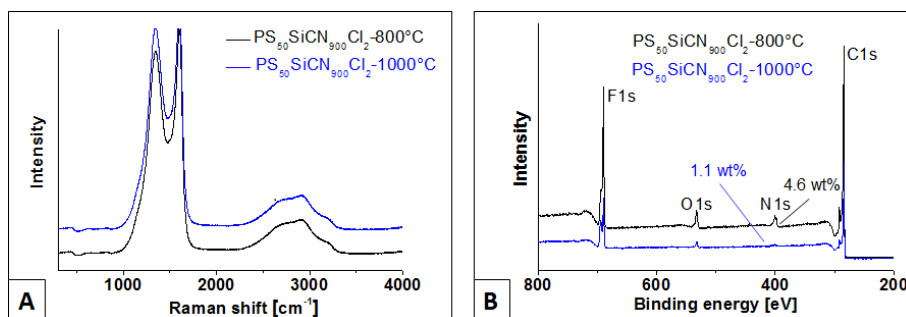


Figure 3.9 Raman spectroscopy (A) and XPS measurements (B) of PS₅₀SiCN₉₀₀Cl₂-800°C and PS₅₀SiCN₉₀₀Cl₂-1000°C.

Recently, the substance class of N-doped carbons gained an increased interest as electrode material in supercapacitors due to the beneficial impact on the electrochemical performance. In this context, the SiCN derived N-doped carbon compounds were tested as electrode material. Two main consequences became evident by the electrochemical characterization.

First, the higher nitrogen and mesopore amount of the compound chlorinated at 800 °C led to an enhancement of the electrochemical capacitance as seen in the cyclic voltammograms in a full cell setup (**Figure 3.10A**). Long term stability measurements were performed analyzing the decay in capacitance over time at 3 V cell voltage. PS₅₀SiCN₉₀₀Cl₂-800°C lasted twice as long as PS₅₀SiCN₉₀₀Cl₂-1000°C until a drop of 20 % in capacitance was reached (**Figure 3.10B**).

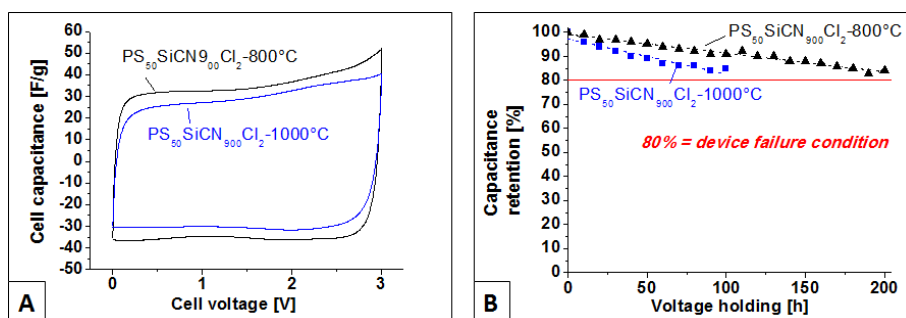


Figure 3.10 Full cell cyclic voltammograms at 3 V cell voltage (A) and long term stability tests at 3 V cell voltage (B) of PS₅₀SiCN₉₀₀Cl₂-800°C and PS₅₀SiCN₉₀₀Cl₂-1000°C with 1-ethyl-3-methylimidazolium tetrafluoroborate (EMIM-BF₄) as electrolyte.

Second, an enhanced capacitance was observed using the ionic liquid 1-ethyl-3-methylimidazolium tetrafluoroborate (EMIM-BF₄) as electrolyte determined by galvanostatic charge/discharge experiments of PS₅₀SiCN₉₀₀Cl₂-800°C (**Figure 3.11A**). This is 20 % higher than for standard electrolytes like tetraethylammonium tetrafluoroborate (TEA-BF₄) in acetonitrile (ACN). In situ resistivity measurements were performed analyzing the electronic properties independent of the electrolyte. The expected behavior of a bell-shaped curve with a

decrease of the normalized resistance at increased potential was observed for the standard electrolyte TEA-BF₄ in ACN with the N-doped carbon electrode (**Figure 3.11B**). However, the combination of EMIM-BF₄ and the SiCN derived N-doped carbon material as electrode showed a nearly constant normalized resistance (**Figure 3.11B**). Thus, the increase of capacitance is a result of the suitable match between the SiCN derived N-doped carbon electrode and the electrolyte EMIM-BF₄.

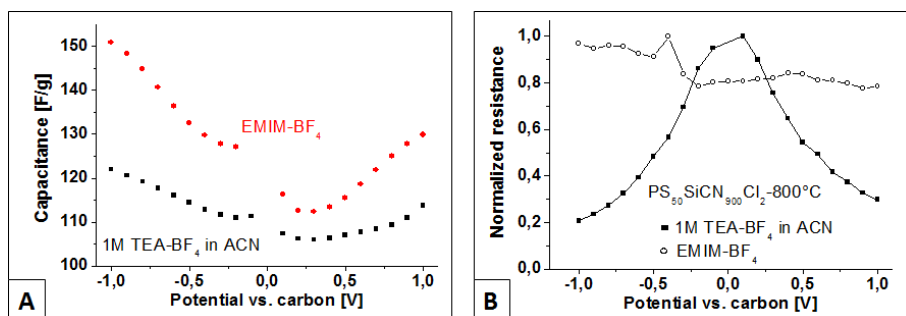


Figure 3.11 GCPL measurements (A) and in situ resistivity measurements with EMIM-BF₄ and TEA-BF₄ in acetonitrile as electrolytes (B) of PS₅₀SiCN₉₀₀Cl₂-800°C.

In the third manuscript in chapter 6, the stabilization of iridium nanoparticles using the PS structured SiCN material as support led to a hierarchical porous SiCN material. The synthesis of the Ir@PS₆₀SiCN material was performed according to chapter 4 using an iridium aminopyridinato complex as metal precursor. The iridium complex was added to a suspension of PS particles, HTT-1800, and DCP. The metal transfer from the complex to the polysilazane HTT-1800 (transmetalation step) started during the short mixing time. The cross-linking of the ceramic precursor was enhanced by iridium catalyzed hydrosilylation and dehydro-coupling. DCP was additionally used as cross-linker stabilizing the subsequent generated pores. The pyrolysis of the structured green body was performed at 1000 °C.

SEM measurements of Ir@PS₆₀SiCN show the requested honey-combed pore structure with homogeneously distributed mesopores in the range of 35 nm (**Figure 3.12A**). Nitrogen sorption analysis determined a large SSA of 450 m²/g and a hierarchically pore size distribution in the micro and meso scale range (**Figure 3.12B**).

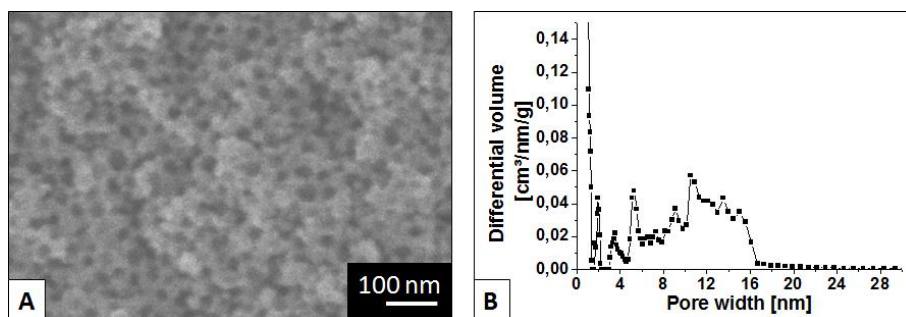


Figure 3.12 SEM image (A) and nitrogen sorption measurement with pore size distribution (B) of Ir@PS₆₀SiCN.

The presence of iridium in the porous SiCN support was verified by energy-dispersive X-ray spectroscopy (EDX) (**Figure 3.13A**). Powder X-ray diffraction (XRD) analysis confirms the presence of iridium nanoparticles with a particle size of about 1 nm (**Figure 3.13B**).

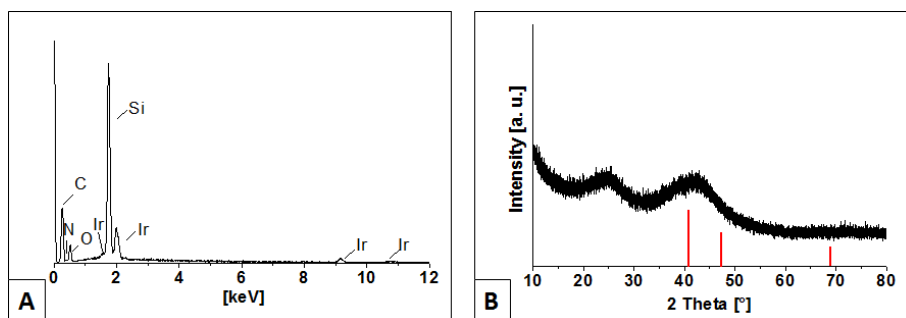


Figure 3.13 EDX measurement (A) and XRD measurement (B) of Ir@PS₆₀SiCN.

Homogenously distributed iridium nanoparticles with a particle size distribution between 0.6 nm and 1.4 nm were verified by TEM measurements. A distance of 221.4 pm between the adjacent lattice planes was determined by HR-TEM measurements indicating the presence of cubic crystalline iridium nanoparticles (**Figure 3.14**).

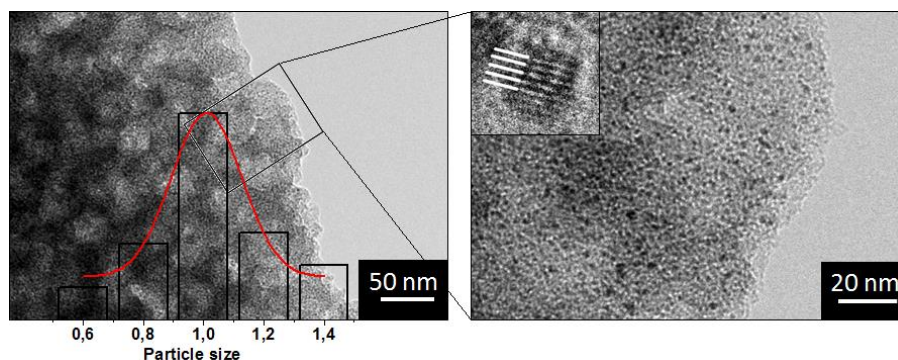
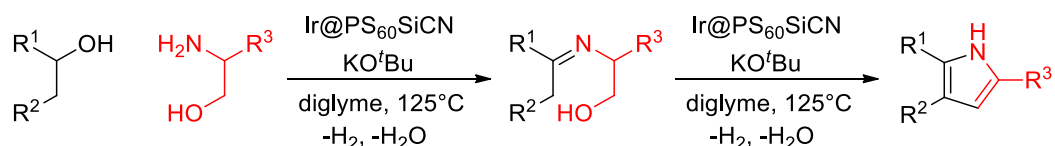


Figure 3.14 TEM measurement with particle size distribution and HR-TEM measurement of Ir@PS₆₀SiCN.

The Ir@PS₆₀SiCN material seems to be a very promising heterogeneous catalyst due to the large SSA and the very small iridium nanoparticles. The sustainable synthesis of N-heterocycles like pyrroles, pyridines, and quinolines was performed using the concept of acceptorless dehydrogenative condensation. The synthesis of 2,5-substituted and 2,3,5-substituted pyrroles were addressed with optimized reaction conditions (**Scheme 3.1**).



Scheme 3.1 Generation of pyrroles starting from secondary alcohols and 1,2-amino alcohols under elimination of water and hydrogen. Reaction conditions: 1,2-amino alcohol (1.5 mmol), secondary alcohol (6 mmol), KOtBu (3 mmol), 0.58 mol% Ir, 1.5 mL diglyme, 24 h at 125 °C.

The variation of the amino alcohol and the secondary alcohol as well as the acceptance of several functional groups in high yields were investigated (**Figure 3.15**).

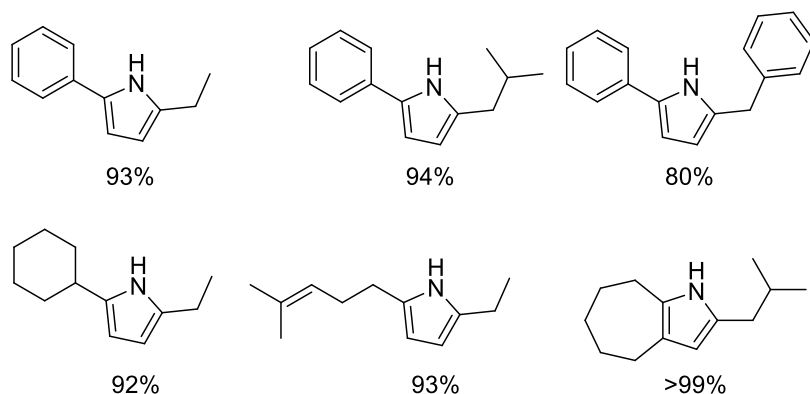
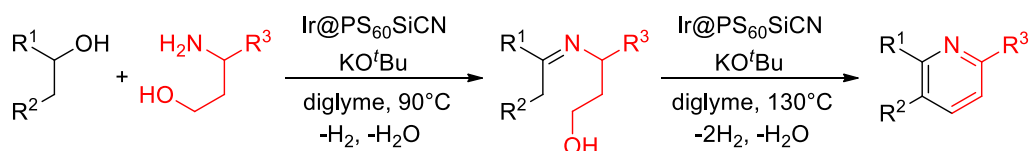


Figure 3.15 Substrate scope of 2,5-substituted and 2,3,5-substituted pyrroles with yields determined by GC.

Next, the synthesis of 2,6-substituted and bicyclic pyridines was addressed in order to extent the substrate scope (**Scheme 3.2**).



Scheme 3.2 Generation of pyridines starting from secondary alcohols and 1,3-amino alcohols under elimination of water and hydrogen. Reaction conditions: 1,3-amino alcohol (1.5 mmol), secondary alcohol (6 mmol), KOtBu (3 mmol), 0.89 mol% Ir, 1.5 mL diglyme, 24 h at 90 °C and 24 h at 130 °C.

It was possible to synthesize a 2,6-alkyl-substituted pyridine as well as bicyclic pyridines with several functional groups in moderate to very good yields starting from cycloheptanol (**Figure 3.16**).

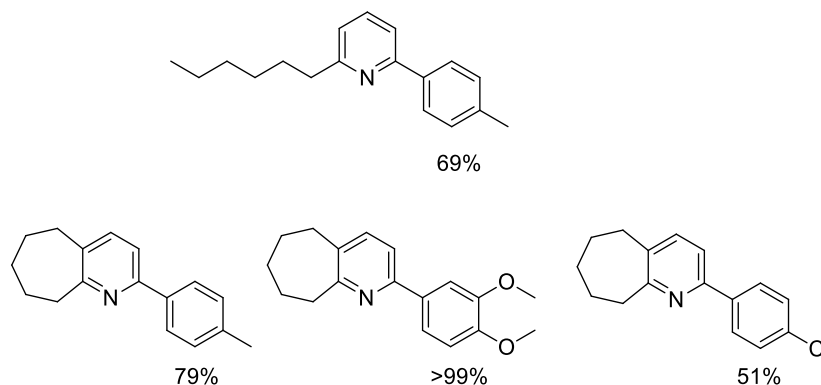
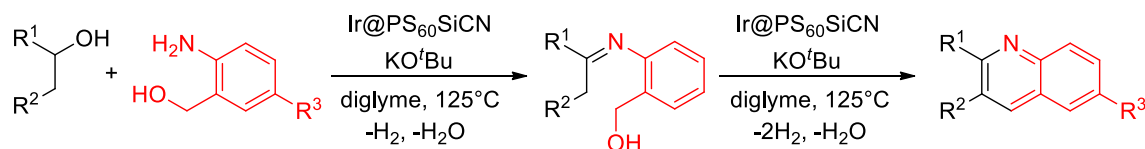


Figure 3.16 Substrate scope of 2,6-substituted and bicyclic pyridines with yields determined by GC.

Furthermore, 2- and 3-substituted as well as 2,3-substituted quinolines were synthesized with the described reaction conditions (**Scheme 3.3**).



Scheme 3.3 Generation of quinolines starting from alcohols and 2-aminobenzyl alcohol derivatives under elimination of water and hydrogen. Reaction conditions: 2-aminobenzyl derivative (1.5 mmol), alcohol (6 mmol), KO^tBu (3 mmol), 0.89 mol% Ir, 1.5 mL diglyme, 24 h at $125^\circ C$.

The tolerance of aryl-, alkyl-, chloro-groups, and cyclic-groups was demonstrated in moderate to very good yields (**Figure 3.17**).

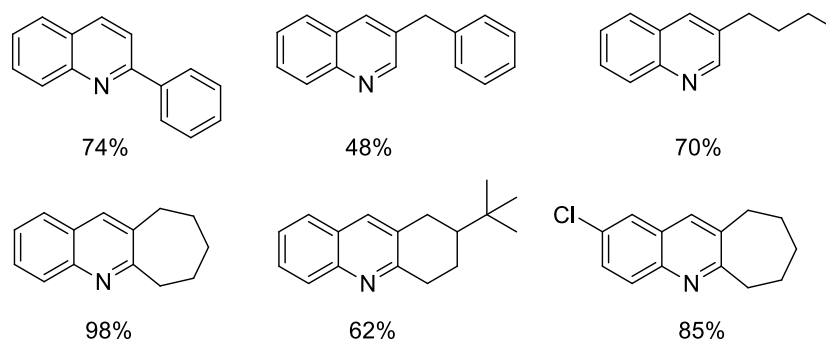


Figure 3.17. Substrate scope of 2- and 3-substituted as well as 2,3-substituted quinolones with yields determined by GC.

Finally, the activity and reusability of the Ir@PS₆₀SiCN catalyst was investigated compared to commercially available heterogeneous iridium catalysts (Ir/C, Ir/Al₂O₃, Ir/CaCO₃) as well as an unstructured Ir@SiCN catalyst. The hierarchical structured Ir@PS₆₀SiCN catalyst showed a good reusability in four successional runs and was significantly more active than the commercially available Ir catalysts and the unstructured Ir@SiCN catalyst. The synthesis of the Ir@SiCN catalyst without a pore building template led to a low SSA. The successful structuring of the Ir@PS₆₀SiCN catalyst causes a high SSA and an open porosity. This leads to a much better accessibility of the homogenously distributed iridium nanoparticles and consequently to the higher activity in the sustainable synthesis of N-heterocycles (**Figure 3.18**).

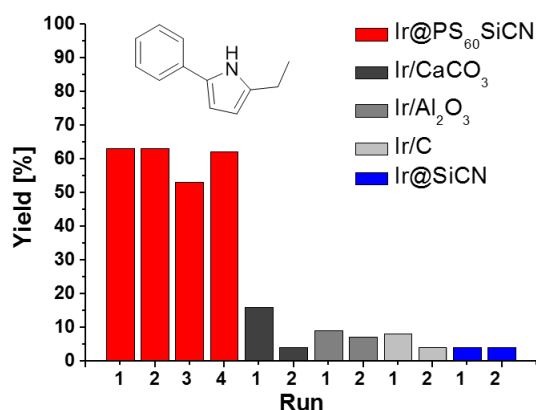


Figure 3.18 Heterogeneous iridium catalyst screening. Reaction conditions: 2-aminobutan-1-ol (1.5 mmol), 1-phenylethanol (6 mmol), KO^tBu (1.5 mmol), 1.32 mol% Ir, 1.5 mL diglyme, 5 h at 120 °C.

In the last manuscript in chapter 7, the demand of high metal accessibility and low metal content was addressed performing an Ir@SiCN coating on a modified polystyrene structured SiCN support. Therefore, the incorporated carbon of the hierarchically porous PS₆₀SiCN₁₀₀₀ material was partial removed as carbon dioxide by calcination. A fixed bed reactor with coupled online GC was used investigating the ideal calcination temperature (**Figure 3.19A**). The PS₆₀SiCN₁₀₀₀ material was calcinated at different temperatures observing an enhanced carbon dioxide release with increasing calcination temperature. A very good removal of carbon was obtained at 500 °C. Finally, the low surface area PS₆₀SiCN₁₀₀₀ material was heated to 500 °C under nitrogen atmosphere, treated with air oxygen for 45 minutes, and cooled down under nitrogen atmosphere obtaining a highly porous material (**Figure 3.19B**).

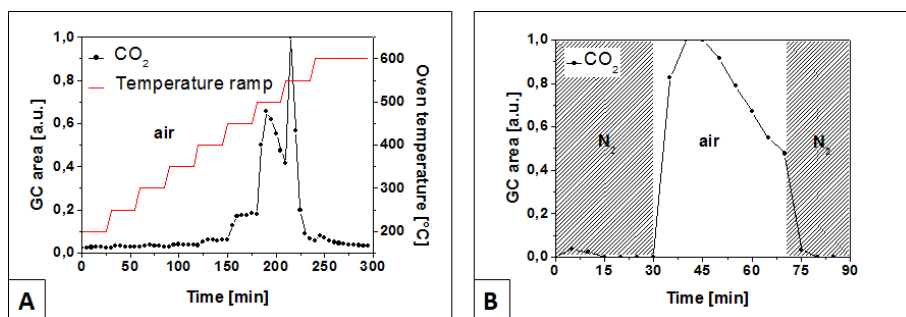


Figure 3.19 Online GC studies. Temperature dependent CO_2 release up to 700 °C (A). Calcination program with heating to 500 °C and cooling down under nitrogen flow obtaining a short calcination window at 500 °C (B).

Nitrogen sorption analysis exhibits an increase of the SSA from 37 m^2/g to 220 m^2/g for the calcinated SiCN material compared to the raw SiCN material. The mesopore amount of the pore volume was increased to 89 % (**Figure 3.20A**). SEM measurements show a honey-combed structure with open porosity after the calcination treatment (**Figure 3.20B**).

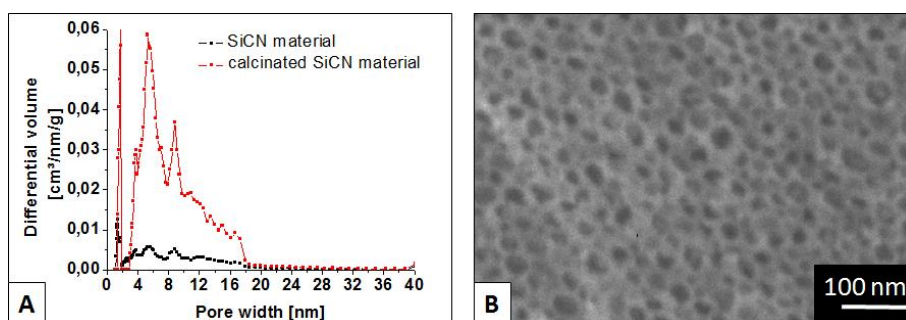


Figure 3.20 Calculated pore size distribution from nitrogen sorption measurements of the calcinated SiCN material and the SiCN material (A) as well as SEM image of the calcinated SiCN material (B).

After the enlargement of the SSA, the calcinated material was used as matrix for the coating with Ir@SiCN obtaining an Ir@SiCN-SiCN core-shell material. Therefore, the matrix material was treated with a mixture of an iridium aminopyridinato complex, HTT-1800, and DCP with a wetting technique and pyrolysed at 1000 °C. The successful coating was indicated by the reduction of the SSA (110 m^2/g) and the pore volume determined by nitrogen sorption measurements (**Figure 3.21A**). Moreover, SEM measurements show an open porosity in the macro scale range (**Figure 3.21B**).

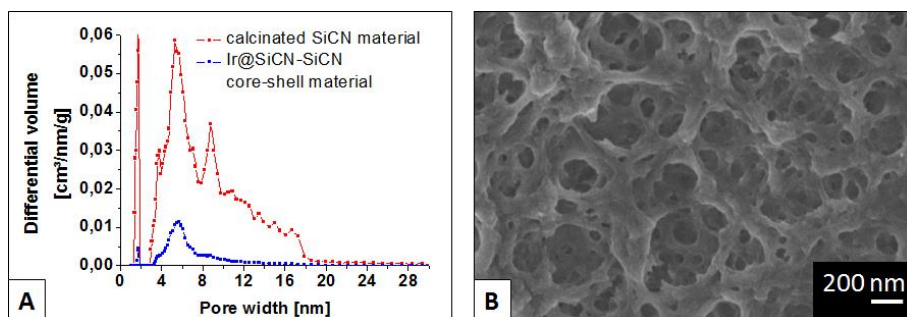


Figure 3.21 Calculated pore size distribution from nitrogen sorption measurements of the Ir@SiCN-SiCN core-shell material compared to the calcinated SiCN material (A) and the SEM image of the Ir@SiCN-SiCN core-shell material (B).

The presence of iridium in the core-shell material was verified by EDX measurements (**Figure 3.22A**). TEM images support this result showing homogenously distributed metal nanoparticles with a particle size distribution between 0.6 nm and 1.6 nm (**Figure 3.22B**). Thus, the coating technique leads to imbedded iridium nanoparticles in a thin SiCN layer on a SiCN support with increased SSA in order to enable a better metal accessibility.

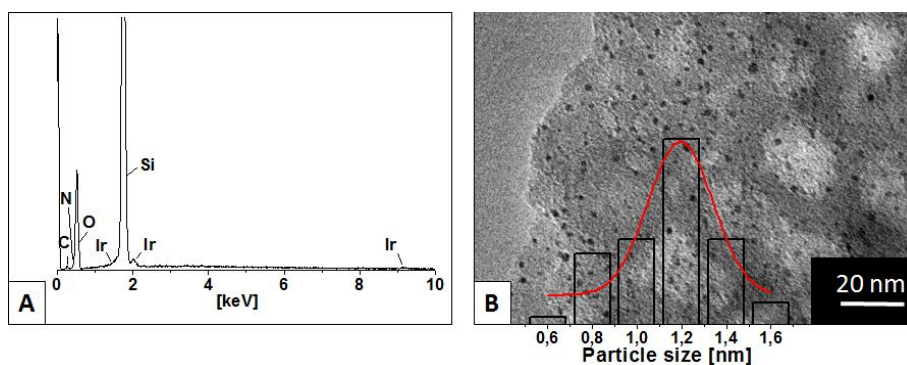


Figure 3.22 EDX measurement (A) and TEM measurement with particle size distribution (B) of the Ir@SiCN-SiCN core-shell material.

3.2 Individual Contribution to Joint Publications

Results presented in this thesis were achieved in collaboration with others and are published or to be submitted as described below. Contributions of all co-authors to the different publications are specified. The corresponding author(s) is (are) denoted by an asterisk note.

Chapter 4

This work is published in *Nanomaterials* **2015**, 5, 425-435 with the title

“Meso-Structuring of SiCN Ceramics by Polystyrene Templates”

Julia-Katharina Ewert, Christine Denner, Martin Friedrich, Günter Motz,^{*} and Rhett Kempe^{*}

I synthesized all compounds, carried out the corresponding characterizations except described below and performed all data analysis. Christine Denner performed SEM measurements and Martin Friedrich TEM measurements. The publication was written by me. Rhett Kempe and Günter Motz supervised this work and were involved in scientific discussions, comments and corrections of the manuscript.

Chapter 5

This work is published in *J. Mater. Chem. A* **2015**, 3, 18906-18912 with the title

“Enhanced Capacitance of Nitrogen-Doped Hierarchical Porous Carbide-Derived Carbon in Matched Ionic Liquids”

Julia-Katharina Ewert, Daniel Weingarth, Christine Denner, Martin Friedrich, Marco Zeiger, Anna Schreiber, Nicolas Jäckel, Volker Presser,^{*} and Rhett Kempe^{*}

I synthesized the polystyrene template and the SiCN ceramic and carried out the corresponding characterizations, except SEM measurements performed by Christine Denner and TEM measurements carried out by Martin Friedrich. I performed all data analysis. Furthermore, I coordinated the material characterization of the N-doped carbon, was contributed to all corresponding data analysis and performed elemental analysis. Daniel Weingarth carried out the chlorination treatment and was contributed to the electrochemical measurements (esp. in situ resistivity) as well as the data analysis. Christine Denner measured SEM and Martin Friedrich carried out TEM measurements of the N-doped carbon material. Marco Zeiger carried out Raman spectroscopy. Anna Schreiber was contributed to electrochemical testing (electrode

preparation and cell measurements). Nicolas Jäckel was contributed to electrochemical measurements and gas sorption measurements for the N-doped carbon. Moreover, I was contributed to the conceptual design of the publication as well as Daniel Weingarth. I wrote the manuscript together with Daniel Weingarth. Volker Presser and Rhett Kempe supervised this work, were contributed to the conceptual design of the manuscript, and were involved in scientific discussions, comments and corrections of the manuscript.

Chapter 6

This work is to be submitted with the title

“A Hierarchical Structured Reusable Iridium Catalyst for the Sustainable Synthesis of Pyrroles, Pyridines, and Quinolines”

Julia-Katharina Ewert, Christine Denner, Martin Friedrich, and Rhett Kempe*

I synthesized all compounds, carried out or coordinated the corresponding characterizations except described below and performed the data analysis. Moreover, the catalytic studies were performed and analyzed by me. Christine Denner performed SEM measurements and Martin Friedrich measured TEM and HR-TEM. The manuscript was written by me. Rhett Kempe supervised this work and were involved in scientific discussions, comments and corrections of the manuscript.

Chapter 7

This work is to be submitted in with the title

“Hierarchical Porous PS₆₀SiCN Material by Controlled Calcination for Ir@SiCN Coating”

Julia-Katharina Ewert, Stefan Schwarz, Christine Denner, Martin Friedrich, and Rhett Kempe*

I synthesized all compounds, carried out or coordinated the corresponding characterizations except described below and performed the data analysis. Christine Denner performed SEM measurements and Martin Friedrich measured TEM. The controlled calcination of the ceramics was performed in a fixed bed reactor with online GC analysis by Stefan Schwarz. The publication was written by me. Rhett Kempe and Günter Motz supervised this work and were involved in scientific discussions, comments and corrections of the manuscript.

4 Meso-Structuring of SiCN Ceramics by Polystyrene Templates

Julia-Katharina Ewert,^[a] Christine Denner,^[a] Martin Friedrich,^[a] Günter Motz^[b] and Rhett Kempe^[a]

[a] Inorganic chemistry II, University Bayreuth, 95440 Bayreuth, Germany.

[b] Institute of Ceramic Materials Engineering, University Bayreuth, 95440 Bayreuth, Germany.

Published in *Nanomaterials* **2015**, 5, 425-435.

Keywords: SiCN; meso-structured; self-sacrificial template method; polystyrene particles

Abstract: A simple one-pot synthesis of well-defined PS-silazane nano-composites (polystyrene, PS) is described. In contrast to the, thus far, used two-step procedure ((1) assembly of a PS template bed and (2) careful filling of the voids between the PS spheres), which is restricted to macro structuring, we are able to simply mix the PS template and a commercially available silazane precursor HTT-1800 in toluene. The key is the alteration of the zeta potential of the PS template leading to a homogeneous dispersion in the silazane-toluene mixture. Removal of solvent gives rise to a highly ordered PS-silazane nano-composites and subsequent pyrolysis leads to mesoporous silicon carbonitride (SiCN) materials. The one-pot procedure has two advantages: easy upscaling and the use of PS spheres smaller than 100 nm in diameter, here 60 nm. The PS template was characterized by photon correlation spectroscopy, zeta potential measurements, scanning electron microscopy (SEM), and thermal gravimetric analysis (TGA). The resulting mesoporous SiCN materials were analyzed by SEM, transmission electron microscopy (TEM), nitrogen sorption analysis, and Fourier transform infrared measurements (FT-IR).

4.1 Introduction

Polymer-derived (PD) silicon carbonitride (SiCN) ceramics are diversely used materials due to their easy processability, chemical resistance, and high thermal stability [1–14]. Among many applications, the use of PD-SiCN ceramics as a promising catalyst support material (M@SiCN) has been described [15–22]. Especially interesting is the generation of very small late transition metal nano particles from metallo-polysilazanes [17–22]. A catalytic reactivity as efficient as for homogeneous catalysts has been observed for Ir@SiCN [22]. Unfortunately, the M@SiCN

catalysts developed thus far show a low specific surface area, which means most of the metal nano particles are not accessible. In this context, the generation of nano-structured high surface area PD-SiCN ceramics is a desirable goal. Such structuring is difficult due to the hydrolysis sensitivity of the polymeric precursors. Out of the methods described thus far, the use of polyolefin templates seems most promising [10].

The group of Wiesner [23] used poly(isoprene-*block*-dimethylaminoethylmethacrylate) (PI-*b*-PDMAEMA) as structure-directing agent leading to a meso-structured SiCN ceramics. Furthermore, they combined their synthesis route using PI-*b*-PDMAEMA as structure-directing agent with polystyrene (PS) spheres as templates to structure at various lengths scales [17]. The group of Kim [24] synthesized poly(vinyl)silazane-*block*-polystyrene (PVSZ-*b*-PS) with self-assembly behavior, which was subsequently converted into an ordered mesoporous SiCN ceramic. Moreover, they combined photolithography and advanced nanofabrication processes resulting in a mesoporous SiCN patterns [25]. Jones and Lodge [26] introduced a hard template inverse replication technique. A microphase-separated polymer blend was used for the formation of a PE (polyethylene) template. The subsequent synthesis led to disordered 3D continuous porous non-oxide ceramics with pores between 60 and 100 nm. Our group produced ultrathin SiCN fibers as well as lamellar morphologies performing a one pot self-assembly and organic-inorganic block copolymer synthesis [27]. A commercially available polysilazane acted as the inorganic block and hydroxy-terminated polyethylene synthesized via coordinative chain transfer polymerization [28] as the organic block component.

The groups of Kim and Kenis [15] established the self-sacrificial template method using PS spheres. A packed bed of PS spheres is assembled in the first step and macroporous SiCN (and SiC) monoliths are obtained after infiltrating the template assembly by a preceramic silazane polymer and subsequent pyrolysis [29,30].

The elegant nano-structuring methods applied thus far have certain limitation. The block copolymer based strategies do either introduce oxygen using acrylic monomers or involve sophisticated block copolymer synthesis. Furthermore, bulk material structuring is demanding. The simple PS template approach has been restricted to macro structuring thus far. Most likely, since infiltration into the beds of PS smaller than 100 nm in diameter is challenging. Polysilazane diffusion into such small voids is very slow.

Herein we report on a simple one-pot synthesis of well-defined PS-silazane nano-composites. In contrast to the so far used two-step procedure: first, settling of the PS templates and, second, careful filling of the voids between the PS spheres, we are able to simply mix the PS templates

and a commercially available silazane precursor in common organic solvents. The key is the alteration of the zeta potential of the PS template to allow homogeneous dispersion of the PS template in the silazane solvent mixture. Removal of the solvent gives rise to the nano-composites and pyrolysis leads to meso-structured SiCN materials. The one-pot procedure has two advantages: easy upscaling and the use of PS spheres smaller than 100 nm in diameter.

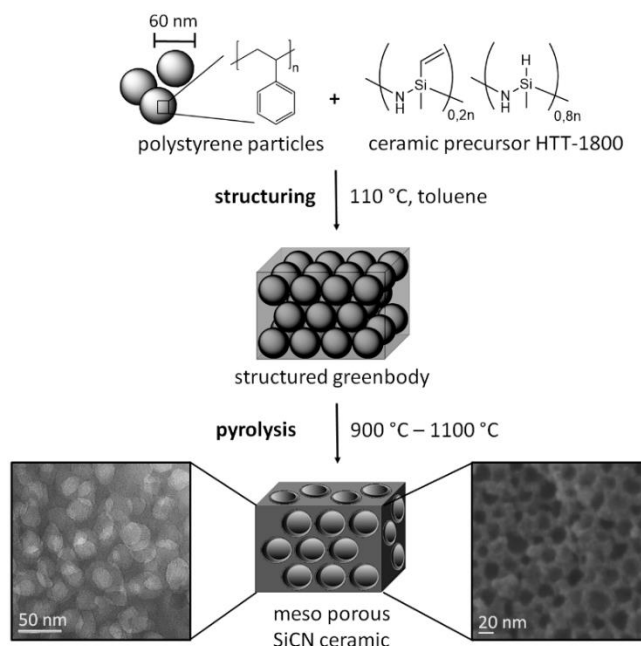
Porous ceramic produced at lower temperatures (900 °C) may be useful for battery applications.

4.2 Results and Discussion

4.2.1 Synthesis of the PS₆₀ Template and the PS₆₀SiCN Ceramics

In the first step, the spherical PS particles were synthesized with a diameter of 60 nm (PS₆₀) via emulsion polymerization. 4.50 g purified styrene (43.23 mmol) and 0.40 g divinylbenzene (3.07 mmol) were dispersed under stirring in degassed ultrapure water. Furthermore, 0.25 g of the surfactant CTAB (0.69 mmol) and 10 mg of the initiator 2,2'-azobis(2-methylpropion-amidine)dihydrochloride (0.04 mmol) were each dissolved in 5 mL ultrapure water. CTAB was added to the dispersion of styrene and divinylbenzene at 80 °C. After 30 min the polymerization was started by adding the initiator and, after 24 h, the polystyrene particles were purified by dialysis and isolated by freeze-drying. The template size of 60 nm is located in the macro scale range and accommodates the shrinking process of the particles to meso size during the pyrolysis [29]. It was essential to generate PS particles with a positive partial charge in order to stabilize a homogeneous dispersion of PS₆₀ in toluene during the structuring step. Particles with a negative partial charge, using potassium persulfate as an initiator, dispersed significantly less well in toluene. The commercial available preceramic polymer HTT-1800 was added obtaining a homogeneous suspension of the polymer template and the preceramic polymer by simple mixing. Cross-linking of HTT-1800 was achieved using the radical initiator dicumylperoxide (DCP) at 110 °C. The ordered polystyrene spheres were sealed in the HTT-1800 matrix. Removing the solvent under vacuum led to a structured green body. To guarantee a comprehensive structuring, the mixing ratio of 2:1 of the PS₆₀ template and the ceramic precursor is essential. We tested a few ratios based on dense packing of PS spheres and the complete filling of the voids by HTT-1800 (2.5:1 ratio). The best structuring was observed at a 2:1 ratio. Larger amounts of HTT-1800 gave rise to partially non-structured materials. The meso-porous structured ceramics PS₆₀SiCN₉₀₀, PS₆₀SiCN₁₀₀₀, and PS₆₀SiCN₁₁₀₀ were obtained after the pyrolysis of the green body

under nitrogen atmosphere at different temperatures (900–1100 °C) with a tailored pyrolysis program (Schema 1).



Scheme 1. Synthesis route leading to meso-structured SiCN ceramics: (1) Structuring: PS₆₀ dispersion in silazane-toluene mixture; pre-crosslinking at 110 °C; removal of solvent, and crosslinking at 110 °C leading to structured green bodies; (2) Pyrolysis with tailored pyrolysis program at 900, 1000, or 1100 °C obtaining PS₆₀SiCN₉₀₀, PS₆₀SiCN₁₀₀₀, and PS₆₀SiCN₁₁₀₀.

4.2.2 Characterization of the PS₆₀ Template

The hydrodynamic radius of the PS particles was calculated by contin analysis (Figure 1A). A narrow particle distribution in the range from 23.7 to 36 nm was achieved. The peak maxima is at 28.6 nm which means an average diameter of 57.2 nm for the PS particles (PS₆₀). Furthermore, a monodisperse behavior is verified.

Particle size and shape of the PS₆₀ template were observed by SEM. The particle size distribution was determined based on the scanning electron microscopy (SEM) image (Figure 1B). An average particle size of 62.8 nm was calculated by Gaussian fit. Moreover, a narrow monodisperse distribution of spherical particles was obtained, which is in agreement with the results of the PCS measurement.

By choice of the initiator and the surfactant the PS particles were generated with a positive partial charge, which was confirmed by zeta potential measurements. The PS₆₀ template exhibits a zeta potential of 47 mV. Compared to PS particles with negative partial charges, the

stabilization of a homogeneous dispersion in nonpolar solvents like toluene is possible enabling the performed one-pot synthesis.

The decomposition temperature of the PS₆₀ template was investigated by TGA under nitrogen atmosphere. The major mass loss occurs between 380 and 445 °C. The PS₆₀ template is totally decomposed at a temperature of 470 °C (Figure 1C). It was important to investigate the decomposition behavior of the template in order to adjust the pyrolysis temperature ($0.5\text{ °C}\cdot\text{min}^{-1}$ between 400 and 500 °C). Thus, the entire elimination of the PS template and the generation of maximum pore density was ensured.

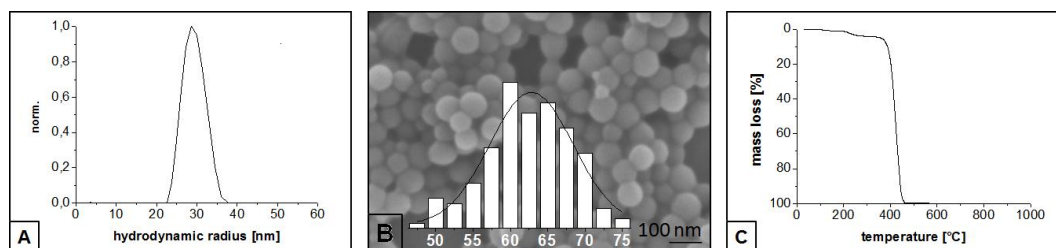


Figure 1. Particle size distribution calculated by CONTIN analysis (A); Scanning electron microscopy (SEM) image with particle size distribution (nm) (B); and thermal gravimetric analysis (TGA) analysis under nitrogen atmosphere (C) of the PS₆₀ template.

4.2.3 Characterization of the PS₆₀SiCN Ceramics

The PS₆₀SiCN compounds were pyrolyzed at 900, 1000, and 1100 °C to investigate the temperature dependent stability of the pores. Porous ceramic produced at low temperatures (900 °C) may also be useful for battery applications [31,32]. The SEM-images identify a honeycomb surface structure with small mesopores for the ceramics PS₆₀SiCN₉₀₀ (Figure 2A,B) and PS₆₀SiCN₁₀₀₀ (Figure 2C,D). According to Kim and coworkers [29] a shrinking process of the PS particles takes place during the pyrolysis of the green body. The total collapse of the surface pores is observed at a pyrolysis temperature of 1100 °C (Figure 2E,F).

TEM-images illustrate the correlation of the pore density and the pyrolysis temperature. Increasing temperatures result in the reduction of the pore density (Figure 3A–F), which confirms the results of the SEM measurements.

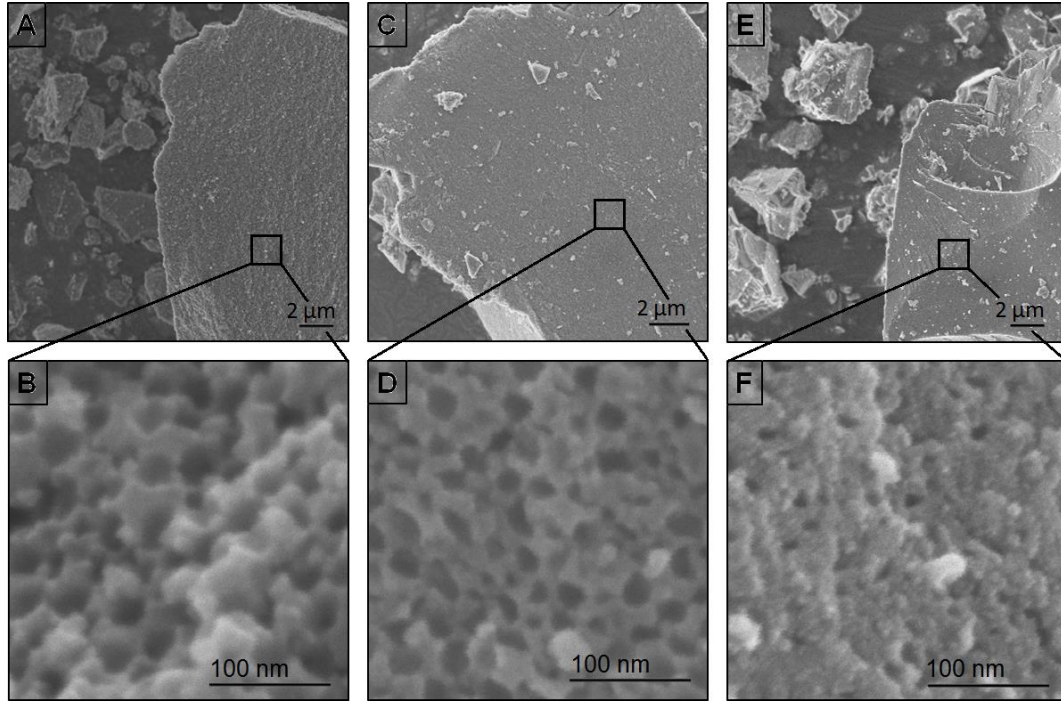


Figure 2. SEM-images of PS₅₀SiCN₉₀₀ (A,B); of PS₅₀SiCN₁₀₀₀ (C,D); and of PS₅₀SiCN₁₁₀₀ (E,F).

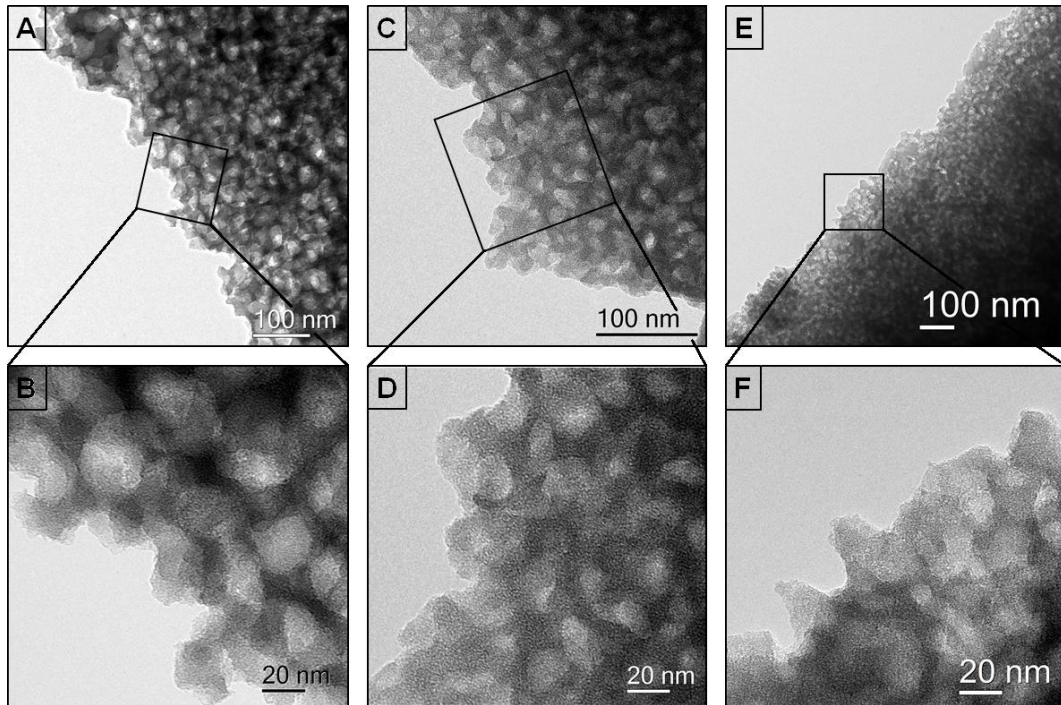


Figure 3. TEM-images of (A,B); of PS₅₀SiCN₁₀₀₀ (C,D); and of PS₅₀SiCN₁₁₀₀ (E,F).

Nitrogen sorption measurements (Figure 4A) of the ceramics show typical Type IV isotherms according to Sing *et al.* [33] The presence of mesopores is indicated by the hysteresis. Large specific surface areas (PS₅₀SiCN₁₁₀₀: 35 m²/g, PS₅₀SiCN₁₀₀₀: 50 m²/g and PS₅₀SiCN₉₀₀: 110 m²/g) correlate with the reduction of pyrolysis temperature indicating the increased

mesopore percentage. The calculated pore size distribution (NLDFT) shows a major pore volume between 4 and 10 nm. Furthermore, larger mesopores up to 24 nm can be observed (Figure 4B). The larger pores are attributed to the surface-located cavities according to the SEM-images. The smaller pores are located inside the material. This trend can also be recognized for the ceramics $\text{PS}_{50}\text{SiCN}_{1000}$ and $\text{PS}_{50}\text{SiCN}_{1100}$. With rising pyrolysis temperature the contribution of high range mesopores decreases, which is in agreement with the nitrogen sorption isotherms.

The FT-IR measurements indicate the presence of SiCN ceramics in regard to the characteristic signals of the HTT-1800 precursor (Figure 4C) [34,35]. The broad peak at 1250 cm^{-1} is typical for SiCN ceramics and accrues from the overlapping of the Si-C-, the Si-N- and the Si-N-Si-bands [32,33].

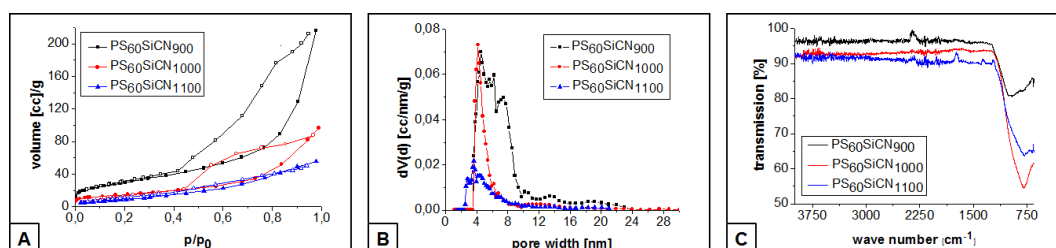


Figure 4. Nitrogen sorption isotherms (A); calculated pore size distribution (B); and Fourier transform infrared measurements (FT-IR) spectra (C) of the ceramics $\text{PS}_{60}\text{SiCN}_{900}$, $\text{PS}_{60}\text{SiCN}_{1000}$, and $\text{PS}_{60}\text{SiCN}_{1100}$.

4.3 Experimental Section

4.3.1 Materials and Methods

All reactions were carried out in a dry argon or nitrogen atmosphere using standard Schlenk or glove box techniques. Non-halogenated solvents were dried over sodium benzophenone ketyl and distilled. (1-Hexadecyl)trimethylammonium bromide (CTAB) (98% purity, abcr, Karlsruhe, Germany), 2,2'-azobis(2-methylpropion-amidine)dihydrochloride (97% purity, Aldrich Chemistry, Steinheim, Germany), KiON HTT1800 (Clariant Advanced Materials GmbH, Frankfurt, Germany) and dicumylperoxide (97% purity, Aldrich Chemistry, Steinheim, Germany) were purchased from commercial sources and used without further purification. Styrene (>99% purity, Sigma Aldrich, Steinheim, Germany) and divinylbenzene (technical grade, 55%, Aldrich Chemistry, Steinheim, Germany) were destabilized over an alumina B column (ICN Biomedicals GmbH, Eschwege, Germany).

Photon correlation spectroscopy (PCS) measurements were carried out with an ALV DLS/SLA-SP 5022F laser goniometer system. A Ne/Ar ion laser ($\lambda = 632.8$ nm) with a constant output of 260 mW was used as power source. The correlation function was generated by an ALV-5000/E multiple tau digital correlator. The decalin bath temperature was regulated to 20 °C with a computer-operated thermostat. The fixed angle measurements were performed with a 90° angle. The data analysis was accomplished by the CONTIN analysis.

Zeta potential measurements were performed with a Zetasizer Nano ZS (Malvern Instruments Limited, Herrenberg, Germany).

Thermal gravimetric analysis (TGA) were performed under nitrogen atmosphere using a Thermowaage L81 (Linseis, Selb, Germany) and a heating rate of 5 K·min⁻¹ up to 900 °C.

CHN analyses were carried out on a Vario elementar EL III.

Ceramization was performed in a high temperature furnace (GERO, Berlin, Germany) under nitrogen atmosphere. The pyrolyzed ceramics were milled in a ball mill “Pulverisette 0” (Fritsch, Idar-Oberstein, Germany) for 20 min.

SEM measurements were carried out using a Zeiss Field-Emission-Scanning-Electron-Microscope (FESEM) “LEO 1530 GEMINI”. The acceleration voltage was 1–5 kV. The samples were sputter-coated with a 1.3 nm layer of platinum.

Transmission electron microscopy (TEM) measurements were performed using a Varian LEO 9220 (Carl Zeiss, 120 kV, Oberkochen, Germany) instrument. The samples were suspended in chloroform and sonicated for 5 min. Two microliters of the suspension were placed on a CF200-Cu-grid (Electron Microscopy Sciences, Hatfield, USA) and allowed to dry.

FT-IR measurements were performed using a Perkin-Elmer FTIR Spectrum 100 over a range from 4400 to 650 cm⁻¹.

Nitrogen sorption analyses were conducted using a Nova2000e (Quantachrome, Odelzhausen, Germany) instrument. The specific surface areas were calculated using p/p_0 -values from 0.05–0.31 (BET). The pore width and average pore volume was calculated by DFT calculations (N₂ at 77 K on carbon (slit pore, NLDFE equilibrium model)).

4.3.2 Preparation

Synthesis of the PS₆₀ template: The emulsion polymerization of the cross-linked polystyrene latex particles with 60 nm diameter were carried out in a three neck round bottom flask with a reflux condenser, a KPG stirrer and a septum. 4.50 g purified styrene (43.23 mmol) and 0.40 g divinylbenzene (3.07 mmol) were dispersed under stirring in 90 mL degased ultrapure water.

An amount of 0.25 g of the surfactant CTAB (0.69 mmol) and 10 mg of the initiator 2,2'-azobis(2-methylpropionamidine)dihydrochloride (0.04 mmol) were each solved in 5 mL ultrapure water. CTAB was added to the dispersion at 80 °C under stirring with 200 rpm. After 30 min the polymerization was started by adding the initiator. After 24 h the polystyrene particles were purified by dialysis and isolated by freeze drying.

Synthesis of the PS₆₀SiCN compounds: In a round bottom Schlenk flask 1.0 g PS₆₀ were degassed applying a vacuum of 10⁻³ mbar for several hours to remove residual water. The PS₆₀-particles were dispersed in 40 mL toluene under stirring. Subsequently, 0.56 g of KiON HTT1800 (7.77 mmol) and 0.05 g dicumylperoxide (1.85 mmol) were added. Without stirring, the suspension was heated to 110 °C for 20 h. The solvent was removed under vacuum and the *in situ* structured preceramic polymer was annealed for 20 h at 110 °C to complete the crosslinking. The PS₅₀SiCN₉₀₀₋₁₁₀₀ green bodies were pyrolyzed under nitrogen flow according to the following program:

$RT \xrightarrow{1\text{ K min}^{-1}, 3\text{ h}} 300\text{ °C} \xrightarrow{1\text{ K min}^{-1}, 3\text{ h}} 400\text{ °C} \xrightarrow{0.5\text{ K min}^{-1}, 3\text{ h}} 500\text{ °C} \xrightarrow{1\text{ K min}^{-1}, 4\text{ h}} 600\text{ °C} \xrightarrow{0.5\text{ K min}^{-1}, 0\text{ h}} 700\text{ °C} \xrightarrow{1\text{ K min}^{-1}, 0.5\text{ h}} 900\text{ °C} - 1100\text{ °C}$

4.4 Conclusions

To the best of our knowledge, meso-porous structured SiCN nano-composites were generated by the self-sacrificial template method for the first time. The processability of monoliths was shown in a one pot synthesis including PS latex particles with the size of 60 nm as template and the commercial inexpensive HTT-1800 as preceramic polymer. The positive partial charge of the polymer template facilitates a homogeneous dispersion of PS₆₀ particles in the silazane solvent mixture enabling easy upscaling. The influence of different pyrolysis temperatures was investigated regarding the stability of the pores. The specific BET surface area and the mesopore percentage correlates with the decrease of the pyrolysis temperature.

For future research, meso-porous SiCN compounds are well-suited materials for the stabilization of metal particles, which provides the application as catalyst supports.

4.5 Acknowledgments

We thank the SFB 840 and the Elitenetzwerk Bayern e.V. for financial support.

Author Contributions

Julia-Katharina Ewert designed the experiments and performed the experiments. Martin Friedrich performed TEM measurements and Christine Denner performed SEM measurements. Julia-Katharina Ewert, Rhett Kempe, and Günter Motz wrote the manuscript.

Conflicts of Interest

The authors declare no conflict of interest.

4.6 References

1. Riedel, R.; Kleebe, H.-J.; Schönfelder, H.; Aldinger, F. A covalent micro/nano-composite resistant to high-temperature oxidation. *Nature* **1995**, *374*, 526–528.
2. Weibelzahl, W.; Motz, G.; Suttor, D.; Ziegler, G. Corrosion stability and mechanical properties of polysilazane-derived SiCN-ceramics. *Key Eng. Mater.* **1999**, *161–163*, 111–114.
3. Kroke, E.; Li, Y.-L.; Konetschny, C.; Lecomte, E.; Fasel, C.; Riedel, R. Silazane derived ceramics and related materials. *Mater. Sci. Eng. R* **2000**, *26*, 97–199.
4. Greil, P. Polymer derived engineering ceramics. *Adv. Eng. Mater.* **2000**, *2*, 339–348.
5. Kleebe, H.J.; Störmer, H.; Trassl, S.; Ziegler, G. Thermal stability of SiCN ceramics studied by spectroscopy and electron microscopy. *Appl. Organomet. Chem.* **2001**, *15*, 858–866.
6. Riedel, R.; Mera, G.; Hauser, R.; Klonczynski, A. Silicon-based polymer-derived ceramics: Synthesis properties and applications—A review. *J. Ceram. Soc. Jpn.* **2006**, *114*, 425–444.
7. Studart, A.R.; Gonzenbach, U.T.; Tervoort, E.; Gauckler, L.J. Processing routes to macroporous ceramics: A review. *J. Am. Ceram. Soc.* **2006**, *89*, 1771–1789.
8. Colombo, P.; Mera, G.; Riedel, R.; Sorarù, G.D. Polymer-derived ceramics: 40 years of research and innovation in advanced ceramics. *J. Am. Ceram. Soc.* **2010**, *93*, 1805–1837.
9. Colombo, P.; Sorarù, G.D.; Riedel, R.; Kleebe, A.; Stech, D.E. *Polymer Derived Ceramics*; Publications Inc.: Lancaster, PA, USA, 2010.

10. Shi, Y.; Wan, Y.; Zhao, D. Ordered mesoporous non-oxide materials. *Chem. Soc. Rev.* **2011**, *40*, 3854–3878.
11. Zaheer, M.; Schmalz, T.; Motz, G.; Kempe, R. Polymer derived non-oxide ceramics modified with late transition metals. *Chem. Soc. Rev.* **2012**, *41*, 5102–5116.
12. Ionescu, E.; Kleebe, H.J.; Riedel, R. Silicon-containing polymer-derived ceramic nanocomposites (PDC-NCs): Preparative approaches and properties. *Chem. Soc. Rev.* **2012**, *41*, 5032–5052.
13. Mera, G.; Navrotsky, A.; Sen, S.; Kleebe, H.-J.; Riedel, R. Polymer-derived SiCN and SiOC ceramics—Structure and energetics at the nanoscale. *J. Mater. Chem. A* **2013**, *1*, 3826.
14. Bernardo, E.; Fiocco, L.; Parcianello, G.; Storti, E.; Colombo, P. Advanced ceramics from preceramic polymers modified at the nano-scale: A review. *Materials* **2014**, *7*, 1927–1956.
15. Sung, I.K.; Mitchell, C.M.; Kim, D.P.; Kenis, P.J.A. Tailored macroporous SiCN and SiC structures for high-temperature fuel reforming. *Adv. Funct. Mater.* **2005**, *15*, 1336–1342.
16. Mitchell, C.M.; Kim, D.P.; Kenis, P. Ceramic microreactors for on-site hydrogen production. *J. Catal.* **2006**, *241*, 235–242.
17. Kamperman, M.; Burns, A.; Weissgraeber, R.; van Vegten, N.; Warren, S.C.; Gruner, S.M.; Baiker, A.; Wiesner, U. Integrating structure control over multiple length scales in porous high temperature ceramics with functional platinum nanoparticles. *Nano Lett.* **2009**, *9*, 2756–2762.
18. Glatz, G.; Schmalz, T.; Kraus, T.; Haarmann, F.; Motz, G.; Kempe, R. Copper-containing SiCN precursor ceramics (Cu@SiCN) as selective hydrocarbon oxidation catalysts using air as an oxidant. *Chem. Eur. J.* **2010**, *16*, 4231–4238.
19. Schmalz, T.; Kraus, T.; Günthner, M.; Liebscher, C.; Glatzel, U.; Kempe, R.; Motz, G. Catalytic formation of carbon phases in metal modified, porous polymer derived SiCN ceramics. *Carbon* **2011**, *49*, 3065–3072.
20. Zaheer, M.; Motz, G.; Kempe, R. The generation of palladium silicide nanoalloy particles in a SiCN matrix and their catalytic applications. *J. Mater. Chem.* **2011**, *21*, 18825.
21. Zaheer, M.; Keenan, C.D.; Hermannsdörfer, J.; Roessler, E.; Motz, G.; Senker, J.; Kempe, R. Robust microporous monoliths with integrated catalytically active metal sites investigated by hyperpolarized ^{129}Xe NMR. *Chem. Mater.* **2012**, *24*, 3952–3963.

22. Forberg, D.; Obenauf, J.; Friedrich, M.; Hühne, S.-M.; Mader, W.; Motz, G.; Kempe, R. The synthesis of pyrroles via acceptorless dehydrogenative condensation of secondary alcohols and 1,2-amino alcohols mediated by a robust and reusable catalyst based on nanometer-sized iridium particles. *Catal. Sci. Technol.* **2014**, *4*, 4188–4192.
23. Kamperman, M.; Garcia, C.B.; Du, P.; Ow, H.; Wiesner, U. Ordered mesoporous ceramics stable up to 1500 degrees C from diblock copolymer mesophases. *J. Am. Chem. Soc.* **2004**, *126*, 14708–14709.
24. Nghiem, Q.D.; Kim, D.J.; Kim, D.P. Synthesis of inorganic–organic diblock copolymers as a precursor of ordered mesoporous SiCN ceramic. *Adv. Mater.* **2007**, *19*, 2351–2354.
25. Nguyen, C.T.; Hoang, P.H.; Perumal, J.; Kim, D.P. An inorganic-organic diblock copolymer photoresist for direct mesoporous SiCN ceramic patterns via photolithography. *Chem. Commun. (Camb)* **2011**, *47*, 3484–3486.
26. Jones, B.H.; Lodge, T.P. High-temperature nanoporous ceramic monolith prepared from a polymeric bicontinuous microemulsion template. *J. Am. Chem. Soc.* **2009**, *131*, 1676–1677.
27. Pillai, S.K.; Kretschmer, W.P.; Denner, C.; Motz, G.; Hund, M.; Fery, A.; Trebbin, M.; Forster, S.; Kempe, R. SiCN nanofibers with a diameter below 100 nm synthesized via concerted block copolymer formation, microphase separation, and crosslinking. *Small* **2013**, 984–989.
28. Pillai, S.K.; Kretschmer, W.P.; Trebbin, M.; Forster, S.; Kempe, R. Tailored nanostructuring of end-group-functionalized high-density polyethylene synthesized by an efficient catalytic version of Ziegler’s “Aufbaureaktion”. *Chem. Eur. J.* **2012**, *18*, 13974–13978.
29. Yan, J.; Hong, L.Y.; Wang, A.J.; Kim, D.P. Facile synthesis of SiCN ceramic foam via self-sacrificial template method. *Solid State Phenom.* **2007**, *124–126*, 727–730.
30. Xiao, Z.; Wang, A.; Kim, D.-P. 3D macroporous SiCN ceramic patterns tailored by thermally-induced deformation of template. *J. Mater. Chem.* **2010**, *20*, 2853–2857.
31. Dibandjo, P.; Graczyk-Zajac, M.; Riedel, R.; Pradeep, V.S.; Soraru, G.D. Lithium insertion into dense and porous carbon-rich polymer-derived SiOC ceramics. *J. Eur. Ceram. Soc.* **2012**, *32*, 2495–2503.
32. Song, T.; Xia, J.; Lee, J.-H.; Lee, D.H.; Kwon, M.-S.; Choi, J.-M.; Wu, J.; Doo, S.K.; Chang, H.; Park, W.I.; *et al.* Arrays of sealed silicon nanotubes as anodes for lithium ion batteries. *Nano Lett.* **2010**, *10*, 1710–1716.

33. Sing, K.S.W.; Everett, D.H.; Haul, R.A.W.; Moscou, L.; Pierotti, R.A.; Rouquerol, J.; Siemieniewska, T. Reporting physisorption data for gas/solid systems. *Pure Appl. Chem.* **1984**, *57*, 603–619.
34. Kriegsmann, H.; Beyer, H. Spektroskopische untersuchungen an Siliciumverbindungen. XIV. IR- und Ramanspektren einiger substituierter Disilylacetylene. *Z. Anorg. Allg. Chem.* **1961**, *311*, 180–185.
35. Choong Kwet Yive, N.S.; Corriu, R.J.P.; Leclercq, D.; Mutin, P.H.; Vioux, A. Silicon carbonitride from polymeric precursors: Thermal cross-linking and pyrolysis of oligosilazane model compounds. *Chem. Mater.* **1992**, *4*, 141–146.

5 Enhanced Capacitance of Nitrogen-Doped Hierarchical Porous Carbide-Derived Carbon in Matched Ionic Liquids

Julia-Katharina Ewert,^[a] Daniel Weingarth,^[b] Christine Denner,^[a] Martin Friedrich,^[a] Marco Zeiger,^[b,c] Anna Schreiber,^[b] Nicolas Jäckel,^[b,c] Volker Presser,^[b,c] and Rhett Kempe^[a]

[a] Anorganische Chemie II (Catalyst Design), Universität Bayreuth, 95440 Bayreuth, Germany

[b] INM - Leibniz Institute for New Materials, Campus D2 2, 66123 Saarbrücken, Germany.

[c] Department of Materials Science and Engineering, Saarland University, Campus D2 2, 66123 Saarbrücken, Germany.

Published in *J. Mater. Chem. A* **2015**, 3, 18906-18912.

Keywords: heteroatom carbons, supercapacitors, energy storage, ionic liquids, soft templating

Abstract: Supercapacitors combine efficient electrical energy storage and performance stability based on fast electrosorption of electrolyte ions at charged interfaces. They are a central element of existing and emerging energy concepts. A better understanding of capacitance enhancement options is essential to exploit the full potential of supercapacitors. Here, we report a novel hierarchically structured N-doped carbon material and a significant capacitance enhancement for a specific ionic liquid. Our studies indicate that matching of the electrode material and the ionic liquid specifically leads to a constant normalized resistance of the electrode material (voltage window up to ± 1 V vs. carbon) and a significant enhancement of the specific capacitance. Such effects are not seen for standard organic electrolytes, non-matched ionic liquids, or non-N-doped carbons. A higher N-doping of the electrode material improves the symmetric full cell capacitance of the match and considerably increases its long-term stability at +3 V cell voltage. This novel observance of enhanced specific capacitance for N-doped carbons with matched ionic liquid may enable a new platform for developing supercapacitors with enhanced energy storage capacity.

5.1 Introduction

Electrochemical capacitors, also known as supercapacitors or ultracapacitors, capitalize on the high efficiency and performance stability of fast electrosorption of electrolyte ions at the charged interface with nanoporous carbon.^{1,2} While derived from abundantly available biomass, commonly used high surface area carbons show only a moderate electrical conductivity, which presents a limitation to effective charge screening, leading to limited energy storage capacity.³ At a device level, this shortcoming is usually compensated by the admixing of conductive additives;⁴ yet, this approach is not an intrinsic solution for the inability to accommodate a high amount of electric charge within the carbon nanopores. The beneficial impact of N-doping on the electrical conductivity and, more generally, the electrochemical performance of supercapacitors has first been investigated by Lota et al. in polymer-derived carbons.⁵ By now, a series of carbon materials with N-doping has been explored, including carbon nanotubes,^{6,7} mesoporous carbon spheres,⁸ biomass-derived porous carbon,⁹ metal–organic frameworks,¹⁰ and graphenelike carbon.¹¹ Nitrogen can be introduced into carbon, generally, top-down or bottom-up. The latter involves the synthesis of a carbon network and subsequent N-doping via annealing, for example in ammonia.¹² Alternatively, N-doping can be accomplished very effectively by using nitrogen-containing precursor materials, including bio-materials like prawn shells or yogurt^{9,13} or ionic liquids.¹⁴ Depending on the synthesis procedure and the maximum synthesis temperature, the maximum amount of N-doping in carbon may reach around 21 mass%.¹⁵ In general, we find lower nitrogen content when employing higher synthesis temperatures¹⁵ and a significant improvement of the electrochemical performance has been reported already for rather low amounts of nitrogen, such as 1–2 mass%.⁵ Besides improving the electrical conductivity and increasing the charge screening ability of carbon,⁷ N-sites at the carbon surface may facilitate charge transfer across the electrode/electrolyte interface. Such redox-sites may contribute significantly to the energy storage mechanism by enabling access to reversible faradaic reactions and possibly pseudocapacitance;^{11,16} yet, this is often accomplished at the cost of sacrificing power handling and longevity to some degree.² Considering the high ion mobility and the possible benefit of redox-related charge storage, most of the investigations of nitrogen-doped carbons have been carried out in aqueous electrolytes, foremost H₂SO₄ (ref. 5, 6 and 17) and KOH.⁵ In such systems, an enhancement of the electrochemical performance is accomplished by the introduction of fast surface redox-reactions of quaternary nitrogen and other N-groups with the protic electrolyte. Only a small

number of studies, so far, have been carried out on organic electrolytes,⁵ including ionic liquids.¹⁸ The latter are a highly promising group of electrolytes that are able to push the voltage limit of supercapacitors to at least 3.5 V even for long-term operation,¹⁹ while benefitting from a non-volatile and temperature-stable nature at the cost of low ion mobility.²⁰ Since the stored amount of energy scales with the square of the cell voltage, ionic liquids are attractive candidates for high-energy supercapacitor devices.²¹ While the results for many of the N-doped carbons are promising, one aspect has somewhat been overlooked: the intricate correlation between ions and the carbon surface. Matching the ionic liquid to an optimized voltage window has recently been demonstrated for pure carbon materials,²² but it is still unclear what selection strategy should be applied for matching an ionic liquid to nitrogen-doped carbon.

Herein, we report a novel hierarchically porous N-doped carbon material obtained from meso-structured polymer derived silicon carbonitride and the electrochemical performances in different ionic liquids. We observe a significantly improved capacitance for one specific ionic liquid and an increased N-doping improves the symmetric full cell capacitance as well as the long-time stability of such cells at high voltage.

5.2 Results and Discussion

5.2.1 Preparation of the hierarchical porous N-doped carbon material

Since the template free synthesis of polymer-derived silicon carbon nitride (SiCN) materials leads neither to micropores nor to mesopores,²³ we decided to synthesize a polystyrene-polysilazane nanocomposite regarding meso-structuring.²⁴ Therefore, positively charged polystyrene (PS) spheres with a diameter of about 50 nm (PS₅₀) were synthesized as structuring templates via emulsion polymerization (Fig. 1; see also ESI, Fig. S1†). The particles were mixed in toluene with commercially available polysilazane HTT-1800. Divinylbenzene (DVB) was used as a cross-linker stabilizing the particles in toluene. Thus, an enhanced yield of residual carbon can be obtained. Evaporation of the solvent gave rise to the nano-composite green body. The green body was pyrolyzed at 900 °C in order to remove the PS₅₀ template and led to the thermally stable meso-structured SiCN material PS₅₀SiCN₉₀₀. (Fig. 1; see also ESI, Fig. S2†). Chlorine treatment, commonly used for the synthesis of carbide-derived carbons (CDC),²⁵ was employed at 800 °C (PS₅₀SiCN₉₀₀Cl₂-800°C) and 1000 °C (PS₅₀SiCN₉₀₀Cl₂-1000°C) to volatilize residual silicon and partially mobilize silicon nitride.²⁶

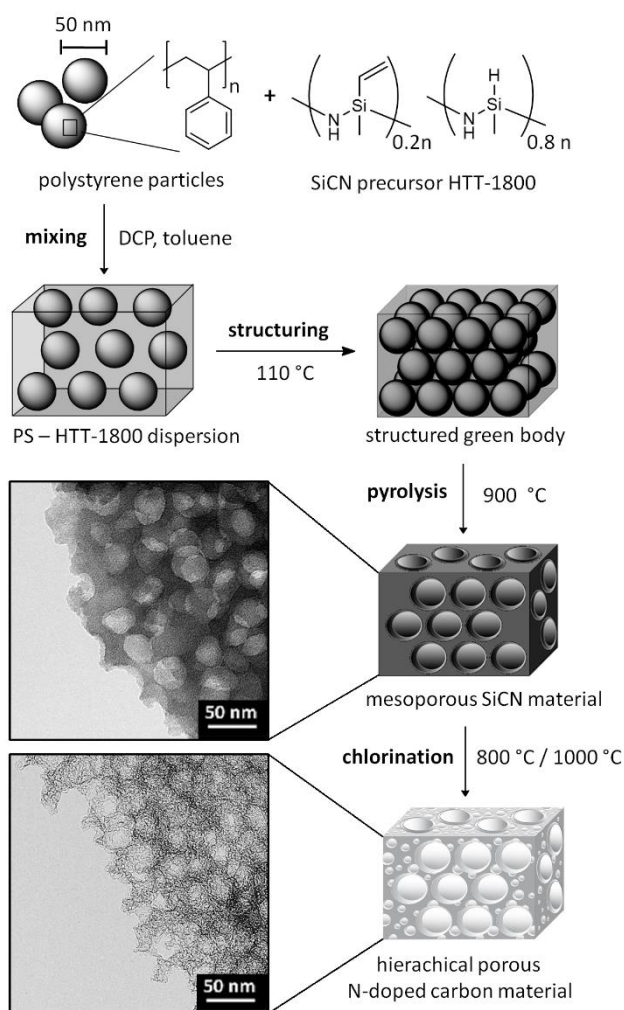


Figure 1. Schematic process of the synthesis of the N-doped hierarchically porous carbon materials and transmission electron microscopy (TEM) images of $\text{PS}_{50}\text{SiCN}_{900}$ (left, top) $\text{PS}_{50}\text{SiCN}_{900}\text{Cl}_2\text{-}800^\circ\text{C}$ (left, bottom) following a three step procedure. (1) Mixing 50 nm polystyrene (PS_{50}) particle template, the commercially available SiCN precursor HTT-1800, and dicumylperoxide (DCP, cross linker) in toluene as well as structuring by removal of the solvent. (2) Pyrolysis at 900 °C obtaining the mesoporous SiCN material $\text{PS}_{50}\text{SiCN}_{900}$. (3) Chlorination at 800 °C or 1000 °C leading to the hierarchical porous N-doped carbon material $\text{PS}_{50}\text{SiCN}_{900}\text{Cl}_2\text{-}800^\circ\text{C}$ and $\text{PS}_{50}\text{SiCN}_{900}\text{Cl}_2\text{-}1000^\circ\text{C}$, respectively.

5.2.2 Material characterization

Transmission electron microscopy (TEM) images of $\text{PS}_{50}\text{SiCN}_{900}\text{Cl}_2\text{-}800^\circ\text{C}$ before and after chlorine treatment are shown in Fig. 1. For scanning electron microscopy (SEM) and TEM images of all materials, see ESI, Fig. S1–S3.† As common for CDC,²⁷ our materials remained conformal after chlorine gas treatment, preserving the structure of the mesoporous SiCN material and adding additional pores so that a very high pore volume (up to $1.67 \text{ cm}^3\text{g}^{-1}$) was reached.

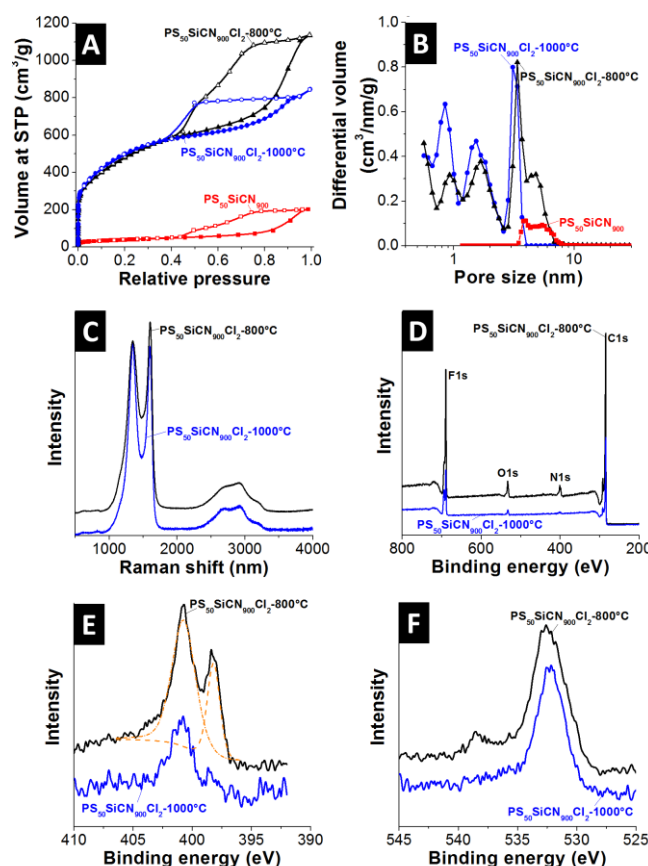


Figure 2. Characterization of the hierarchically porous nitrogen-doped carbon materials (A) Nitrogen sorption isotherms and (B) calculated pore size distribution of the ceramic template and the chlorinated materials. (C) Raman spectra of the samples PS₅₀SiCN₉₀₀-800°C and PS₅₀SiCN₉₀₀-1000°C, (D) XPS survey spectra of the samples PS₅₀SiCN₉₀₀-800°C and PS₅₀SiCN₉₀₀-1000°C, (E) N1s high resolution spectrum of PS₅₀SiCN₉₀₀-800°C and PS₅₀SiCN₉₀₀-1000°C, (F) O1s high resolution spectrum of PS₅₀SiCN₉₀₀-800°C and PS₅₀SiCN₉₀₀-1000°C.

The SiCN material PS₅₀SiCN exhibits a characteristic nitrogen sorption isotherm typical for a purely mesoporous material (Fig. 2A).²⁸ The nitrogen gas sorption isotherms of the material after chlorine gas treatment were a combination of the IUPAC Type I and Type IV isotherm with a pronounced Type H2 hysteresis in reflectance of the mixed micro- and mesoporous pore structure (Fig. 2B). Compared to the mesoporous SiCN material (107 m²g⁻¹), the BET surface area strongly increases as a result of chlorine etching at 800 °C to 1745 m²g⁻¹ and at 1000 °C to 1817 m²g⁻¹ (Table 1). PS₅₀SiCN₉₀₀Cl₂-800°C is dominated by mesopores, 71% of the pore volume (Table 1). In contrast, PS₅₀SiCN₉₀₀Cl₂-1000°C shows approximately a one-to-one distribution of micro- and mesopores at a lower total pore volume (1.19 cm³g⁻¹ instead of 1.67 cm³g⁻¹). The smaller pore volume may result from an enhanced carbon sintering and pore coalescing at 1000 °C.²⁹ The hierarchical pore size distributions observed for both N-doped carbon materials facilitates access of ionic liquid ions to the pores (Table 1). The diameter of

the largest mesopores is significantly smaller than 50 nm (diameter of the used PS templates) due to incomplete cracking of the PS template during pyrolysis (Fig. 2B).

The materials after chlorine gas treatment showed Raman spectra with pronounced D- and G-peaks around 1350 cm^{-1} and 1590 cm^{-1} , respectively, as typical for incompletely graphited carbons (Fig. 2C).³⁰ With increased chlorination temperature, the degree of carbon ordering increases indicated by the small decrease of the integral I_D/I_G signal ratio from 2.3 to 2.1.

The insertion of nitrogen into the carbon network was confirmed by X-ray photoelectron emission spectroscopy (XPS) (Fig. 2D–F and Table 1) and elemental analysis (EA) (Table 1). The chlorination temperature had a strong effect on N-doping. The decrease of the temperature during the chlorination process caused a lower nitrogen removal and a higher amount of nitrogen in the final carbon material (Table 1).¹⁵

Table 1. Pore characteristics derived from nitrogen gas sorption at liquid nitrogen temperature and nitrogen content calculated from ^aelemental analysis (EA) and ^bX-ray photoelectron spectra (XPS) for the samples after chlorine gas treatment.

	PS ₅₀ SiCN ₉₀₀	PS ₅₀ SiCN ₉₀₀ Cl ₂ -800°C	PS ₅₀ SiCN ₉₀₀ Cl ₂ -1000°C
BET SSA (m ² /g)	106	1745	1817
DFT SSA (m ² /g)	117	1536	1516
V _{total} (cm ³ /g)	0.27	1.67	1.19
V _{micropores} (cm ³ /g)	0	0.47	0.59
V _{mesopores} (cm ³ /g)	0.27	1.19	0.60
Pore size average (nm)	4.4	3.3	2.0
N (mass%) ^a	Not measured	5.5	1.6
N (mass%) ^b	Not measured	4.6	1.1

5.2.3 Electrochemical measurements

Next, we investigated the electrochemical behavior of the N-doped carbon materials. As seen from the cyclic voltammograms (CV) of PS₅₀SiCN₉₀₀Cl₂-800°C (Fig. 3A) and PS₅₀SiCN₉₀₀Cl₂-1000°C (Fig. 3B), stable electrochemical performance is obtained in the studied voltage window (up to -1 V vs. carbon, equivalent to 2 V cell voltage).³¹ As shown for galvanostatic charge/discharge data (ESI, Fig. S4A and S4B†), a maximum specific capacitance of 151 F g^{-1} at -1 V vs. carbon is seen for PS₅₀SiCN₉₀₀Cl₂-800°C in combination with 1-ethyl-3-methylimidazolium tetrafluoroborate (EMIM-BF₄), reflecting the behavior of the CV curves. In contrast, 1 M tetraethylammonium tetrafluoroborate (TEA-BF₄) in acetonitrile (ACN) results in 121 F g^{-1} and 122 F g^{-1} for neat 1-ethyl-3-methylimidazolium bis(trifluoromethyl-sulfonyl)imide (EMIM-TFSI). The same behavior is seen for PS₅₀SiCN₉₀₀Cl₂-1000°C, with a maximum

capacitance of 149 F g⁻¹ for EMIM-BF₄ and only 126 F g⁻¹ for 1 M TEA-BF₄ in either propylene carbonate (PC) or ACN. The only difference between the latter two solvents, as seen from the CV in Fig. 3B, is the lower ion mobility during charging and discharging for PC. Neat 1-butyl-3-methylimidazolium tetrafluoroborate (BMIM-BF₄) also yields a lower capacitance, namely 134 F g⁻¹. The capacitance values of different N-doped carbon electrodes with aqueous and nonaqueous electrolytes found in the literature are compared in Table 2.

Table 2. Comparison of the capacitance values of different N-doped carbon supercapacitor electrodes with aqueous and non-aqueous electrolytes in literature.

Publication	Electrolyte	Capacitance (F/g)
[5]	1 M H ₂ SO ₄	95-201
[5]	1 M TEA-BF ₄ / ACN	52-114
[17]	1 M H ₂ SO ₄	up to 264
[32]	1 M H ₂ SO ₄	95-182
[33]	1 M H ₂ SO ₄	205
[34]	1 M LiPF ₆ in EC/DMC	159
[35]	6 M KOH	202
[36]	6 M KOH	up to 420

To find a possible explanation for the difference in capacitance, the ohmic resistance of the N-doped carbon materials was measured in the charged state of the electrodes.^{37,38} This way, it was possible to address the change in electronic properties uninfluenced by the electrolyte. As seen in Fig. 3C, an expected behavior is recorded for the standard electrolyte based on ACN, namely a characteristic bell-shaped curve with a decrease in normalized resistance at increased potential. As shown in Fig. 3B and C the PC-based electrolyte shows comparable capacitance values compared to the ACN based electrolyte, indicating that the resistance behavior is also very similar (cf. ref. 38). For the EMIM-BF₄ system, no decrease in normalized resistance is measured (Fig. 3C), indicating interactions of the electrolyte with the electrode material, considering that only the electrolyte was changed. This is additionally confirmed by measuring the in situ resistivity of EMIM-BF₄ in a standard activated carbon (YP80F from Kuraray, Fig. S4C†). Here, the typical voltage-dependency of the normalized resistance is seen again for EMIM-BF₄. Thus, the unique behavior of a virtually constant profile of the electrical conductivity is only achieved by a suitable match between the electrode material (i.e., N-doped carbon) and the electrolyte. Additionally, the pore hierarchy supports the ion transport. In principle, larger pores (like mesopores) facilitate ion mobility in micrometer-sized particles, while, at the same time, a large amount of mesopores is essential to enable a high specific capacitance (i.e., high ion storage

ability).³⁹ Noticeably, the CV shape does not indicate the occurrence of any further processes, such as ion depletion or surface saturation.^{1b} This is further supported when comparing the cyclic voltammograms of SiC-CDC-800°C and PS₅₀SiCN₉₀₀Cl₂-800°C (Fig. S4D†). The performance of the non N-doped material is clearly inferior to that of PS₅₀SiCN₉₀₀Cl₂-800°C in terms of capacitance and rate capability.

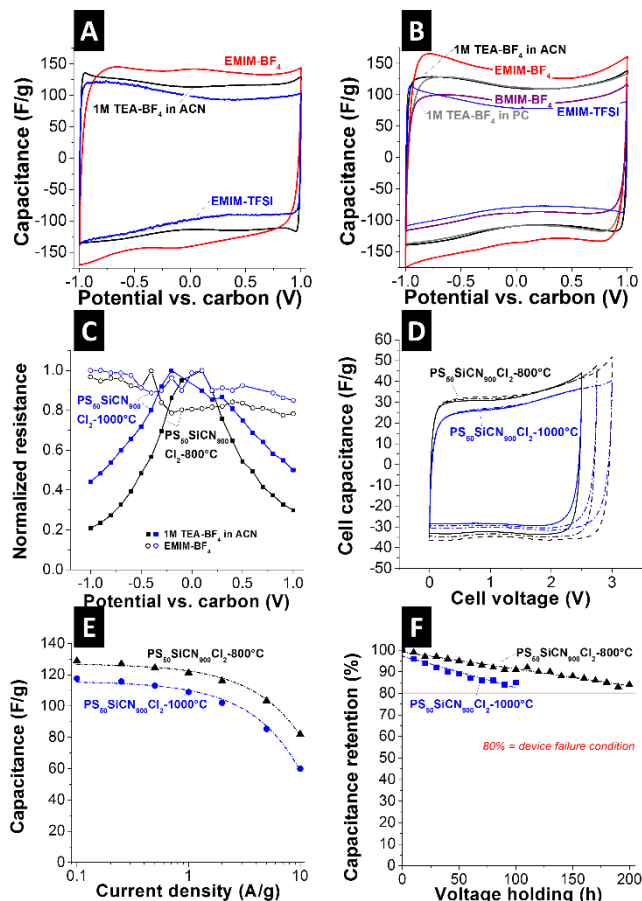


Figure 3. Cyclic voltammograms of PS₅₀SiCN₉₀₀Cl₂-800 (A) and PS₅₀SiCN₉₀₀Cl₂-1000°C (B) in the range of ± 1 V vs. carbon. Scan rate: 10 mV/s (C) In situ resistivity measurements for PS₅₀SiCN₉₀₀Cl₂-800°C and PS₅₀SiCN₉₀₀Cl₂-1000°C with 1 M TEA-BF₄ and EMIM-BF₄ as electrolyte. (D) Full cell cyclic voltammograms of PS₅₀SiCN₉₀₀Cl₂-800°C and PS₅₀SiCN₉₀₀Cl₂-1000°C with EMIM-BF₄ as electrolyte, scan rate: 10 mV/s. (E) Rate handling behavior of PS₅₀SiCN₉₀₀Cl₂-800°C and PS₅₀SiCN₉₀₀Cl₂-1000°C. (F) Long term stability test at 3 V cell voltage of PS₅₀SiCN₉₀₀Cl₂-800°C and PS₅₀SiCN₉₀₀Cl₂-1000°C in EMIM-BF₄.

To check whether the performance of a single electrode as presented before can be translated to a full cell, symmetric full cells were constructed (Fig. 3D). First, the potential window was opened successively up to 3 V cell voltage with a scan rate of 10 mVs⁻¹. The cell capacitance of PS₅₀SiCN₉₀₀Cl₂-800°C (ca. 34 Fg⁻¹) is higher than that of PS₅₀SiCN₉₀₀Cl₂-1000°C (ca. 30 Fg⁻¹). Note that the values for the cell capacitance can be transformed to the specific

capacitance (for one electrode) by multiplying by a factor of 4. The data from cyclic voltammetry agree well with galvanostatic charge/discharge measurements. At a low current density of 0.1 Ag^{-1} , the specific capacitance of $\text{PS}_{50}\text{SiCN}_{900}\text{Cl}_2\text{-}800^\circ\text{C}$ (129 Fg^{-1}) is higher than that of $\text{PS}_{50}\text{SiCN}_{900}\text{Cl}_2\text{-}1000^\circ\text{C}$ (118 Fg^{-1}). Up to 2 Ag^{-1} , both materials display a high rate capability before the capacitance fades at higher current densities.

Finally, the long-term stability at 3 V cell voltage was tested by voltage floating.⁴⁰ Both cells are characterized by a decay in capacitance over time (Fig. 3F); however, $\text{PS}_{50}\text{SiCN}_{900}\text{Cl}_2\text{-}800^\circ\text{C}$ lasted approximately twice as long as $\text{PS}_{50}\text{SiCN}_{900}\text{Cl}_2\text{-}1000^\circ\text{C}$ at an elevated voltage of 3 V. A drop of 20% in capacitance, the common device failure definition in industry,⁴ was not seen within 200 h for $\text{PS}_{50}\text{SiCN}_{900}\text{Cl}_2\text{-}1000^\circ\text{C}$ in EMIM-BF₄. The cycling stability up to 3 V cell voltage (ESI, Fig. S5†) indicates that after a drop in capacitance at the beginning the cell approaches a stable performance after 1000 cycles.

5.3 Conclusion

In summary, we synthesized a hierarchically porous N-doped carbon material with different distributions of meso- and micropores as well as varied N-doping. Both N-doped materials show significant capacitance enhancement for the ionic liquid EMIM-BF₄ in comparison to 1 M TEA-BF₄ in ACN or EMIM-TFSI. In addition, N-doped carbon in combination with EMIM-BF₄ shows a nearly constant normalized resistance from -1 V to +1 V. Distinct differences were observed for both electrode materials in symmetric full cells. The nitrogen-rich carbon material shows a higher cell capacitance and twice as high long-term stability at 3 V cell voltage.

For the moment, the mechanisms causing the enhanced specific capacitance for the matched ionic liquid EMIM-BF₄ compared to other electrolytes (such as EMIM-TFSI or when using organic solvents) remain unclear. Yet, the electrochemical data show that processes like ion sieving or ion saturation cannot cause the phenomenon. Instead, electrical conductivity shows an anomalous enhancement in electrical conductivity of the N-doped carbon electrode material only when using EMIMBF₄. Noticeably, this is not seen for conventional porous carbon (i.e., without N-doping). The unique solid-state response of N-doped carbon to a specific ionic liquid is an intriguing effect to be unraveled in future work.

5.4 Experimental Section

Materials

Synthesis was performed in a dry argon atmosphere using standard Schlenk techniques. Halogenated solvents were dried over P_2O_5 and non-halogenated solvents over sodium benzophenone ketyl. All chemicals were purchased from commercial sources with a purity over 95% and used without further purification unless described detailed below.

Synthesis of the PS₅₀ template

The cross-linked polystyrene particles with an average diameter of 50 nm were synthesized by emulsion polymerization. Therefore, a three neck round bottom flask with a KPG stirrer and a reflux condenser was used. Divinylbenzene (DVB, technical grade, 55 %, Sigma Aldrich) and styrene (> 99 % purity, Sigma Aldrich) were purified by destabilization (alumina B column, ICN Biomedicals GmbH). A dispersion of 4.10 g styrene (39.39 mmol) and 0.40 g DVB (3.07 mmol) was stirred in 90 mL ultrapure water. The dispersion was degassed for 30 min. After that, a solution of 0.25 g (1-hexadecyl)trimethylammonium-bromide (0.69 mmol) (CTAB, 98 % purity, abcr GmbH) in 5 mL ultrapure water was added under stirring (200 rpm) at 80 °C. After 0.5 h, 0.01 g 2,2-azobis(2-methylpropion-amidine)dihydrochloride (0.04 mmol) (97 % purity, Sigma Aldrich) was added initiating the polymerization. Polystyrene particles were dialyzed for purification and freeze dried.

Synthesis of PS₅₀SiCN₉₀₀ material

For several hours the polystyrene template PS₅₀ was evacuated removing residual water. After that, a solution of 0.50 g of KiON HTT1800 (7.77 mmol) (Clariant Advanced Materials GmbH) and 0.05 g dicumylperoxide (1.85 mmol) (97 % purity, Sigma Aldrich) in 40 mL toluene was added under stirring. The dispersion was heated to 110 °C for 24 h without stirring. After removal of the solvent the in situ structured green body was treated at 110 °C for 24 h finalizing the cross-linking. The PS₅₀SiCN₉₀₀ green body was pyrolyzed under a nitrogen atmosphere according to the following procedure: to 300 °C at 1 °Cmin⁻¹ (held for 3 h), to 400 °C at 1 °Cmin⁻¹ (held for 3 h), to 500 °C at 0.5 °Cmin⁻¹ (held for 3 h), to 600 °C at 1 °Cmin⁻¹ (held for 4 h), to 700 °C at 0.5 °Cmin⁻¹ (no holding time), and finally to 900 °C at 1 °Cmin⁻¹ (held for 0.5 h). A Gero furnace was used for this task.

Synthesis of N-doped carbon

For the chlorine treatment around 3 g of $\text{PS}_{50}\text{SiCN}_{900}$ powder was put into a graphite crucible and placed in a quartz tube furnace (Gero F-A 40-200). The tube was flushed with a constant argon flow of 20 sccm for at least 8 h. During heating, chlorine and hydrogen treatment, the argon background flow was set to 100 sccm. The heating rate was $15\text{ }^{\circ}\text{Cmin}^{-1}$ and the oven was held for 6 h at each chlorination temperature ($600\text{ }^{\circ}\text{C}$, $800\text{ }^{\circ}\text{C}$, and $1000\text{ }^{\circ}\text{C}$). During the dwell time, the chlorine gas flow was set to 10 sccm. After cooling to $600\text{ }^{\circ}\text{C}$ with $15\text{ }^{\circ}\text{Cmin}^{-1}$, the chlorine gas flow was stopped and 10 sccm hydrogen gas was applied for 3 h to remove residual chlorine. At the end, the furnace was cooled down to room temperature with a constant argon flow of 20 sccm. The same procedure was followed for the synthesis of SiC-CDC- 800°C (Precursor: Nano SiC, Plasmachem; average particle size ca. 20–30 nm).

Materials characterization

Elemental analyses were carried out on a Vario elemental EL III. Thermal gravimetric analysis (TGA) was carried out under a nitrogen atmosphere using a Thermowaage L81 (Linseis, Germany). With a heating rate of $5\text{ }^{\circ}\text{C min}^{-1}$ the sample was heated to $900\text{ }^{\circ}\text{C}$. Photon correlation spectroscopy (PCS) was performed using an ALV DLS/SLA-SP 5022F laser goniometer system. The power source was a Ne/Ar ion laser ($1\frac{1}{4}\text{ }632.8\text{ nm}$ at 260 mW). By using an ALV-5000/E multiple tau digital correlator the correlation function was generated. The decalin bath temperature was $20\text{ }^{\circ}\text{C}$, regulated by using a computer-operated thermostat. 90° fixed angle measurements were carried out. Data were analyzed by the CONTIN analysis. On a Zeiss field emission SEM LEO 1530 GEMINI scanning electron microscopy (SEM) was performed. The acceleration voltage was up to 5 kV and the materials were sputter-coated with a 1.3 nm platinum layer. Fourier transform infrared (FTIR) measurements were carried out using a Perkin-Elmer FTIR Spectrum 100 (from 4400 to 650 cm^{-1}). Raman spectra of the raw materials were recorded with a Renishaw inVia Raman system using an Nd-YAG laser (532 nm) with 0.2 mW power at the sample surface. The peak analysis and peak fitting were performed assuming one Lorentzian peak for both the D-mode and G-mode. Nitrogen gas sorption measurements ($-196\text{ }^{\circ}\text{C}$) of the electrodes (i.e., carbon + binder) were performed with an Autosorb iQ system (Quantachrome, USA). The materials were outgassed at $150\text{ }^{\circ}\text{C}$ for 10 h in a vacuum. The specific surface area was calculated using the ASiQwin-software using the Brunauer–Emmett–Teller (BET) equation in the linear relative pressure range of 0.01–0.2. The SSA and pore size distribution (PSD) were also calculated via quenched-solid density functional theory (QSDFT) with a hybrid model for

slit and cylindrical pores and pore size between 0.56 and 37.5 nm. Samples for transmission electron microscopy (TEM) were dispersed and sonicated in chloroform and placed on a copper grid (CF200-Cu-grid, Electron Microscopy Sciences, Hatfield, PA, USA). The TEM images were taken with a Varian LEO 9220 (120 kV, Carl Zeiss) and a JEOL 2100F system at 200 kV. X-ray photoelectron spectroscopy (XPS) measurements were performed using a VG ESCALAB 220iXL spectrometer (Thermo Fisher Scientific) equipped with an Al-Ka mono-source (power: 150 W; spot diameter: 500 mm) and a magnetic lens system. The spectra were recorded in constant analyzer energy mode at a pass energy of 20 eV. The XPS was calibrated using the Ag 3d_{5/2}, the Cu 2p_{3/2}, and the Au 4f_{7/2} lines as reference signals. The full-width half maximum (FWHM) of the Ag 3d_{5/2} line was measured to be 0.62 eV at a pass energy of 20 eV. The data were evaluated using the Advantage software provided by Thermo Fisher Scientific. The background subtraction was performed according to Shirley⁴¹ and atomic sensitivity factors were used according to Scofield.⁴²

Electrode preparation

Electrodes were prepared using sample powder dispersed in ethanol. After homogenization in a mortar, 5–10 mass% of dissolved polytetrafluoroethylene (PTFE, 60 mass% solution in water from Sigma Aldrich) were added as binders. While kneading, the slurry became more viscous and the resulting material was rolled with a rolling machine (MTI HR01, MIT Corp.) to a 200 ± 20 mm thick free standing electrode and dried at 120 °C at 2 kPa for 24 h. We employed a custom-built polyether ether ketone (PEEK) cell with spring loaded titanium pistons as a three electrode system described elsewhere.⁴⁰ The cells employed electrodes with 12 mm diameter, a glass-fiber separator (GF/A (for full cells) or GF/D (for half cells)) from (Whatman, USA), and carbon-coated aluminum foil current collectors (type Zflo 2653, Coveris Advanced Coatings). PTFEbound YP-50F was used as the reference electrode.⁴³ The assembled cells were dried at 120 °C for 12 h at 2 kPa in an inert gas glovebox (MBraun Labmaster 130, O₂ and H₂O < 1 ppm) and, after cooling to room temperature, vacuum-filled with 1 M tetraethylammonium tetrafluoroborate (TEA-BF₄) of electrochemical grade (i.e., water content < 20 ppm), acetonitrile (ACN) or propylene carbonate (PC) purchased from BASF. The used ionic liquids 1-ethyl-3-methylimidazolium bis(trifluoromethylsulfonyl)imide (EMIM-TFSI; > 99 %, Sigma Aldrich) and 1-ethyl-3-methylimidazolium tetrafluoroborate (EMIM-BF₄; > 99 %, IoLiTec Ionic Liquids Technologies) were degassed using a Schlenk tube in a Si-oil

bath heated to 100 °C and a vacuum of 1 Pa was applied for at least 6 h to remove residual gas and water.

Electrochemical testing: the electrochemical measurements were carried out using a potentiostat/galvanostat VSP300 from Bio-Logic, with cyclic voltammetry (CV), galvanostatic cycling with potential limitation (GCPL), and electrical impedance spectroscopy (EIS). CVs were recorded in half cell mode at 1, 10, 100 and 1000 mV s⁻¹ in the potential range of 0 to 1 V vs. carbon with activated carbon (YP50, Kuraray chemicals) as the reference electrode.^{43,44} GCPL in half cell mode was performed to access the maximum available capacitance values from discharge in the range of ± 1 V. The cell was charged for 10 min up to the desired potential and then discharged to 0 V. The capacitance was determined in 100 mV steps. Full cells were prepared for further testing in CV and GCPL mode. The CVs were recorded up to 3 V with 10 mV s⁻¹. In GCPL mode, the current density was increased in several steps from 0.1 Ag⁻¹ to 10Ag⁻¹ with 10 s resting period between charging/discharging to access information on the IR-drop. The voltage holding experiments were performed at 3 V cell voltage with 10 h holding periods followed by 3 galvanostatic charge/discharge cycles to determine the capacitance. This was repeated for at least 10 times. The galvanostatic cycling experiments (see ESI, Fig. S5†) were performed at 1 Ag⁻¹.⁴⁰ The in situ resistance measurements were conducted with a system described in ref. 37. The working electrode was galvanostatically charged to the favored potential and after cell charging, the working electrode cable was removed and a multimeter was used for measuring the resistance between the other two gold contacts (accuracy: ± 1.5 %). This two-contact-point electrical conductivity probe for in situ measurements at various states of electrode charge was shown to yield data consistent with a four-point probe setup by Kastening et al. shown in ref. 45.

5.5 Acknowledgements

DW, MZ, NJ, and VP thank Prof. Eduard Arzt (INM) for his continuing support and acknowledge funding from the German Federal Ministry for Research and Education (BMBF) in support of the nanoEES3D project (award number 03EK3013) as part of the strategic funding initiative energy storage framework. RK thanks the SFB 840 for financial support and JKE the Elitenetzwerk Bayern e. V. for a grant. We thank Annett Rabis (Paul Scherrer Institute, Switzerland) for performing the XPS measurements.

5.6 Notes and References

- 1 (a) P. Simon and Y. Gogotsi, *Nat. Mater.*, 2008, **7**, 845; (b) J. Segalini, E. Iwama, P.-L. Taberna, Y. Gogotsi and P. Simon, *Electrochem. Commun.*, 2012, **1**, 63.
- 2 F. Beguin, V. Presser, A. Balducci and E. Frackowiak, *Adv. Mater.*, 2014, **26**, 2219.
- 3 (a) H. Gerischer, R. McIntyre, D. Scherson and W. Storck, *J. Phys. Chem.*, 1987, **91**, 1930; (b) A. A. Kornyshev, N. B. Luque and W. Schmickler, *J. Solid State Electrochem.*, 2014, **18**, 1345.
- 4 F. Beguin and E. Frackowiak, *Supercapacitors*, Wiley, Weinheim, 2013.
- 5 G. Lota, B. Grzyb, H. Machnikowska, J. Machnikowski and E. Frackowiak, *Chem. Phys. Lett.*, 2005, **404**, 53.
- 6 L. G. Bulusheva, E. O. Fedorovskaya, A. G. Kurennya and A. V. Okotrub, *Phys. Status Solidi B*, 2013, **250**, 2586.
- 7 J. D. Wiggins-Camacho and K. J. Stevenson, *J. Phys. Chem. C*, 2009, **113**, 19082.
- 8 J. Tang, J. Liu, C. Li, Y. Li, M. O. Tade, S. Dai and Y. Yamauchi, *Angew. Chem., Int. Ed.*, 2015, **54**, 588.
- 9 R. J. White, M. Antonietti and M.-M. Titirici, *J. Mater. Chem.*, 2009, **19**, 8645.
- 10 (a) J. Tang, R. Salunkhe, J. Liu, N. L. Torad, M. Imura, S. Furukawa and Y. Yamauchi, *J. Am. Chem. Soc.*, 2015, **137**, 1572; (b) R. R. Salunkhe, J. Tang, Y. Kamachi, T. Nakato, J. H. Kim and Y. Yamauchi, *ACS Nano*, 2015, **9**, 6288; (c) N. L. Torad, R. R. Salunkhe, Y. Li, H. Hamoudi, M. Imura, Y. Sakka, C.-C. Hu and Y. Yamauchi, *Chem.–Eur. J.*, 2014, **20**, 7895.
- 11 X. Fan, C. Yu, J. Yang, Z. Ling and J. Qiu, *Carbon*, 2014, **70**, 130.
- 12 J. Zhou, Z. Zhang, W. Xing, J. Yu, G. Han, W. Si and S. Zhuo, *Electrochim. Acta*, 2015, **153**, 68.
- 13 M. Wahid, G. Parte, D. Phase and S. Ogale, *J. Mater. Chem. A*, 2015, **3**, 1208.
- 14 (a) S. Zhang, K. Dokko and M. Watanabe, *Chem. Mater.*, 2014, **26**, 2915–2926; (b) N. Fechler, T.-P. Fellingner and M. Antonietti, *Adv. Mater.*, 2013, **25**, 75.
- 15 S. Zhang, S. Tsuzuki, K. Ueno, K. Dokko and M. Watanabe, *Angew. Chem., Int. Ed.*, 2015, **54**, 1302.
- 16 Y. Hu, H. Liu, Q. Ke and J. Wang, *J. Mater. Chem. A*, 2014, **2**, 11753.
- 17 (a) D.-Y. Kang and J. H. Moon, *Sci. Rep.*, 2014, **4**, 5392; (b) D.-D. Zhou, W.-Y. Li, X.-L. Dong, Y.-G. Wang, C.-X. Wang and Y.-Y. Xia, *J. Mater. Chem. A*, 2013, **1**, 8488.

- 18 P. Tamilarasan and S. Ramaprabhu, *J. Nanosci. Nanotechnol.*, 2015, **15**, 1154.
- 19 D. Weingarth, I. Czekaj, Z. Fei, A. Foelske-Schmitz, P. J. Dyson, A. Wokaun and R. Kötz, *J. Electrochem. Soc.*, 2012, **159**, 611.
- 20 W.-Y. Tsai, R. Lin, S. Murali, L. Li Zhang, J. K. McDonough, R. S. Ruoff, P.-L. Taberna, Y. Gogotsi and P. Simon, *Nano Energy*, 2013, **2**, 403.
- 21 A. Brandt, S. Pohlmann, A. Varzi, A. Balducci and S. Passerini, *MRS Bull.*, 2013, **38**, 554.
- 22 K. L. Van Aken, M. Beidaghi and Y. Gogotsi, *J. Mater. Chem. A*, 2015, **54**, 4806.
- 23 M. Zaheer, C. D. Keenan, J. Hermannsdörfer, E. Roessler, G. Motz, J. Senker and R. Kempe, *Chem. Mater.*, 2012, **24**, 3952–3963.
- 24 (a) M. Kamperman, A. Burns, R. Weissgraeber, N. van Vegten, S. C. Warren, S. M. Gruner, A. Baiker and U. Wiesner, *Nano Lett.*, 2009, **9**, 2756; (b) B. H. Jones and T. P. Lodge, *J. Am. Chem. Soc.*, 2009, **131**, 1676; (c) S. K. Pillai, W. P. Kretschmer, C. Denner, G. Motz, M. Hund, A. Fery, M. Trebbin, S. Förster and R. Kempe, *Small*, 2013, **9**, 984; (d) J.-K. Ewert, C. Denner, M. Friedrich, G. Motz and R. Kempe, *Nanomaterials*, 2015, **5**, 425.
- 25 (a) M. Rose, Y. Korenblit, E. Kockrick, L. Borchardt, M. Oschatz, S. Kaskel and G. Yushin, *Small*, 2011, **7**, 1108; (b) V. Presser, M. Heon and Y. Gogotsi, *Adv. Funct. Mater.*, 2011, **21**, 810.
- 26 S.-H. Yeon, P. Reddington, Y. Gogotsi, J. E. Fischer, C. Vakifahmetoglu and P. Colombo, *Carbon*, 2010, **48**, 201.
- 27 Y. Gogotsi, A. Nikitin, H. Ye, W. Zhou, J. E. Fischer, B. Yi, H. C. Foley and M. W. Barsoum, *Nat. Mater.*, 2003, **2**, 591.
- 28 K. S. W. Sing, D. H. Everett, R. A. V. Haul, L. Moscou, R. A. Pierotti, J. Rouquerol and T. Siemieniewska, *Pure Appl. Chem.*, 1985, **57**, 603.
- 29 R. Dash, J. Chmiola, G. Yushin, Y. Gogotsi, G. Laudisio, J. Singer, J. Fischer and S. Kucheyev, *Carbon*, 2006, **44**, 2489.
- 30 A. C. Ferrari and J. Robertson, *Phys. Rev. B: Condens. Matter Mater. Phys.*, 2000, **61**, 14095.
- 31 S. Zhang and N. Pan, *Adv. Energy Mater.*, 2015, **5**, 1401401.
- 32 N. D. Kim, W. Kim, J. B. Joo, S. Oh, P. Kim, Y. Kim and J. Yi, *J. Power Sources*, 2008, **180**, 671.
- 33 W. Kim, J. B. Joo, N. Kim, S. Oh, P. Kim and J. Yi, *Carbon*, 2009, **47**, 1407.

- 34 W. Li, D. Chen, Z. Li, Y. Shi, Y. Wan, G. Wang, Z. Jiang and D. Zhao, *Carbon*, 2007, **45**, 1757.
- 35 L. F. Chen, X. D. Zhang, H. W. Liang, M. Kong, Q. F. Guan, P. Chen, Z. Y. Wu and S. H. Yu, *ACS Nano*, 2012, **6**, 7092.
- 36 L. L. Zhang, X. Zhao, H. Ji, M. D. Stoller, L. Lai, S. Murali, S. McDonnell, B. Cleveger, R. M. Wallace and R. S. Ruoff, *Energy Environ. Sci.*, 2012, **5**, 9618–9625.
- 37 P. W. Ruch, R. Kötz and A. Wokaun, *Electrochim. Acta*, 2009, **54**, 4451.
- 38 D. Weingarth, M. Zeiger, N. Jackel, M. Aslan, G. Feng and V. Presser, *Adv. Energy Mater.*, 2014, **4**, 1400316.
- 39 (a) X. Wen, D. Zhang, L. Shi, T. Yan, H. Wang and J. Zhang, *J. Mater. Chem.*, 2012, **22**, 23835; (b) Z. Peng, D. Zhang, T. Yan, J. Zhang and L. Shi, *Appl. Surf. Sci.*, 2013, **282**, 965; (c) H. Jiang, P. S. Lee and C. Li, *Energy Environ. Sci.*, 2013, **6**, 41; (d) X. Wen, D. Zhang, T. Yan, J. Zhang and L. Shi, *J. Mater. Chem. A*, 2013, **1**, 12334; (e) H. Wang, L. Shi, T. Yan, J. Zhang, Q. Zhong and D. Zhang, *J. Mater. Chem. A*, 2014, **2**, 4739; (f) Q. Wang, J. Yan, Y. Wang, T. Wei, M. Zhang, X. Jing and Z. Fan, *Carbon*, 2014, **67**, 119.
- 40 D. Weingarth, A. Foelske-Schmitz and R. Kötz, *J. Power Sources*, 2013, **225**, 84.
- 41 D. A. Shirley, *Phys. Rev. B: Condens. Matter Mater. Phys.*, 1972, **5**, 4709.
- 42 J. H. Scofield, *J. Electron Spectrosc. Relat. Phenom.*, 1976, **8**, 129.
- 43 D. Weingarth, A. Foelske-Schmitz, A. Wokaun and R. Kötz, *Electrochem. Commun.*, 2012, **18**, 116.
- 44 P. W. Ruch, D. Cericola, M. Hahn, R. Kötz and A. Wokaun, *J. Electroanal. Chem.*, 2009, **636**, 128.
- 45 B. Kastening, M. Hahn and J. Kramerskötter, *J. Electroanal. Chem.*, 1994, **374**, 159.

5.7 Supporting Information

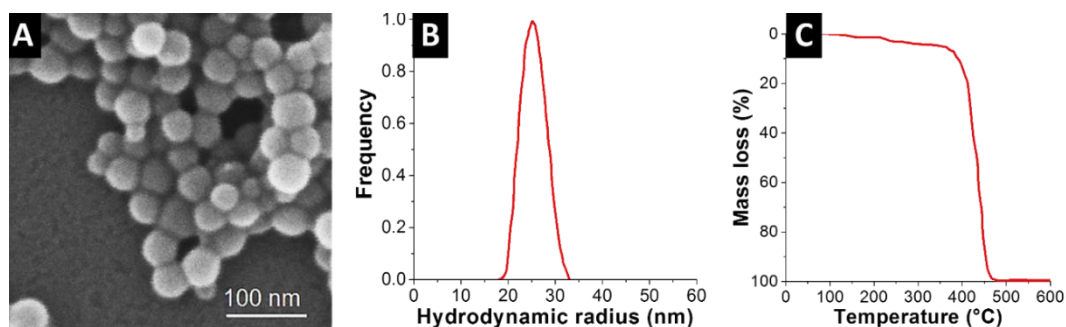


Figure S1. (A) Scanning electron micrograph of the polystyrene PS₅₀. (B) Photon correlation spectrum of PS₅₀ shows a narrow particle size distribution in the range of 19.7 nm and 31.3 nm with a peak at 24.8 nm. (C) Thermogravimetric analysis of PS₅₀ shows a mayor mass loss between 400 and 470 °C (using a heating rate of 0.5 °C/min, nitrogen atmosphere).

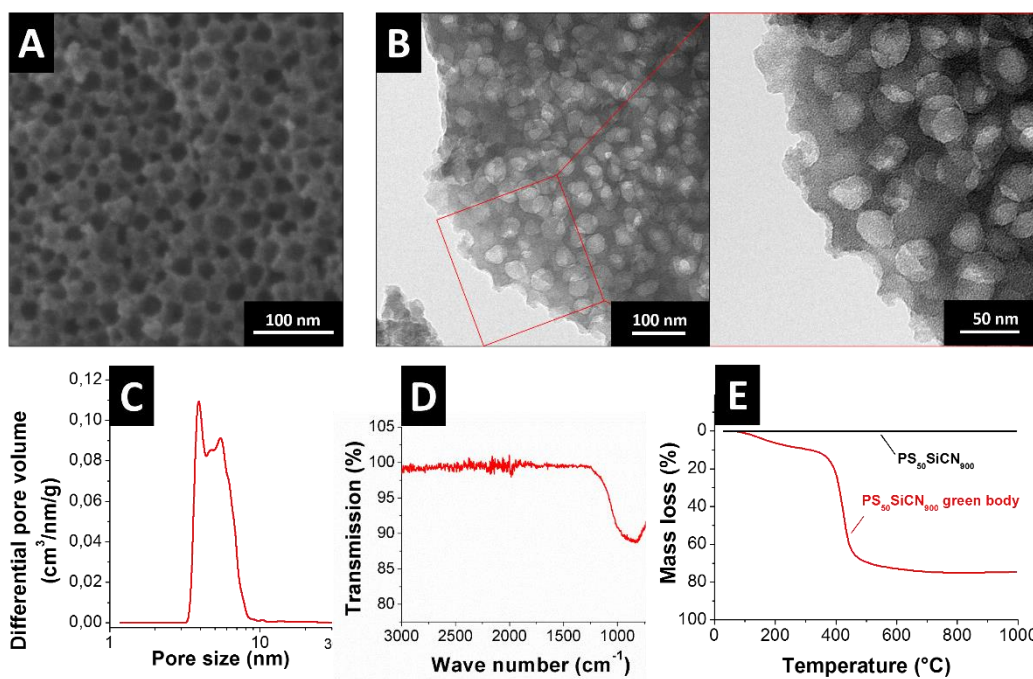


Figure S2. (A) SEM image and (B) TEM image of PS₅₀SiCN₉₀₀ verify the pore structure. (C) Pore size distribution of PS₅₀SiCN₉₀₀, measured by nitrogen gas sorption at -196 °C, shows presence of mesopores and a BET surface area of 130 m²/g. (D) FT-IR measurement of PS₅₀SiCN₉₀₀ exhibits the characteristic broad SiCN peak between 1250 cm⁻¹ and 750 cm⁻¹. (E) TGA measurements of the PS₅₀SiCN₉₀₀ green body and the PS₅₀SiCN₉₀₀ material.

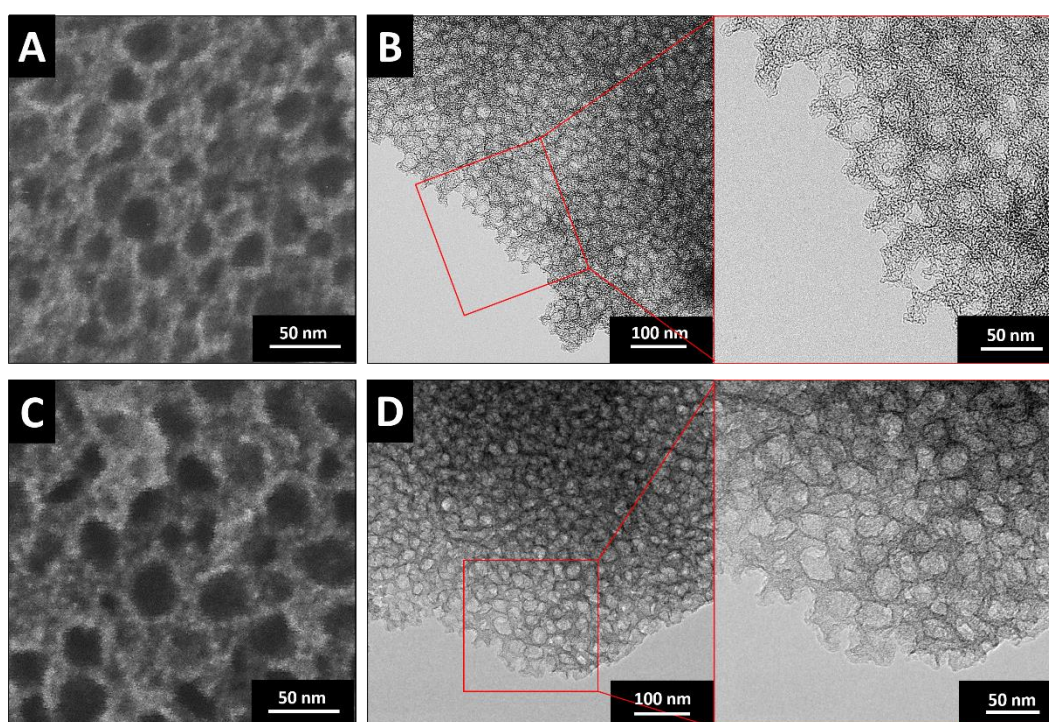


Figure S3. (A) SEM image and (B) TEM image of $\text{PS}_{50}\text{SiCN}_{900}\text{Cl}_2\text{-}800^\circ\text{C}$. (C) SEM image and (D) TEM image of $\text{PS}_{50}\text{SiCN}_{900}\text{Cl}_2\text{-}1000^\circ\text{C}$. Both materials show the honeycombed pore structure of the ceramic template.

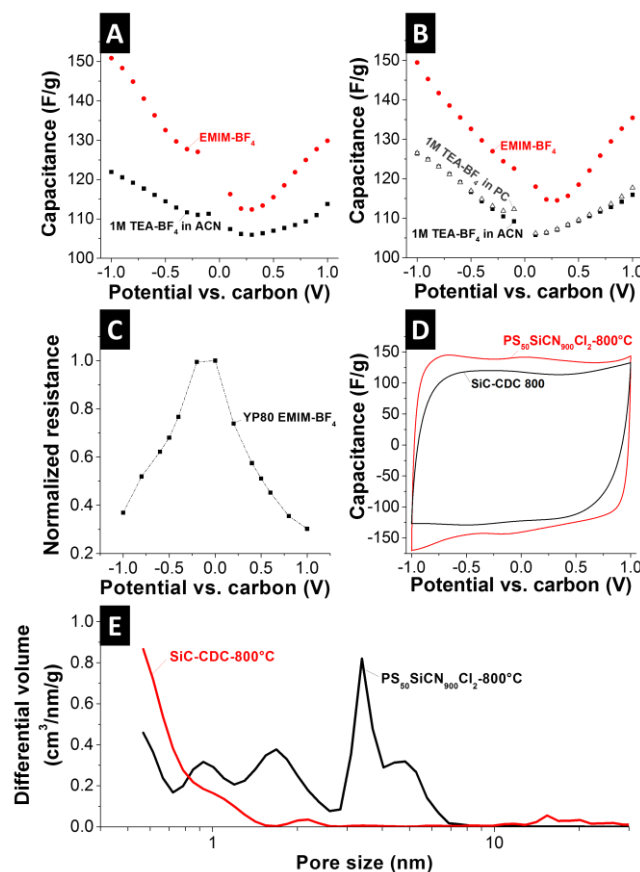


Figure S4. Comparison of the specific capacitance determined by GCPL for (A) $\text{PS}_{50}\text{SiCN}_{900}\text{Cl}_2\text{-}800^\circ\text{C}$ and (B) $\text{PS}_{50}\text{SiCN}_{900}\text{Cl}_2\text{-}1000^\circ\text{C}$. (C) In situ resistivity measurement of YP 80F with EMIM- BF_4 as electrolyte. (D) Cyclic voltammograms of SiC-CDC 800 and $\text{PS}_{50}\text{SiCN}_{900}\text{Cl}_2\text{-}800^\circ\text{C}$ in EMIM- BF_4 as electrolyte, scan rate: 10 mV/s. (E) Calculated pore size distribution of SiC-CDC 800°C and $\text{PS}_{50}\text{SiCN}_{900}\text{Cl}_2\text{-}800^\circ\text{C}$.

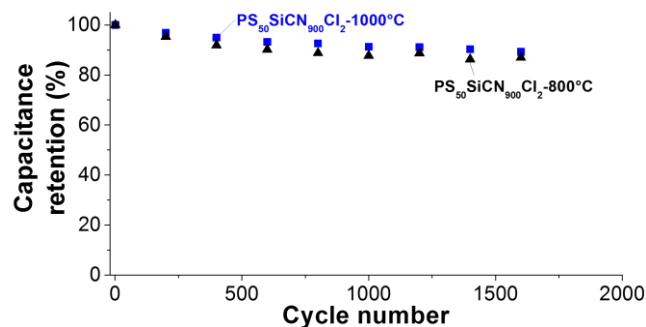


Figure S5. Cycling stability of $\text{PS}_{50}\text{SiCN}_{900}\text{Cl}_2\text{-}800^\circ\text{C}$ and $\text{PS}_{50}\text{SiCN}_{900}\text{Cl}_2\text{-}1000^\circ\text{C}$ in EMIM- BF_4 as electrolyte at 1 A/g.

6 A Hierarchical Structured Reusable Iridium Catalyst for the Sustainable Synthesis of Pyrroles, Pyridines, and Quinolines

Julia-Katharina Ewert,^[a] Martin Friedrich,^[a] Christine Denner,^[a] Rhett Kempe^[a]

[a] Institute of Inorganic Chemistry II, University Bayreuth, 95440 Bayreuth, Germany

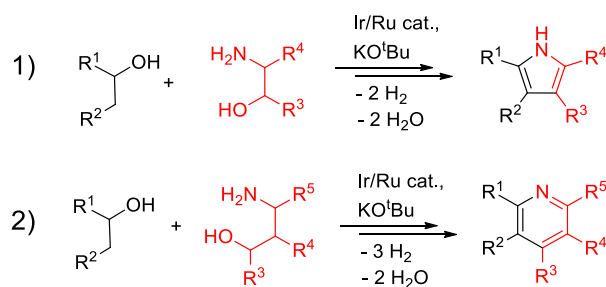
To be submitted.

Keywords: polyolefin structuring, polystyrene template, iridium, heterogeneous catalysis, sustainable chemistry

Abstract: The limitation of fossil fuels requires sustainable synthesis protocols for the generation of fine chemicals. In this context, the usage of platform chemicals processed from biomass is of great interest. Here, we present the sustainable synthesis of N-heterocycles mediated by a silicon carbonitride supported Ir catalyst. The catalyst material was obtained using a polystyrene based structuring approach recently developed by our group. We showed a broad substrate scope for lot pyrroles, pyridines, and quinolines as well as the tolerance of various functional groups. Our catalyst exhibits an excellent activity and good reusability compared to commercially available Ir catalysts.

6.1 Introduction

Environmental concerns and the limited exploitability of fossil carbon resources like crude oil call for the usability of alternative preferentially renewable resources and protocols to synthesize chemicals from them. Out of the available biomass, lignocellulose is especially attractive since it is abundantly available and indigestible.¹ Since lignocellulose can be processed to alcohols efficiently,² the development of alcohol re-functionalization reactions is a highly desired goal in modern chemistry or sustainable synthesis.³ Recently, the groups of Milstein,⁴ Seito⁵ and us^{3,6} developed a broadly applicable catalytic synthesis in which the combination of condensation and dehydrogenation allows the selective linkage of different alcohols to important classes of aromatic N-heterocyclic compounds like pyrroles and pyridines (**Scheme 1**). A similar approach was reported by Beller and coworkers.⁷



Scheme 1. Synthesis of pyrroles (1) as well as pyridines (2) starting from alcohols and amino alcohols under elimination of water and hydrogen.

Homogenous iridium and ruthenium catalysts have been mainly used for these reactions. The use of reusable easy-to-handle catalysts having similar activities and selectivity profiles as the homogenous catalysts that have been used so far seemed attractive to us.⁸

Here, we report on the synthesis of a hierarchically structured, silicon carbonitride (SiCN) supported iridium catalyst (Ir@PS₆₀SiCN) that mediates the efficient synthesis of pyrroles, pyridines, and quinolines from alcohols and amino alcohols (**Scheme 1**). The catalyst is significantly more active than commercially available Ir catalysts and shows a better reusability. SiCN-transition-metal nanocomposites (M@SiCN) have emerged as a promising class of catalysts recently.^{8,9} The SiCN matrix allows the stabilization of unusual small metal nanoparticles based on the coordinative saturation of the metal ions or clusters by the N atoms of the support during the catalyst synthesis.¹⁰ The SiCN support itself is highly attractive since it is thermally very robust and chemically inert.¹¹ A deficiency of the M@SiCN nanocomposite catalysts used so far is the low specific surface area of the SiCN support. Out of the existing protocols to mesostructured SiCN by polyolefines,^{9a,12} we used the polystyrene (PS) method recently introduced by our group.^{12h}

6.2 Results and Discussion

The hierarchical structured iridium catalyst was synthesized based on our PS synthesis route (Ir@PS₆₀SiCN, **Figure 1**).^{12h} An Ir-aminopyridinato-complex was used to introduce iridium in the porous SiCN support. Cross-linking of the commercial available polysilazane HTT-1800 takes place by iridium catalyzed hydrosilylation and dehydro-coupling.⁸ The generated pores were additionally stabilized using dicumylperoxide (DCP) as cross-linker.

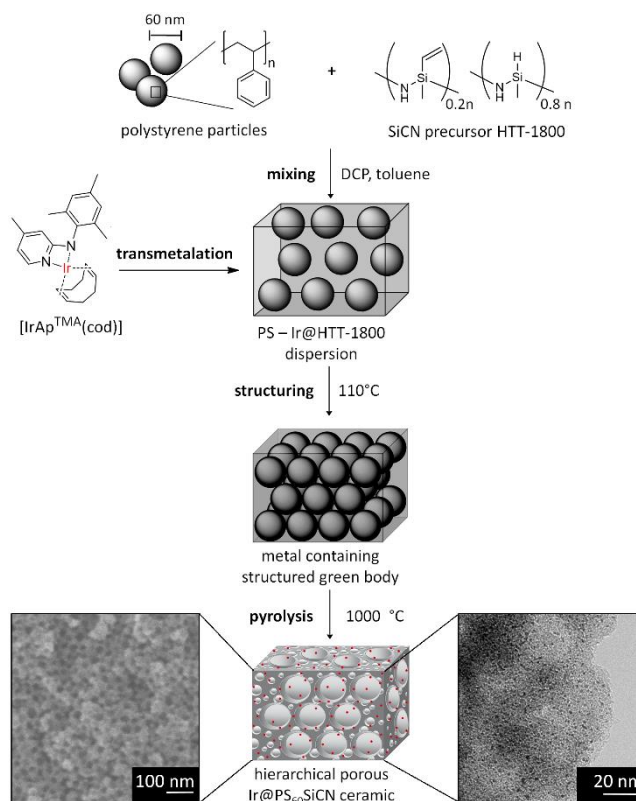


Figure 1. Synthesis route of the Ir@PS₆₀SiCN catalyst: 1) Mixing 60 nm polystyrene (PS₆₀) template, HTT-1800, and DCP in toluene. Addition of [IrAp^{TMA}(cod)] complex leading to transmetalation. 2) Structuring by cross-linking at 110 °C and removal of the solvent leading to a metal containing structured green body. 3) Pyrolysis with a tailored pyrolysis program at 1000 °C obtaining Ir@PS₆₀SiCN. SEM (see left side) and TEM (see right side) analysis verify the highly porous structure as well as the homogenous distribution of iridium nanoparticles.

We verified homogeneously distributed pores in the mesopore range (35 nm diameter) for the Ir@PS₆₀SiCN material by SEM measurements (**Figure 1** and **Figure 2A**). The iridium catalyst exhibits a specific surface area of 450 m²/g according to nitrogen sorption measurements (**Figure 2B**) after activation. Moreover, a pore size distribution in the micro and meso scale range was determined (**Figure 2C**). Characteristic iridium signals were observed by EDX measurements (**Figure 3A**). Powder XRD measurements (**Figure 3B**) indicate the presence of iridium nanoparticles with a particle diameter of about 1 nm. Moreover, the amorphous character of the SiCN material obtained from HTT-1800 was verified. Homogeneously distributed metal particles with a particle size distribution between 0.6 nm and 1.4 nm were shown by TEM measurements (**Figure 1** and **Figure 3C**). HR-TEM measurements indicate the presence of cubic crystalline iridium nanoparticles based on the characteristic distance of 221.4 pm between the adjacent lattice planes (**Figure 3C**). An iridium content of 12.0 wt% was determined by ICP-OES measurements.

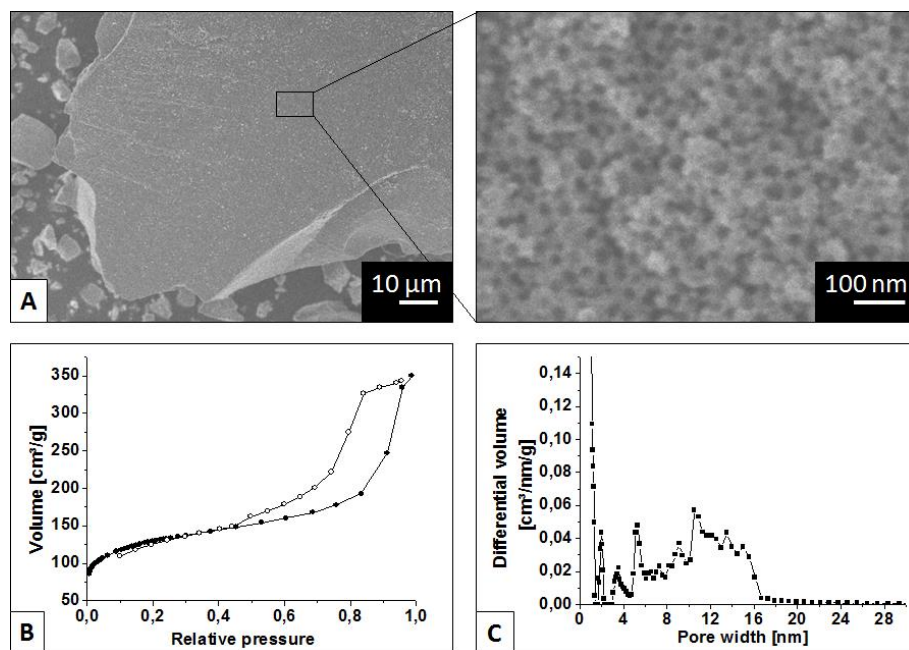


Figure 2. SEM measurement (A), nitrogen sorption measurements with isotherm (B), and the calculated pore size distribution (C) of the hierarchical porous Ir@PS₆₀SiCN material.

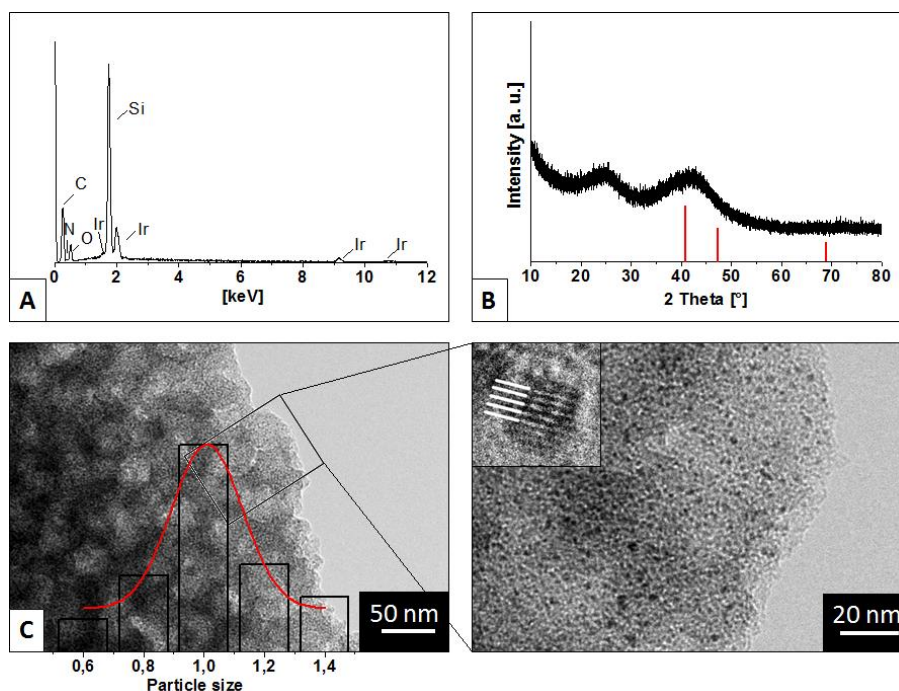


Figure 3. EDX measurement (A), powder XRD measurement (red: reflexes of cubic crystalline iridium, reference card 00-046-1044) (B), and TEM measurement with the particle size distribution of the iridium particles and HR-TEM measurement (C) of the hierarchical porous Ir@PS₆₀SiCN material.

Next, we applied the hierarchical porous Ir@PS₆₀SiCN material in the catalytic synthesis of aromatic N-heterocycles, namely pyrroles, pyridines, and quinolines. The reaction of 2-aminobutan-1-ol and 1-phenylethanol to **1a** (Table 1) was used as model reaction to find the

best reaction conditions. Optimized reaction conditions led to a conversion of 93 % of **1a** using 0.58 mol% iridium, two equivalents KO^tBu as base, and an alcohol/amino alcohol ratio of 2/1 at 125 °C according to Ref 8. With these suitable conditions in hand, we addressed the issue of substrate scope. The reaction of 1-phenylethanol with different 1,2-amino alcohols led to 2,5-disubstituted pyrroles (**Table 1**, **1a-c**) in excellent yields for two examples. Aliphatic substituents, branched alcohols, and aryl groups were introduced. Furthermore, we varied the secondary alcohol. 2,5-disubstituted pyrroles with 1-cyclohexyl-1-ethanol (**Table 1**, **1d**) as well as olefin functions (**Table 1**, **1e**) were applicable. The reaction of cyclic alcohols led to bicyclic (2,3,5-substituted) pyrroles (**Table 1**, **2**).

Table 1. Synthesized 2,5-substituted and 2,3,5-substituted pyrroles ^a

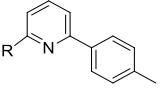
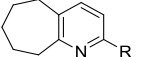
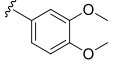
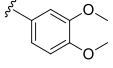
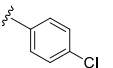
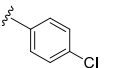
$ \begin{array}{c} \text{R}^1\text{-CH(OH)-CH}_3 + \text{H}_2\text{N-CH(R}^2\text{)-CH}_2\text{OH} \xrightarrow[\text{- 2 H}_2\text{O, - 2 H}_2]{\text{Ir@PS}_{80}\text{SiCN, 2 eq. KO}^t\text{Bu}} \text{R}^1\text{-CH(R}^2\text{)-CH=CH-NH-R}^2 \\ \text{1a - e} \end{array} $			
$ \begin{array}{c} \text{Cyclic Alcohol} + \text{H}_2\text{N-CH(R}^2\text{)-CH}_2\text{OH} \xrightarrow[\text{- 2 H}_2\text{O, - 2 H}_2]{\text{Ir@PS}_{80}\text{SiCN, 2 eq. KO}^t\text{Bu}} \text{Bicyclic Pyrrole} \\ \text{2} \end{array} $			
Entry	Product		Yield [%] ^{b, c}
1		1a R = Et	93
2		1b R = i-Bu	94 (90)
3		1c R = Bn	80
4 ^d		1d R = cyclohexyl	92
5 ^e		1e R =	93 (87)
6		2 R = i-Bu	> 99

^a Reaction conditions: 1,2-amino alcohol (1.5 mmol), secondary alcohol (6 mmol), KO^tBu (3 mmol), 0.58 mol% Ir, 1.5 mL diglyme, 24 h at 125 °C oil bath temperature. ^b Yields determined by GC (*n*-dodecane as internal standard).

^c Yields of isolated products are given in parentheses. ^d 130 °C. ^e 0.89 mol% Ir.

Next, the substance class of pyridines was addressed. We adopted the optimized reaction conditions of the pyrrole synthesis.^{6a} The conversion of secondary alcohols with 1,3-amino alcohols led to 2,6-substituted pyridines. An alkyl-substituted pyridine (**Table 2**, **3**) was synthesized in good yield. Moreover, the formation of bicyclic pyridines starting from cycloheptanol was accomplished. Aryl-, methoxy-, and chloro-groups were well tolerated with moderate to excellent yields (**Table 2**, **4a-c**).

Table 2. Synthesized 2,6-substituted and bicyclic pyridines ^a

$ \begin{array}{c} \text{R}^1\text{CH(OH)CH}_2\text{R}^2 + \text{HOCH}_2\text{CH(R}^3\text{)CH(R}^4\text{)NH}_2 \\ \xrightarrow[\text{- 2 H}_2\text{O, - 3 H}_2]{\text{Ir@PS}_{60}\text{SiCN, 2 eq. KO}^t\text{Bu}} \\ \text{R}^1\text{CH(R}^2\text{)CH(R}^3\text{)CH(R}^4\text{)N} \\ \textbf{3} \end{array} $		
$ \begin{array}{c} \text{Cycloalkanol} + \text{HOCH}_2\text{CH(R}^2\text{)CH(R}^3\text{)NH}_2 \\ \xrightarrow[\text{- 2 H}_2\text{O, - 3 H}_2]{\text{Ir@PS}_{60}\text{SiCN, 2 eq. KO}^t\text{Bu}} \\ \text{Bicyclic Pyridine} \\ \textbf{4a - c} \end{array} $		
Entry	Product	Yield [%] ^{b, c}
1	 3 R = n-hexyl	69 (65)
3	 4a R = <i>p</i> -xylene	79
4	 4b R = 	>99 (97)
5 ^d	 4c R = 	51

^a Reaction conditions: 1,3-amino alcohol (1.5 mmol), secondary alcohol (6 mmol), KO^tBu (3 mmol), 0.89 mol% Ir, 1.5 mL diglyme, 24 h at 90 °C and 24 h at 130 °C oil bath temperature. ^b Yields determined by GC (*n*-dodecane as internal standard). ^c Yields of isolated products are given in parentheses.

^d 1.48 mol% Ir.

Furthermore, the synthesis of quinolines was performed. Thereby, 2- and 3-substituted quinolines were obtained in moderate to good yields (**Table 3, 5a-c**). Again, aryl- and alkyl-groups were tolerated. Additionally, 2,3-substituted quinolines were successfully synthesized in good to very good yields (**Table 3, 6a-c**). The tolerance of cycloheptanol (**Table 3, 6a**) as well as the tolerance of chloro-groups (**Table 3, 6b**) and branched alcohols (**Table 3, 6c**) was demonstrated.

Table 3. Synthesized 2-and 3-substituted as well as 2,3-substituted quinolones ^a

Entry	Product		Yield [%] ^{b, c}
1		5a R = Ph	74
2		5b R = Bn	48
3		5c R = n-Bu	70 (69)
4		6a n = 2; R = H	98 (94)
6		6b n = 1; R = i-Bu	62
7 ^d		6c n = 2; R = H	85

^a Reaction conditions: 2-aminobenzyl derivate (1.5 mmol), alcohol (6 mmol), KO^tBu (3 mmol), 0.89 mol% Ir, 1.5 mL diglyme, 24 h at 125 °C oil bath temperature. ^b Yields determined by GC (*n*-dodecane as internal standard). ^c Yields of isolated products are given in parentheses. ^d 110 °C, KO^tBu (1.5 mmol), 1.67 mol% Ir.

Finally, we investigated the activity and reusability of the structured SiCN catalyst compared to different commercially available heterogeneous iridium catalysts (Ir/C, Ir/Al₂O₃, Ir/CaCO₃) as well as an unstructured Ir@SiCN catalyst. The reaction of 2-aminobutan-1-ol and 1-phenylethanol to 2-ethyl-5-phenyl-1H-pyrrole was chosen as test reaction. After each run, the catalysts were washed with water and either methanol or acetone to eliminate residues. As seen in **Figure 3**, all commercially available catalysts were less efficient than the Ir@PS₆₀SiCN system using the same amount of iridium. Neither of the additionally tested catalysts obtained more than 16 % yield in the first run. A significant activity loss was already observed in the second run for Ir/C and Ir/CaCO₃. The porous SiCN supported system achieved a good reusability in four successional runs. Moreover, the Ir@PS₆₀SiCN catalyst is significant more active than the unstructured Ir@SiCN catalyst. The Ir@SiCN catalyst was synthesized without a pore building template and exhibits only a low SSA without any porosity. The PS based structuring procedure of the Ir@PS₆₀SiCN catalyst results in an open porosity and a high SSA. This leads to a much better accessibility of the iridium nanoparticles explaining the higher activity in catalytic reactions.

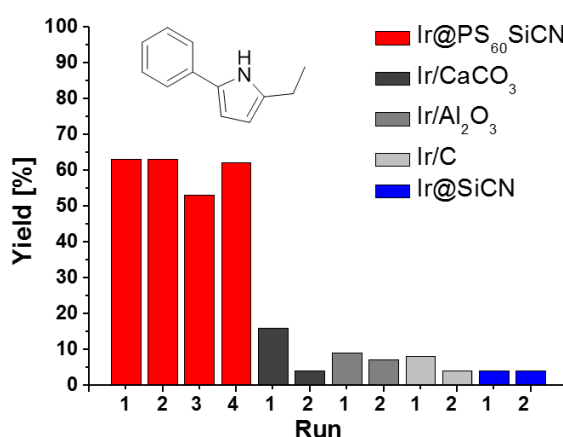


Figure 3. Heterogeneous iridium catalyst screening. Reaction conditions: 2-aminobutan-1-ol (1.5 mmol), 1-phenylethanol (6 mmol), KO^tBu (1.5 mmol), 1.32 mol% Ir, 1.5 mL diglyme, 5 h at 120 °C oil bath temperature.

6.3 Conclusion

We introduced a hierarchical structured SiCN iridium nanocomposite catalyst with high specific surface area. The robust Ir@PS₆₀SiCN catalyst exhibited an excellent accessibility of the nanometer-sized iridium particles. We accomplished the sustainable synthesis of N-heterocycles like pyrroles, pyridines, and quinolines starting from alcohols and amino alcohols. A broad substrate scope and the tolerance of diverse functional groups was shown. Our Ir catalyst exhibited an excellent activity and good reusability compared to commercially available heterogeneous iridium catalysts.

6.4 Experimental Section

6.4.1 Catalyst synthesis

A dispersion of 1.00 g degassed PS₆₀-particles in 40 mL toluene was stirred with 500 mg of HTT-1800 (7.77 mmol), 50 mg DCP (1.85 mmol), and 410 mg [IrAp^{TMA}(cod)]⁸ (0.78 mmol). Without stirring, the suspension was heated to 110 °C for 24 h. The cross-linking process of the in situ structured green body was completed at 110 °C (24 h) after removal of the solvent. The Ir@PS₆₀SiCN catalyst was obtained following pyrolysis under nitrogen atmosphere at 1000 °C. (Detailed experimental procedure see Supporting Information).

6.4.2 General method for synthesis of N-heterocycles

In a pressure tube, alcohol, amino alcohol, and KO^tBu were solved in diglyme and added to the catalyst. The catalysis was carried out at the respectively reaction time and temperature under stirring. The reaction mixture was cooled to room temperature and quenched with water. For GC analysis, *n*-dodecane was added as internal standard and the product was extracted with diethyl ether. Isolated products were purified by column chromatography (see Supporting Information).

6.5 Acknowledgements

We thank the SFB 840 and the Elitenetzwerk Bayern e.V. for financial support, Dr. Wolfgang Milius and Florian Puchtler for XRD measurements and Dr. Gunter Ilgen and the BayCEER institute for ICP-OES measurements.

6.6 References

- 1 C. O. Tuck, E. Perez, I. T. Horvath, R. A. Sheldon, M. Poliakoff, *Science* **2012**, 337, 695-699.
- 2 T. P. Vispute, H. Zhang, A. Sanna, R. Xiao, G. W. Huber, *Science* **2010**, 330, 1222-1227.
- 3 S. Michlik, R. Kempe, *Nature Chem.* **2013**, 5, 140-144.
- 4 a) D. Srimani, Y. Ben-David, D. Milstein, *Angew. Chem. Int. Ed.* **2013**, 52, 4012-4015; b) D. Srimani, Y. Ben-David, D. Milstein, *Chem. Commun.* **2013**, 49, 6632-6634.
- 5 K. Iida, T. Miura, J. Ando, S. Saito, *Org. Lett.* **2013**, 15, 1436-1439.
- 6 a) S. Michlik, R. Kempe, *Angew. Chem. Int. Ed.* **2013**, 52, 6326-6329; b) S. Ruch, T. Irrgang, R. Kempe, *Chem. Eur. J.* **2014**, 20, 13279-13285.
- 7 a) M. Zhang, X. Fang, H. Neumann, M. Beller, *J. Am. Chem. Soc.* **2013**, 135, 11384-11388; b) J. Schranck, A. Tlili, M. Beller, *Angew. Chem. Int. Ed.* **2013**, 52, 7642-7644; c) M. Zhang, H. Neumann, M. Beller, *Angew. Chem. Int. Ed.* **2013**, 125, 625-629.
- 8 D. Forberg, J. Obenauf, M. Friedrich, S.-M. Hühne, W. Mader, G. Motz, R. Kempe, *Catal. Sci. Technol.* **2014**, 4, 4188-4192.
- 9 a) M. Kamperman, A. Burns, R. Weissgraeber, N. van Vegten, S. C. Warren, S. M. Gruner, A. Baiker, U. Wiesner, U. *Nano Lett.* **2009**, 9, 2756-62; b) G. Glatz, T. Schmalz,

- T. Kraus, F. Haarmann, G. Motz, R. Kempe, *Chem. Eur. J.* **2010**, *16*, 4231-4238; c) M. Zaheer, G. Motz, R. Kempe, *J. Mater. Chem.* **2011**, *21*, 18825-18831; d) M. Zaheer, C. D. Keenan, J. Hermannsdörfer, E. Roessler, G. Motz, J. Senker, R. Kempe, *Chem. Mater.* **2012**, *24*, 3952-3963.
- 10 M. Zaheer, T. Schmalz, G. Motz, R. Kempe, *Chem. Soc. Rev.* **2012**, *41*, 5102-5116.
- 11 P. Colombo, G. D. Sorarú, R. Riedel, A. Kleebe, D. E. Stech, Polymer Derived Ceramics; Publications Inc.: Lancaster, PA, USA, **2010**.
- 12 a) M. Kamperman, C. B. Garcia, P. Du, H. Ow, U. Wiesner, *J. Am. Chem. Soc.* **2004**, *126*, 14708-14709; b) J. Wan, A. Alizadeh, S. T. Taylor, P. R. L. Malenfant, M. Manoharan, S. M. Loureiro, *Chem. Mater.* **2005**, *17*, 5613-5617; c) J. Wan, P. R. L. Malenfant, S. T. Taylor, S. M. Loureiro, M. Manoharan, *Mater. Sci. Eng. A* **2007**, *463*, 78-88; d) B. H. Jones, T. P. Lodge, *J. Am. Chem. Soc.* **2009**, *131*, 1676-1677; e) C. T. Nguyen, P. H. Hoang, J. Perumal, D.-P. Kim, *Chem. Commun.* **2011**, *47*, 3484-3486; f) S. K. Pillai, W. P. Kretschmer, C. Denner, G. Motz, M. Hund, A. Fery, M. Trebbin, S. Forster, R. Kempe, *Small* **2013**, *9*, 984-989; g) J.-K. Ewert, C. Denner, M. Friedrich, G. Motz, R. Kempe, *Nanomaterials* **2015**, *5*, 425-435; h) J.-K. Ewert, D. Weingarth, C. Denner, M. Friedrich, M. Zeiger, A. Schreiber, N. Jäckel, V. Presser, R. Kempe, *J. Mater. Chem. A* **2015**, *3*, 18906-18912.

6.7 Supporting Information

6.7.1 Experimental Section

Materials

All reactions were carried out in a dry argon or nitrogen atmosphere using standard Schlenk or glove box techniques. Nonhalogenated solvents were dried over sodium benzophenone ketyl. Deuterated solvents were ordered from Cambridge Isotope Laboratories, vented, stored over molecular sieves and distilled. (1-Hexadecyl)trimethylammonium bromide (CTAB) (98% purity, abcr, Karlsruhe, Germany), 2,2'-azobis(2-methylpropion-amidine)dihydrochloride (97% purity, Aldrich Chemistry, Steinheim, Germany), KiON HTT1800 (Clariant Advanced Materials GmbH, Frankfurt, Germany) and dicumylperoxide (97% purity, Aldrich Chemistry, Steinheim, Germany) were purchased from commercial sources and used without further purification. Styrene (>99% purity, Sigma Aldrich, Steinheim, Germany) and divinylbenzene (technical grade, 55%, Aldrich Chemistry, Steinheim, Germany) were destabilized over an alumina B column (ICN Biomedicals

GmbH, Eschwege, Germany). The Ir-catalysts Ir/C (1 mass-% iridium), Ir/CaCO₃ (5 mass% iridium), and Ir/Al₂O₃ (1 mass-% iridium) were received from Alfa Aesar. All further chemicals were purchased from commercial sources with purity over 95 % and used without further purification.

Methods

Ceramization was performed in a high temperature furnace (GERO, Berlin, Germany) under nitrogen atmosphere. The pyrolysed ceramic were milled in a ball mill “Pulverisette 0” (Fritsch, Idar-Oberstein, Germany) for 20 min. *SEM* and *EDX* measurements were carried out using a Zeiss Field-Emission-Scanning-Electron-Microscope (FESEM) “LEO 1530 GEMINI”. The acceleration voltage was 1–5 kV. The samples were sputter-coated with a 1.3 nm layer of platinum. *TEM* measurements were performed using a Varian LEO 9220 (Carl Zeiss, 120 kV, Oberkochen, Germany) instrument. The samples were suspended in chloroform and sonicated for 5 min. Two microliters of the suspension were placed on a CF200-Cu-grid (Electron Microscopy Sciences, Hatfield, USA) and allowed to dry. *HR-TEM* was performed using a Philips CM300 FEG/UT (300 kV) instrument. The sample was suspended in chloroform and sonicated for 2 min. A drop of the suspended sample was placed on a grid with lacy carbon film and dried. *Nitrogen sorption analysis* were conducted using a Nova2000e (Quantachrome, Odelzhausen, Germany) instrument. The specific surface areas were calculated using *p/p₀*-values from 0.05–0.31 (BET). The pore width and average pore volume was calculated by DFT calculations (N₂ at 77 K on carbon (slit/cylindric pore, NLDFT equilibrium model)). *Powder X-ray* diffractograms were recorded using a STOE STADI-P-diffractometer (CuK_α radiation, $\lambda = 1,54178 \text{ \AA}$) in θ -2 θ -geometry and with a position sensitive detector. *ICP-OES* measurements were carried out using a Vista-pro radical model from VARIAN. The sample was solved in a mixture of 4.5 mL HCl (32 %, p.a.), 1.5 mL HNO₃ (65 %, distilled) and 1 mL HF (40 %) and heated in a microwave for 7 min at 170 °C (80 % power), for 7 min at 180 °C (85 % power) and for 20 min at 1795 °C (90 % power). *NMR* spectra were received using an INOVA 300 MHz spectrometer at 298 K. Chemical shifts are reported in ppm relative to the deuterated solvent. *Gas chromatography* analysis were performed using an Agilent Technologies 6890N Network gas chromatograph equipped with a flame ionization detector (FID) and a MN HP-5 capillary column (30.0 m x 32 μ m x 0.25 μ m) using *n*-dodecane as internal standard and diethyl ether as solvent. *GC-MS* analyses were performed using an Agilent Technologies 7890A/MSD 5975C system equipped with a HP-5MS column (30.0 m x 32 μ m x 0.25 m)

Synthesis of Ir@PS₆₀SiCN

In a round bottom Schenk flask 1.00 g degased PS₆₀-particles^{S1} were dispersed in 40 mL toluene under stirring. Subsequently, 500 mg of HTT1800 (7.77 mmol), 50 mg dicumylperoxide (1.85 mmol) and 410 mg [IrAp^{TMA}(cod)]^{S2} (0.78 mmol) were added and stirred for 10 min. Without stirring, the suspension was heated to 110 °C for 24 h. After removal of the solvent the crosslinking process of the in situ structured green body was completed at 110 °C (24 h). The Ir@PS₆₀SiCN green body was pyrolysed under nitrogen atmosphere according to the following program:

$RT \xrightarrow{1\text{ K min}^{-1}, 3\text{ h}} 300\text{ °C} \xrightarrow{1\text{ K min}^{-1}, 3\text{ h}} 400\text{ °C} \xrightarrow{0.5\text{ K min}^{-1}, 3\text{ h}} 500\text{ °C} \xrightarrow{1\text{ K min}^{-1}, 4\text{ h}} 600\text{ °C} \xrightarrow{0.5\text{ K min}^{-1}, 0\text{ h}} 700\text{ °C} \xrightarrow{1\text{ K min}^{-1}, 0.5\text{ h}} 1000\text{ °C}$

The resulting ceramic monoliths were milled for 20 min obtaining a ceramic powder. The iridium content of 12.0 wt% of the Ir@PS₆₀SiCN material was determined by ICP-OES measurements.

Synthesis of Ir@SiCN

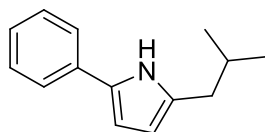
The unstructured Ir@SiCN catalyst used for the comparison of different heterogeneous iridium catalyst was synthesized and handled as described in the literature.^{S2}

Synthesis of N-heterocycles

The Ir@PS₆₀SiCN catalyst was activated prior to the catalytic reactions (typically 200 mg Ir@PS₆₀SiCN, 5 mmol NaOH, 1 mL H₂O, 3 mL MeOH, 60 °C, 8 h). In a pressure tube, 6 mmol alcohol, 1.5 mmol amino alcohol, and 3 mmol KO^tBu were solved in 1.5 mL diglyme and added to the appropriate amount of Ir@PS₆₀SiCN catalyst. The synthesis of pyrroles and quinolines was carried out at 125 °C for 24 h under stirring. The synthesis of pyridines was performed for 24 h at 90 °C and subsequently for 24 h at 130 °C. The reaction mixture was cooled to room temperature and quenched with water. The product was extracted with diethyl ether and *n*-dodecane was added as internal standard for GC analysis. Isolated products were purified by column chromatography (see product characterization).

The Ir@PS₆₀SiCN catalyst was washed with water and methanol for three time between the catalytic runs during the reusability studies. All other catalysts were washed with water and acetone for three times.

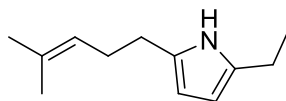
6.7.2 Product Characterization



1b: 2-isobutyl-5-phenyl-1H-pyrrole

1.7 mg iridium, 1-phenylethanol (726 μL , 6.0 mmol), 2-amino-4-methylpentan-1-ol (192 μL , 1.5 mmol), 1.5 mL diglyme, KO^tBu (343 mg, 3.0 mmol), 24 h at 120 °C (oil bath temperature). Purification by column chromatography 50 : 1 pentane : Et₂O; Yield: 269 mg = 1.35 mmol = 90 % as colourless solid. $M(\text{C}_{14}\text{H}_{17}\text{N}) = 199.2 \text{ g mol}^{-1}$.

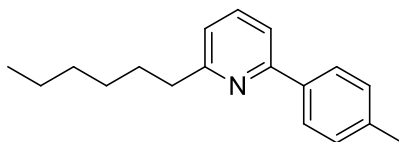
¹H NMR (300 MHz, CDCl₃, 298 K): δ = 8.10 (s_br, 1H), 7.48-7.45 (m, 2H), 7.39-7.34 (m, 2H), 7.22-7.17 (m, 1H), 6.47-6.45 (m, 1H), 6.01-5.99 (m, 1H), 2.54 (d, J = 7.0 Hz, 2H), 2.00-1.86 (m, 1H), 1.00 (d, J = 7.0 Hz, 6H) ppm. ¹³C NMR (75 MHz, CDCl₃, 298 K): δ = 133.3, 133.0, 130.5, 128.8, 125.6, 123.3, 108.0, 106.1, 37.4, 29.3, 22.5 ppm. MS (EI, m/z): 199.2 (M^+).



1e: 2-ethyl-5-(4-methyl-pent-3-enyl)-1H-pyrrole

1.7 mg iridium, 6-methyl-5-hepten-2-ol (916 μL , 6.0 mmol), 2-amino-butan-1-ol (141 μL , 1.5 mmol), 1.5 mL diglyme, KO^tBu (343 mg, 3.0 mmol), 24 h at 120 °C (oil bath temperature). Purification by column chromatography 70 : 1 pentane : Et₂O; Yield: 231 mg = 1.30 mmol = 87 % as yellow oil. $M(\text{C}_{12}\text{H}_{19}\text{N}) = 177.2 \text{ g mol}^{-1}$.

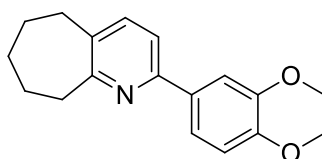
¹H NMR (300 MHz, CDCl₃, 298 K): δ = 7.67 (s_br, 1H), 5.81-5.80 (m, 2H), 5.25-5.20 (m, 1H), 2.63-2.57 (m, 4H), 2.31 (q, J = 7.6 Hz, 2H), 1.73 (s, 3H), 1.62 (s, 3H), 1.25 (t, J = 7.6 Hz, 2H) ppm. ¹³C NMR (75 MHz, CDCl₃, 298 K): δ = 132.8, 132.4, 131.2, 124.1, 104.8, 103.9, 28.4, 28.0, 25.8, 21.0, 17.8, 13.8 ppm. MS (EI, m/z): 177.2 (M^+).



3a: 2-hexyl-6-(p-tolyl)pyridine

2.6 mg iridium, octan-2-ol (952 μ L, 6.0 mmol), 3-amino-3-(p-tolyl)propan-1-ol (248 mg, 1.5 mmol), 1.5 mL diglyme, KO^tBu (343 mg, 3.0 mmol), 24 h at 90 °C and 24 h at 130 °C (oil bath temperature). Purification by column chromatography 40 : 1 pentane : Et₂O; Yield: 247 mg = 0.97 mmol = 65 % as yellow oil. $M(C_{18}H_{23}N) = 253.4 \text{ g mol}^{-1}$.

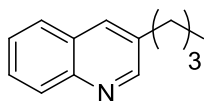
¹H NMR (300 MHz, CDCl₃, 298 K): δ = 7.96 (d, J = 8.20 Hz, 2H), 7.66-7.61 (m, 1H), 7.54-7.51 (m, 1H), 7.32-7.27 (m, 2H), 7.09-7.06 (m, 1H), 2.92-2.87 (m, 2H), 2.44 (s, 3H), 1.90-1.80 (m, 2H), 1.48-1.32 (m, 6H), 0.97-0.93 (m, 3H) ppm. ¹³C NMR (75 MHz, CDCl₃, 298 K): δ = 162.3, 156.8, 138.5, 136.7, 129.4, 126.9, 120.7, 117.3, 38.6, 31.8, 29.8, 29.2, 22.7, 21.28, 14.2 ppm. MS (EI, m/z): 253.4 (M^+).



4b: 2-(3,4-dimethoxyphenyl)-6,7,8,9-tetrahydro-5H-cyclohepta[b]pyridine

2.6 mg iridium, cycloheptanol (725 μ L, 6.0 mmol), 3-amino-3-(3,4-dimethoxyphenyl)propan-1-ol (317 mg, 1.5 mmol), 1.5 mL diglyme, KO^tBu (343 mg, 3.0 mmol), 24 h at 90 °C and 24 h at 130 °C (oil bath temperature). Purification by column chromatography 40 : 1 \rightarrow 20 : 1 pentane : Et₂O; Yield: 412 mg = 1.45 mmol = 97 % as yellow oil. $M(C_{18}H_{21}NO_2) = 283.4 \text{ g mol}^{-1}$.

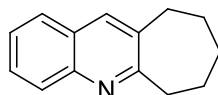
¹H NMR (300 MHz, CDCl₃, 298 K): δ = 7.53 (d, J = 2.3 Hz, 1H), 7.38-7.35 (m, 1H), 7.27 (s, 2H), 6.81 (d, J = 8.2 Hz, 1H), 3.87 (s, 3H), 3.80 (s, 3H), 3.02-2.99 (m, 2H), 2.69-2.65 (m, 2H), 1.79-1.74 (m, 2H), 1.66-1.55 (m, 4H) ppm. ¹³C NMR (75 MHz, CDCl₃, 298 K): δ = 163.0, 153.7, 149.4, 149.1, 137.2, 136.0, 132.9, 119.2, 117.3, 111.1, 110.0, 56.0, 55.9, 39.8, 35.0, 32.6, 28.2, 26.7 ppm. MS (EI, m/z): 283.4 (M^+).



5c: 3-butylquinoline

2.6 mg iridium, hexan-1-ol (746 μL , 6.0 mmol), (2-aminophenyl)methanol (185 mg, 1.5 mmol), 1.5 mL diglyme, KO^tBu (343 mg, 3.0 mmol), 24 h at 125 $^{\circ}\text{C}$ (oil bath temperature). Purification by column chromatography 10 : 1 \rightarrow 5 : 1 pentane : Et_2O ; Yield: 191 mg = 1.03 mmol = 69 % as yellow oil. $M(\text{C}_{13}\text{H}_{15}\text{N}) = 185.1 \text{ g mol}^{-1}$.

^1H NMR (300 MHz, CDCl_3 , 298 K): $\delta = 8.77$ (d, $J = 1.7 \text{ Hz}$, 1H), 8.07 (d, $J = 8.2 \text{ Hz}$, 1H), 7.86 (s, 1H), 7.74-7.71 (m, 1H), 7.62-7.60 (m, 1H), 7.50-7.45 (m, 1H), 2.78-2.73 (m, 2H), 1.73-1.62 (m, 2H), 1.45-1.32 (m, 2H), 0.97-0.92 (m, 3H) ppm. ^{13}C NMR (75 MHz, CDCl_3 , 298 K): $\delta = 152.1$, 146.8, 135.3, 134.0, 129.1, 128.4, 128.2, 127.3, 126.4, 33.2, 32.9, 22.3, 13.9 ppm. MS (EI, m/z): 185.1 (M^+).

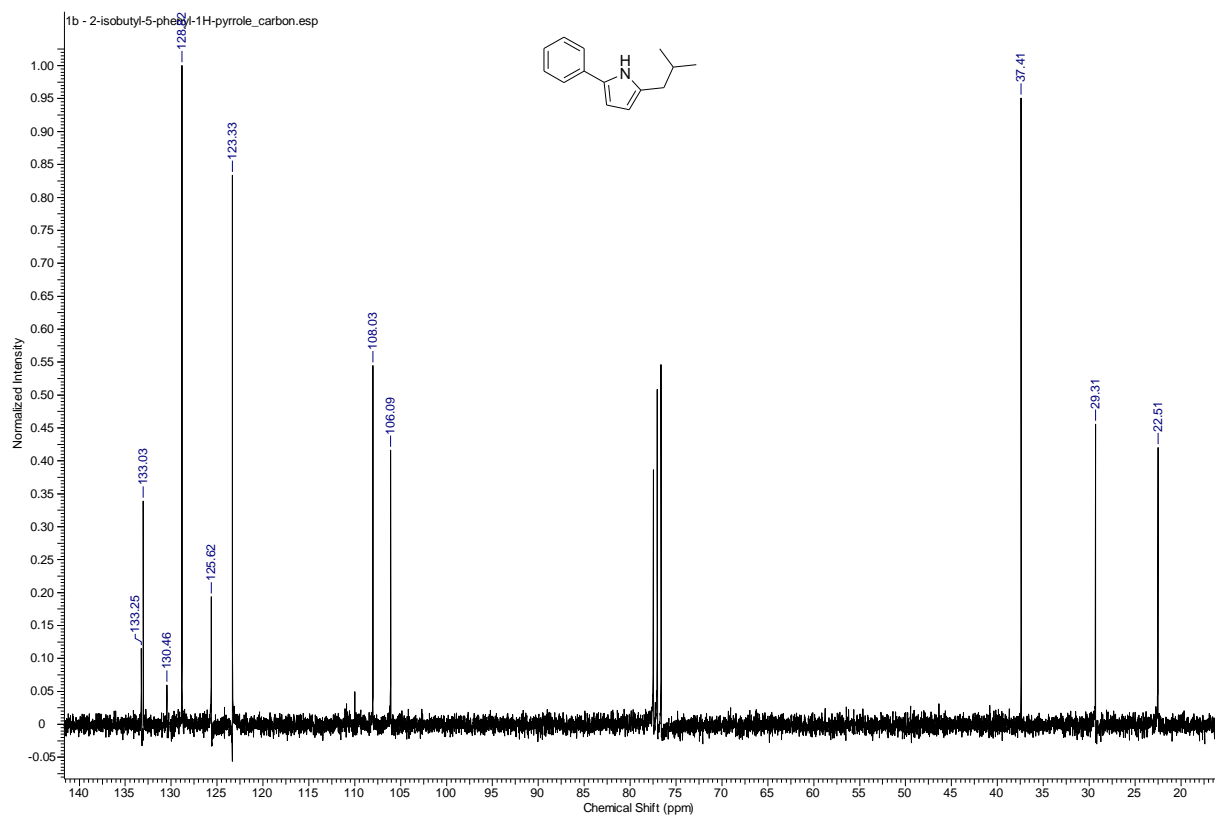
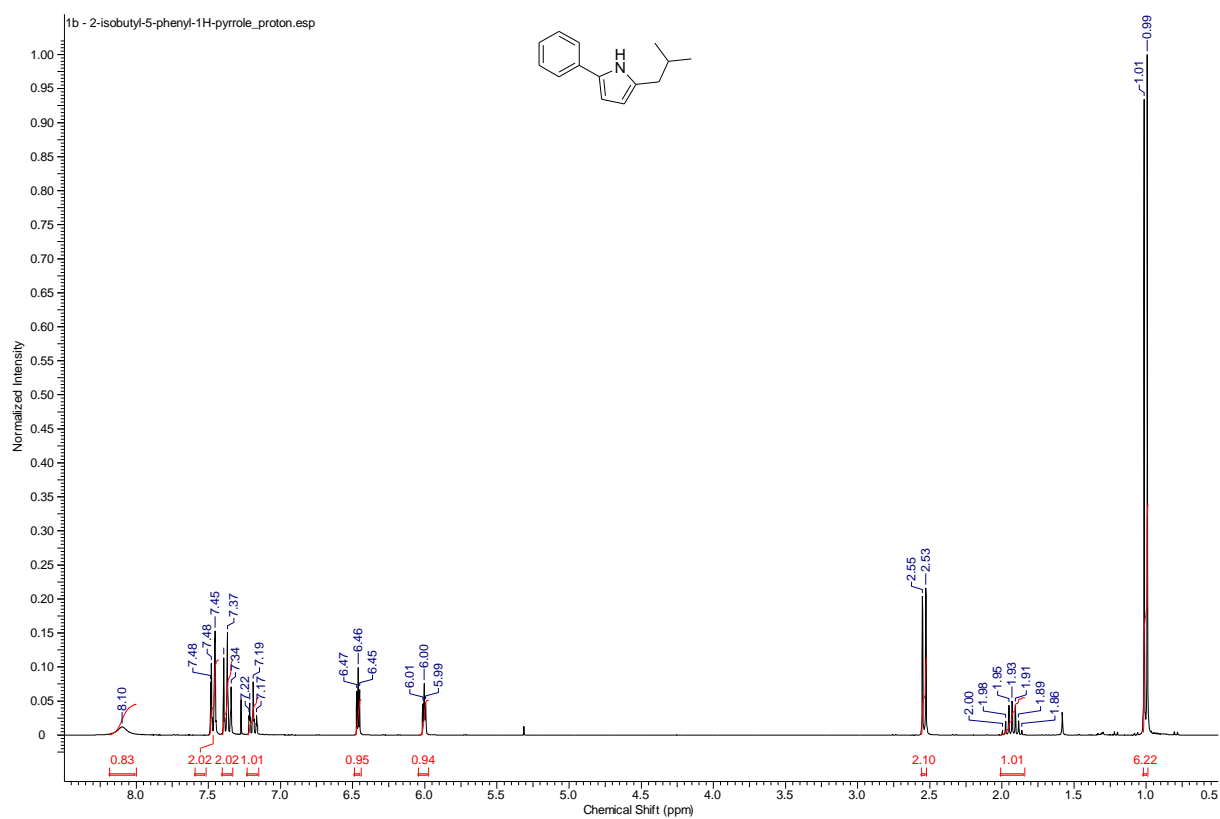


6a: 7,8,9,10-tetrahydro-6H-cyclohepta[b]quinoline

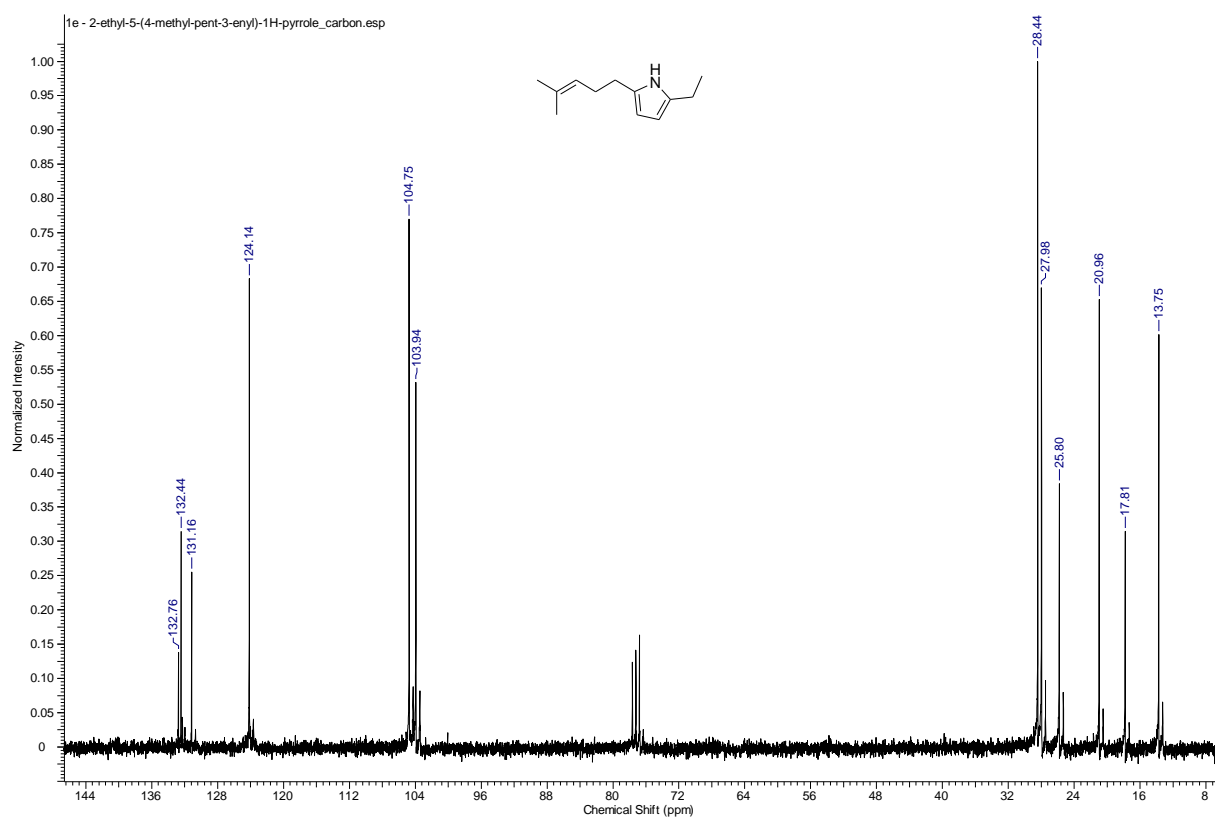
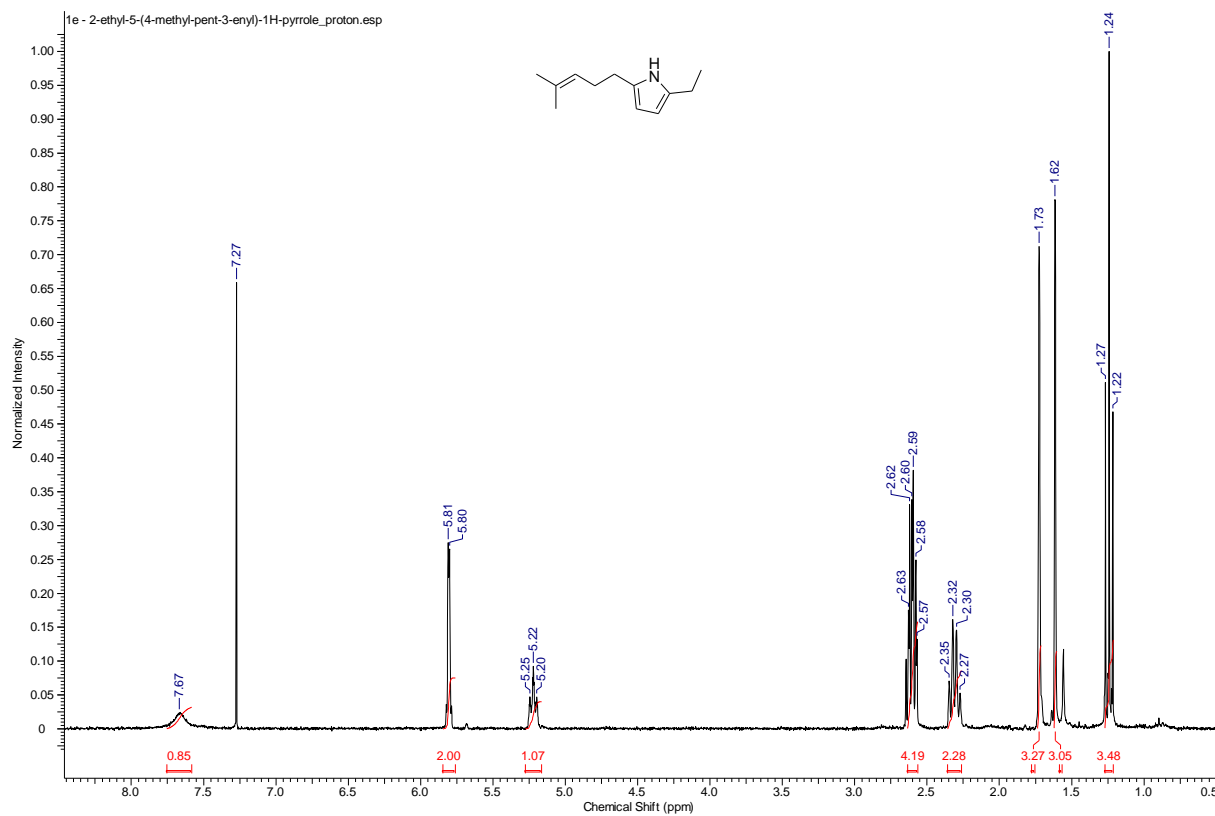
2.6 mg iridium, cycloheptanol (725 μL , 6.0 mmol), (2-aminophenyl)methanol (185 mg, 1.5 mmol), 1.5 mL diglyme, KO^tBu (343 mg, 3.0 mmol), 24 h at 125 $^{\circ}\text{C}$ (oil bath temperature). Purification by column chromatography 10 : 1 \rightarrow 5 : 1 pentane : Et_2O ; Yield: 191 mg = 1.03 mmol = 69 % as yellow oil. $M(\text{C}_{14}\text{H}_{15}\text{N}) = 197.3 \text{ g mol}^{-1}$.

^1H NMR (300 MHz, CDCl_3 , 298 K): $\delta = 8.01$ (d, $J = 8.8 \text{ Hz}$, 1H), 7.79 (s, 1H), 7.71-7.69 (m, 1H), 7.64-7.59 (m, 1H), 7.47-7.42 (m, 1H), 3.23-3.20 (m, 2H), 2.95-2.92 (m, 2H), 1.92-1.71 (m, 6H) ppm. ^{13}C NMR (75 MHz, CDCl_3 , 298 K): $\delta = 163.3$, 152.7, 138.2, 137.3, 136.9, 134.3, 128.8, 128.0, 117.6, 39.7, 35.0, 32.6, 28.1, 26.6 ppm. MS (EI, m/z): 197.3 (M^+).

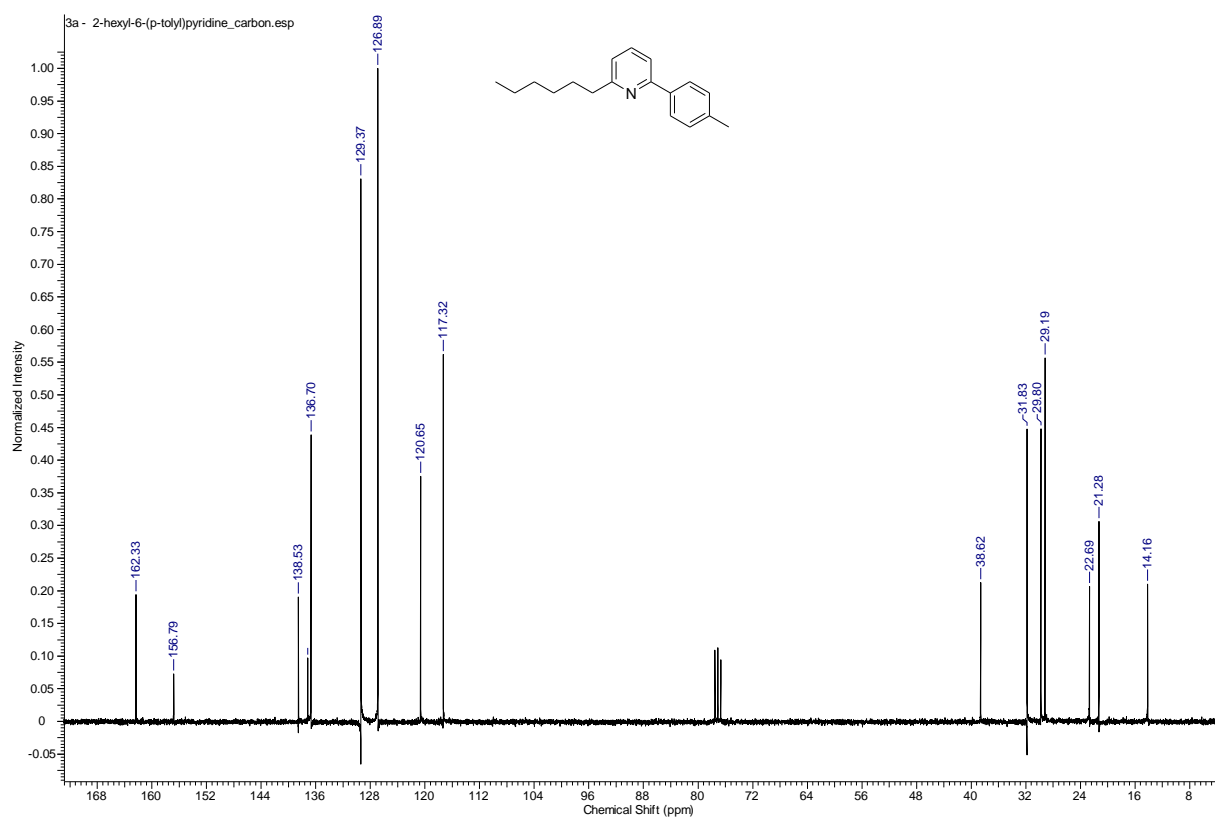
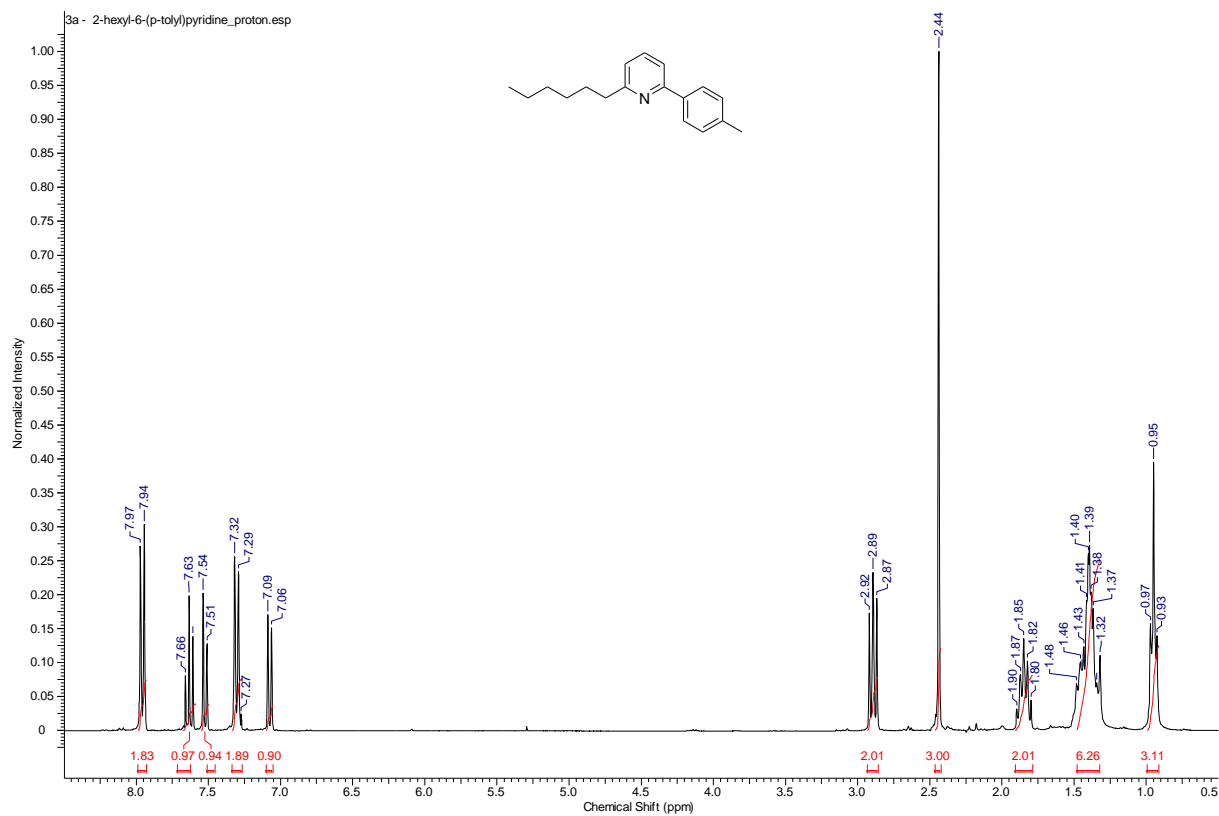
6 A Hierarchical Structured Reusable Iridium Catalyst for the Sustainable Synthesis of Pyrroles, Pyridines, and Quinolines



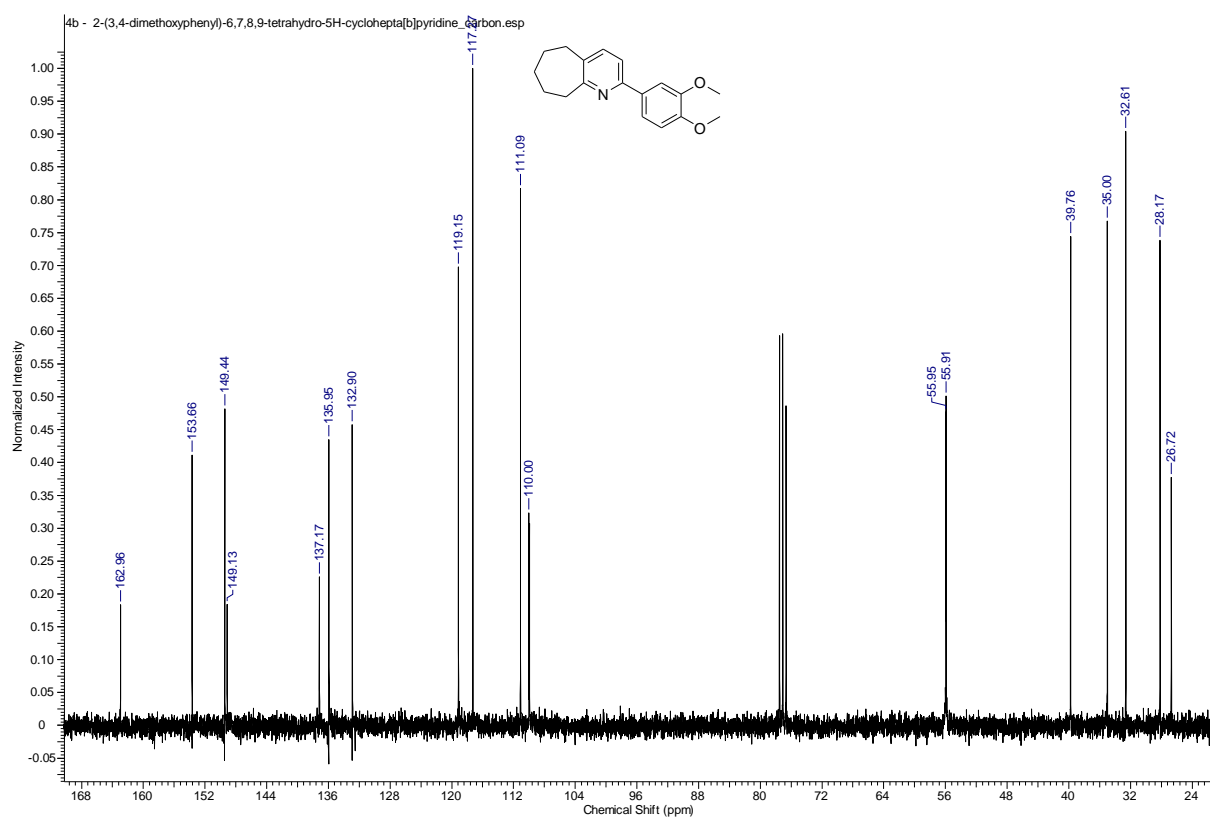
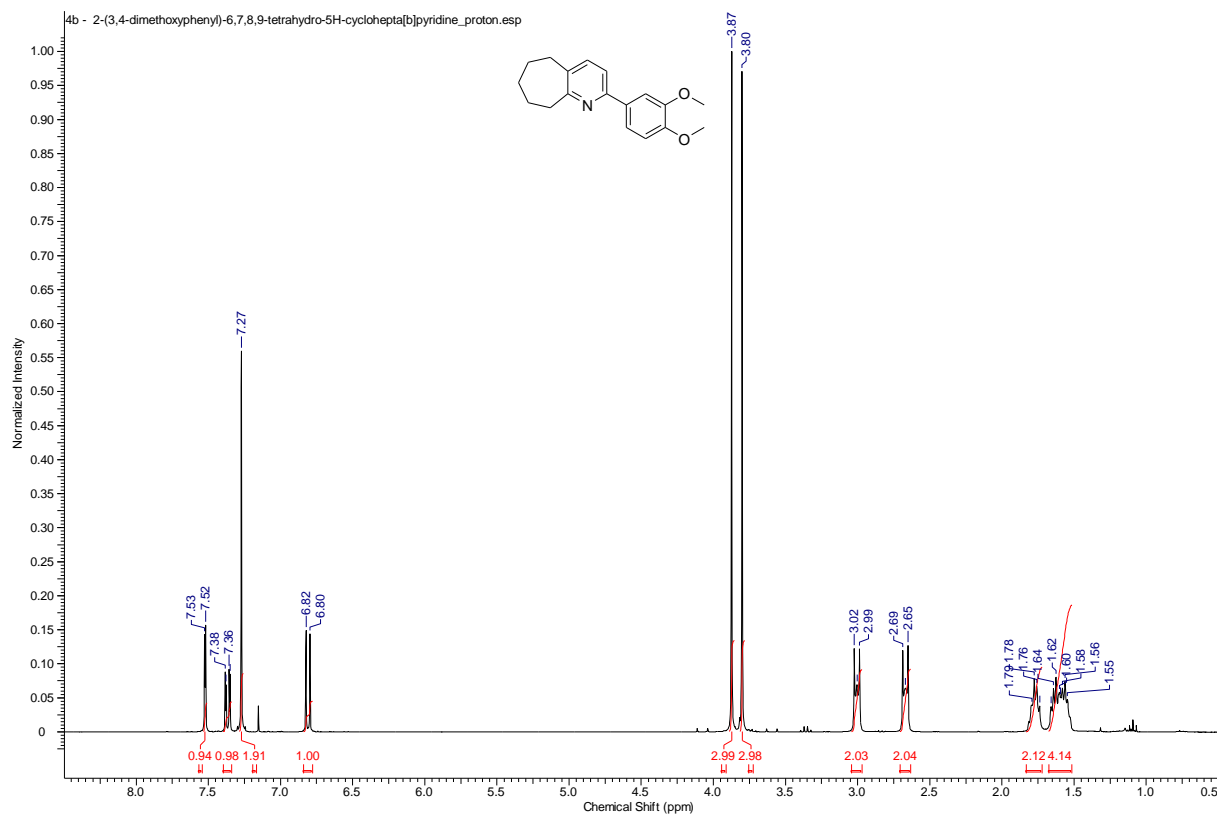
6 A Hierarchical Structured Reusable Iridium Catalyst for the Sustainable Synthesis of Pyrroles, Pyridines, and Quinolines



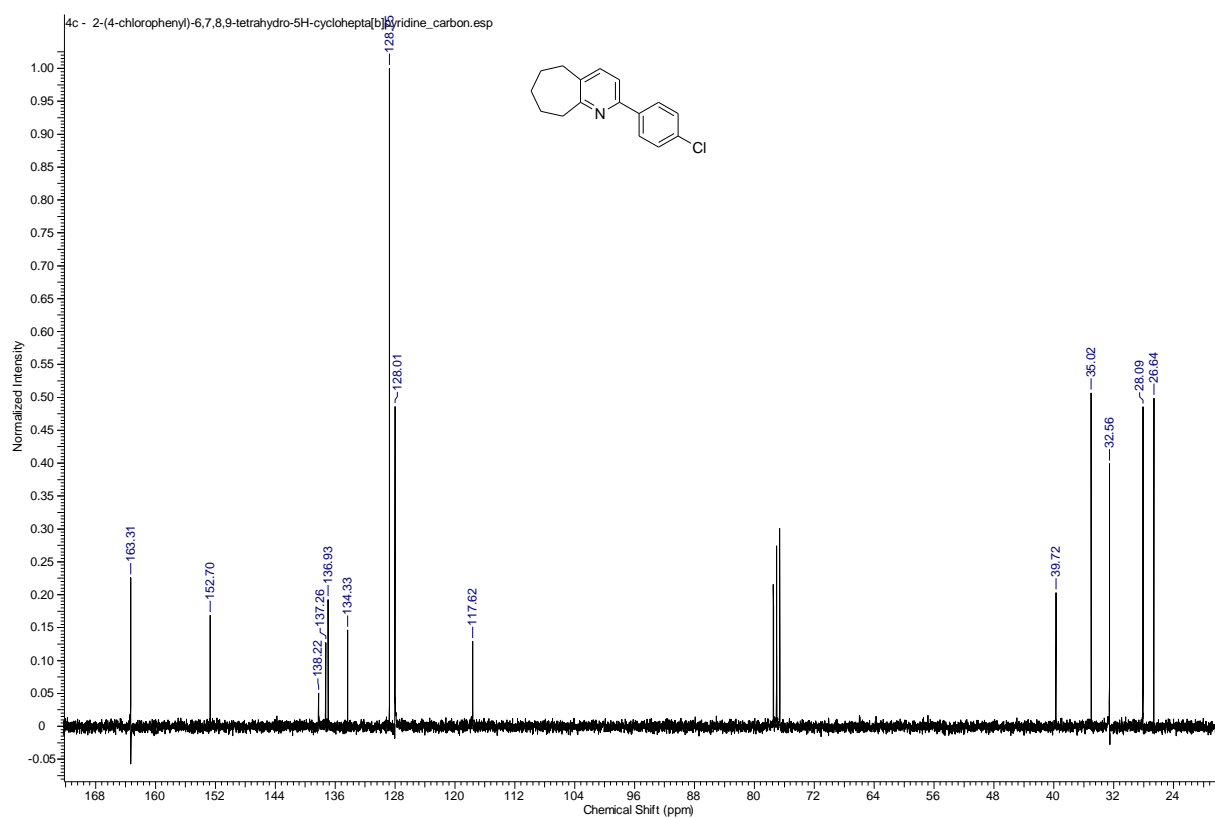
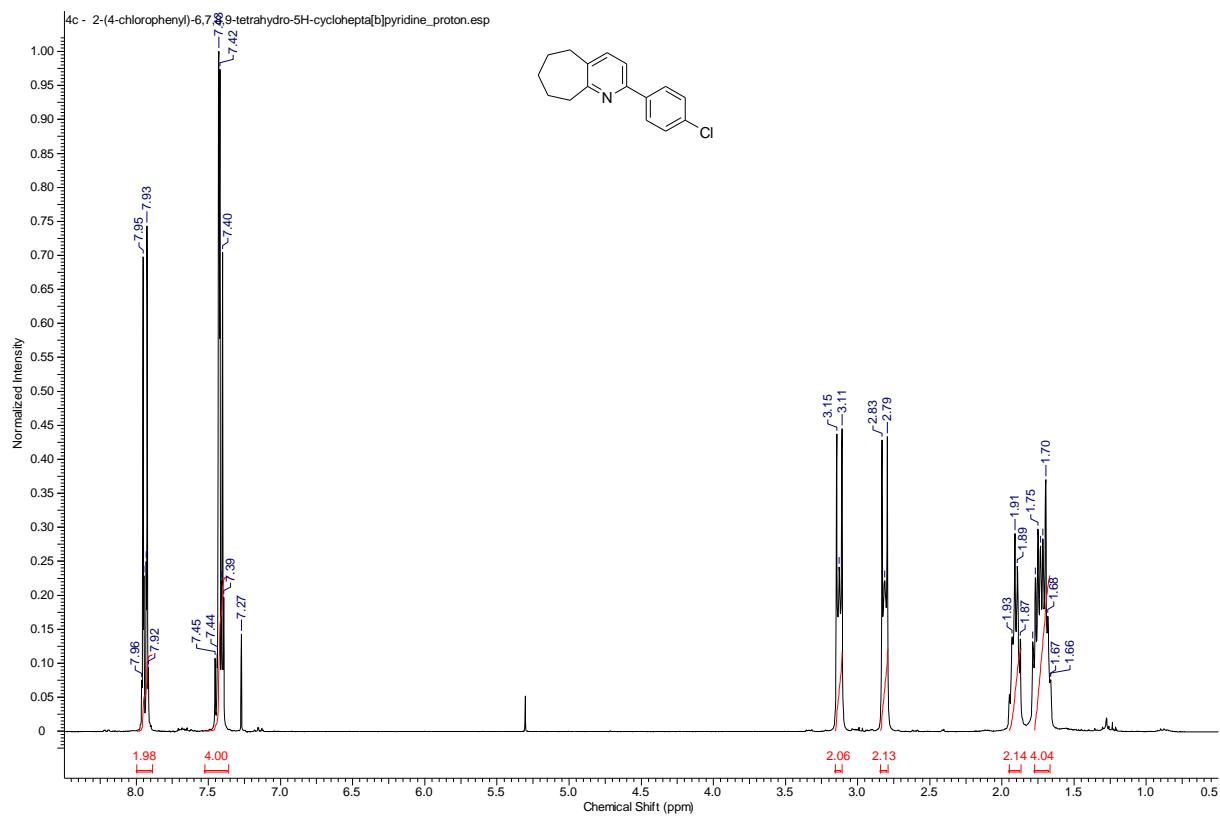
6 A Hierarchical Structured Reusable Iridium Catalyst for the Sustainable Synthesis of Pyrroles, Pyridines, and Quinolines



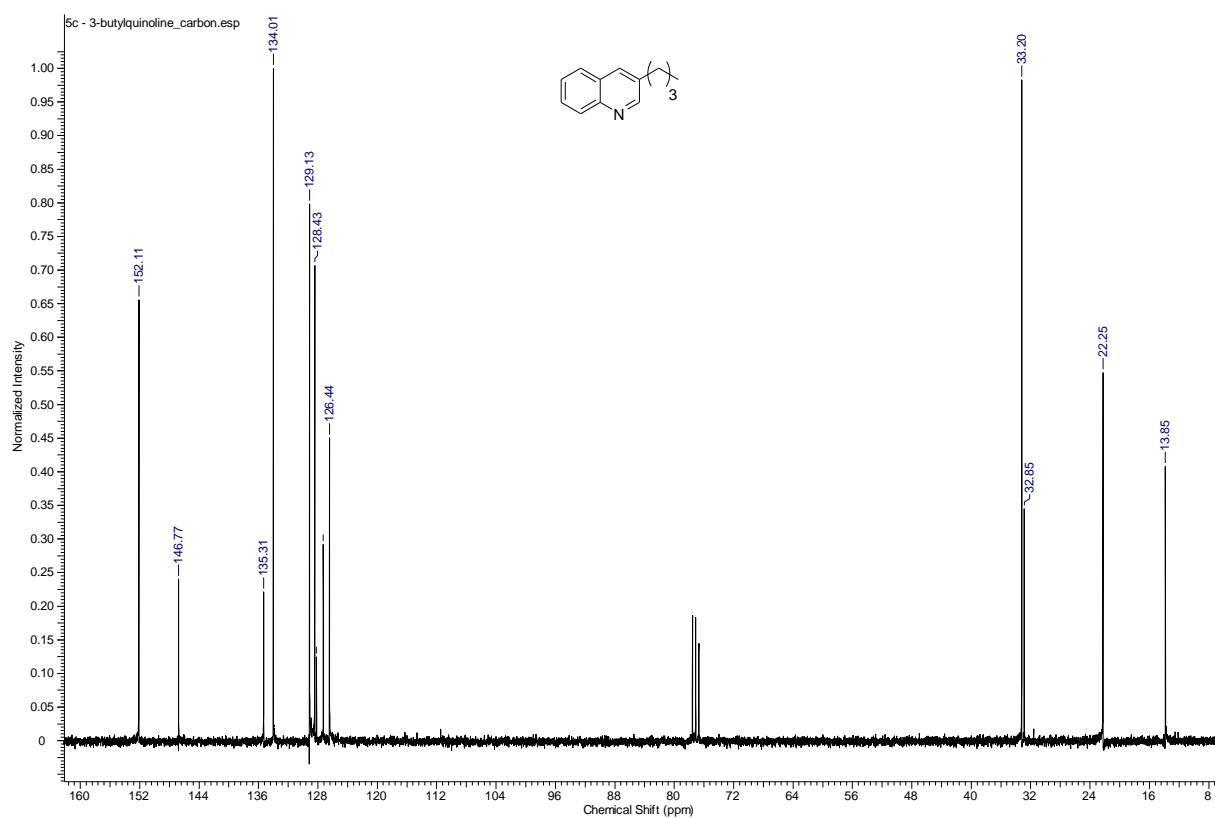
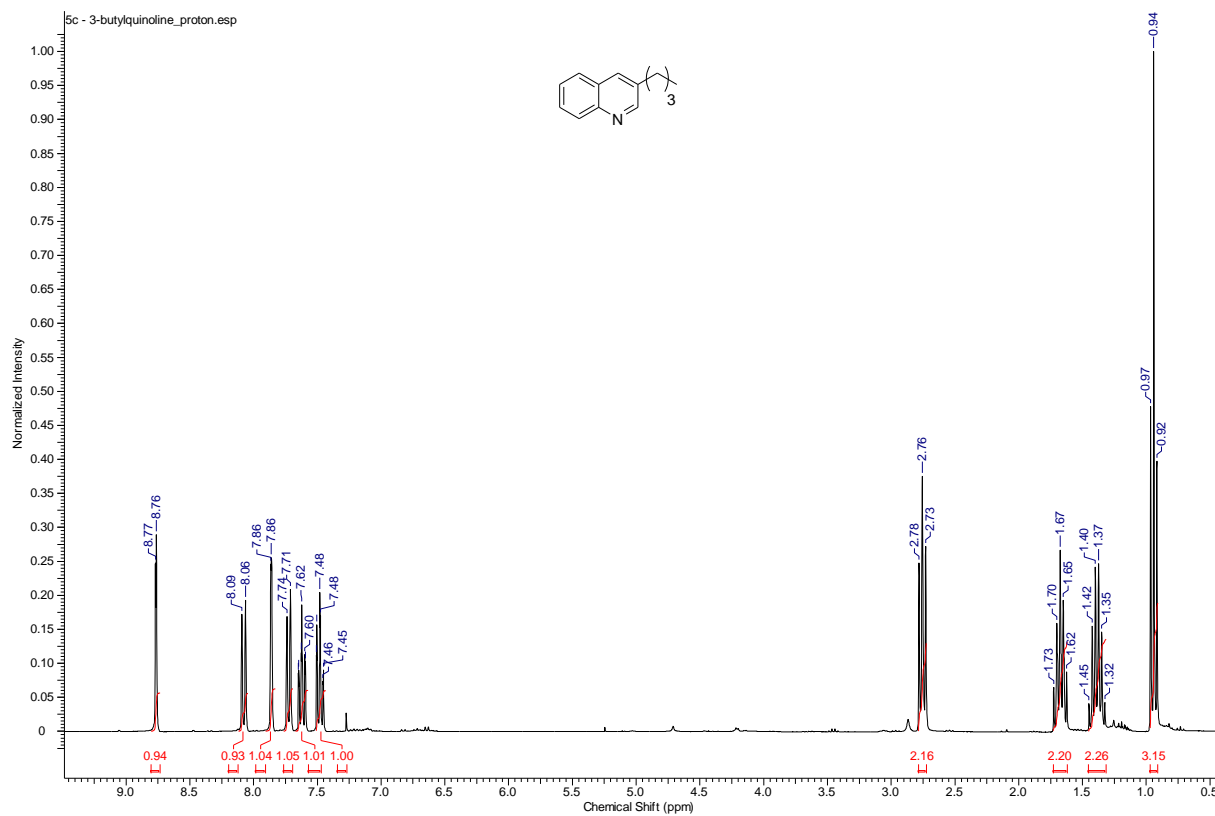
6 A Hierarchical Structured Reusable Iridium Catalyst for the Sustainable Synthesis of Pyrroles, Pyridines, and Quinolines



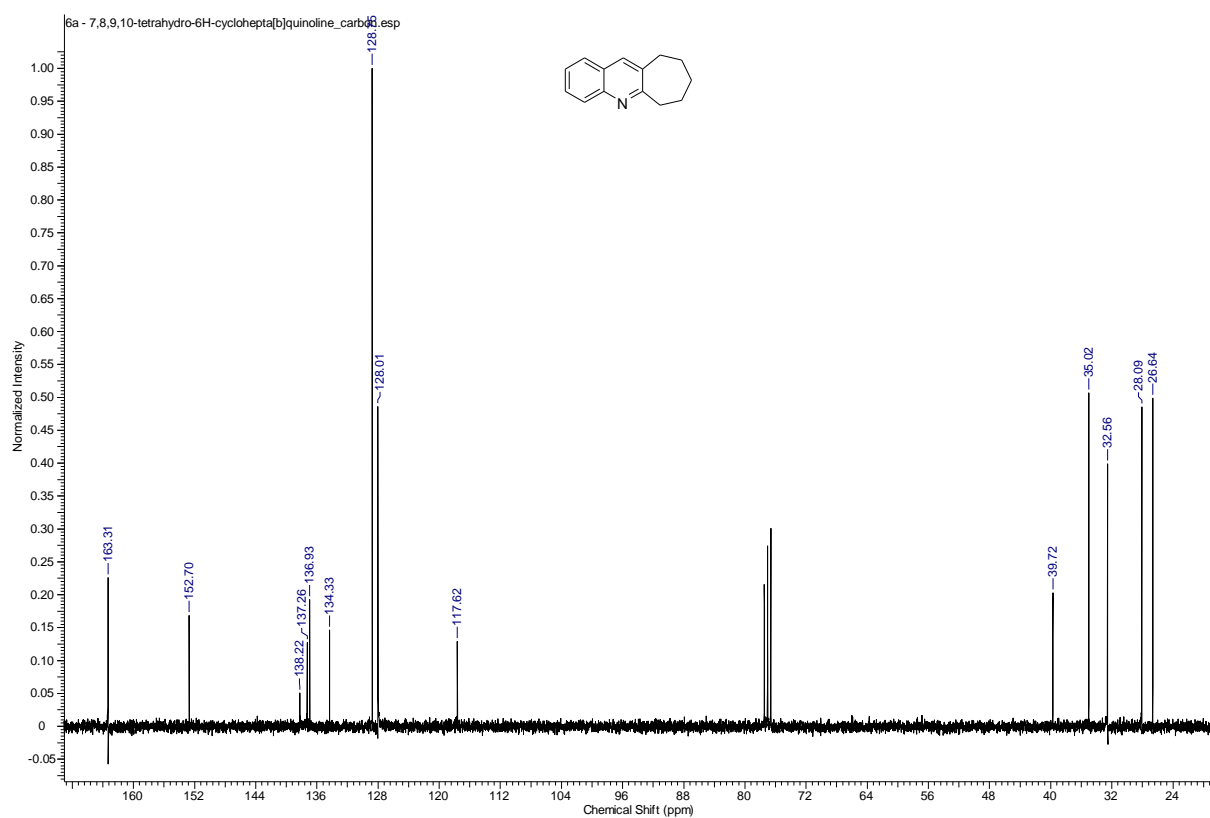
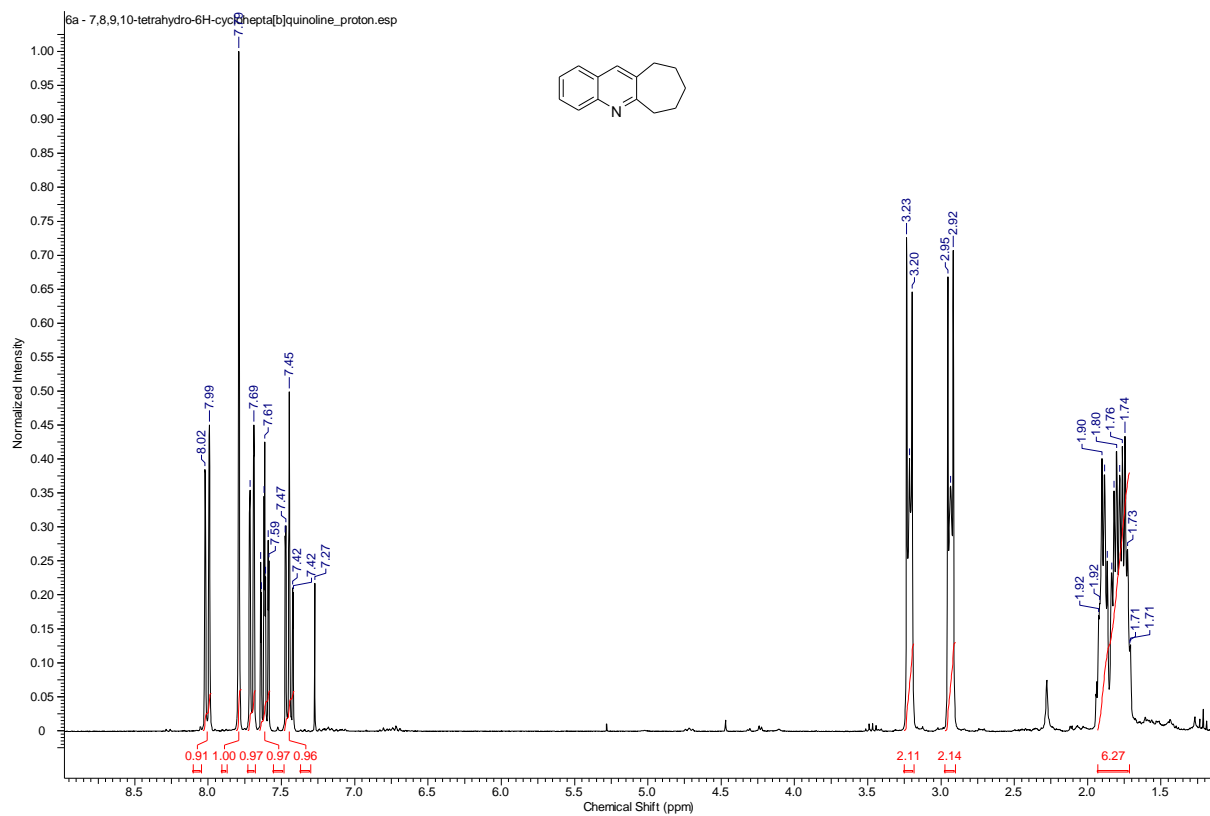
6 A Hierarchical Structured Reusable Iridium Catalyst for the Sustainable Synthesis of Pyrroles, Pyridines, and Quinolines



6 A Hierarchical Structured Reusable Iridium Catalyst for the Sustainable Synthesis of Pyrroles, Pyridines, and Quinolines



6 A Hierarchical Structured Reusable Iridium Catalyst for the Sustainable Synthesis of Pyrroles, Pyridines, and Quinolines



6.8 References

- S1 J.-K. Ewert, C. Denner, M. Friedrich, G. Motz, R. Kempe, *Nanomaterials* **2015**, 5, 425-435.
- S2 D. Forberg, J. Obenauf, M. Friedrich, S.-M. Hühne, W. Mader, G. Motz, R. Kempe, *Catal. Sci. Technol.* **2014**, 4, 4188-4192.

7 Coating of an Ir@SiCN Nanocomposite on a Hierarchically Porous (Micro/Meso) SiCN Support

Julia-Katharina Ewert,^[a] Stefan Schwarz,^[a] Christine Denner,^[a] Martin Friedrich,^[a] Rhett Kempe^[a]

[a] Institute of Inorganic Chemistry II, University Bayreuth, 95440 Bayreuth, Germany

To be submitted.

Keywords: silicon carbonitride ceramics, polyolefin structuring, polystyrene, calcination, metal coating

Abstract: Polymer derived (PD) silicon carbonitride (SiCN) ceramics are well known supports for the stabilization of transition metal nanoparticles. Such SiCN-transition metal nanocomposites (M@SiCN) are applicable as chemical inert and air-stable catalysts. The preferably entire accessibility of the incorporated metal is of great interest considering a highly active and economical catalyst system. The thin metal coating of a highly porous support material is a promising way to address this demand. Herein, we present the coating of an Ir@SiCN nanocomposite on a micro- and mesoporous SiCN support leading to an Ir@SiCN-SiCN core-shell system.

7.1 Introduction

Polymer derived ceramics (PDC), in particular PD-SiCN ceramics are promising support materials for heterogeneous catalyst systems. They are attractive due to their chemical resistance and the high thermal stability.¹ Additionally, the covalent bonded nitrogen of the SiCN network enables the stabilization of very small metal nanoparticles² leading to efficient M@SiCN catalysts.³ Nevertheless, such M@SiCN catalysts are accompanied by a low metal accessibility. An excellent accessibility of the metal particles is important considering the catalyst activity as well as economical aspects. Therefore, a large SSA with a high porosity degree is necessary. Several research groups developed synthesis protocols in order to generate mesoporous PD-SiCN materials with high SSAs by nanostructuring procedures.⁴ There are three pathways known in literature leading to meso structured PD-SiCN ceramics using polyolefin templates.

The first method utilizes an organic block-copolymer as structure-directing agent (SDA) and an inorganic polymer as ceramic precursor. A microphase separation is accomplished due to the compatibility of the ceramic precursor with one block of the SDA. The main problem of this method is the oxygen entry caused by acrylic monomers.⁵ In the second method, a block-copolymer with an inorganic block as ceramic precursor and an organic block as a porogen (responsible for pore formation during pyrolysis) is used. This method is based on the self-assembly character of the block-copolymer and the resulting microphase separation generating a meso structured ceramic.⁶ The third pathway is the so called self-sacrificial method. Here, polyolefin templates like mesoporous polyethylene⁷ or PS spheres⁸ are used as template. Strong etching reagents can be avoided because of the thermal decomposition of the templates. Moreover, oxygen containing monomers are needless. The following research groups investigated porous PD-SiCN ceramics as support materials for catalytic reactions. The group of Wiesner generated the first Pt@SiCN catalyst with a high degree of porosity for the total oxidation of methane using an block-copolymer as SDA.^{5d} Our group introduced micropores in a Ni@SiCN catalyst by a thermal treatment at 600 °C under inert atmosphere enabling a SSA of 400 m²/g for the selective hydrogenation of alkynes.⁹ Moreover, our group introduced a mesoporous SiCN material using an activated carbon template and observed SSAs between 200-470 m²/g after the oxidative removal of the template.¹⁰ This material was coated with palladium using the incipient wetness impregnation technique and obtained an efficient Pd@SiCN catalyst for the methane oxidation.

Herein, we present the coating of an Ir@SiCN nanocomposite on a hierarchically porous SiCN support^{8a} leading to an Ir@SiCN-SiCN core-shell system. The introduced Ir@SiCN coating procedure was realizable following the easy shaping character of PD-SiCN ceramics.^{1h,m} A large SSA was achieved by oxidative reduction of the incorporated carbon of the SiCN material. The efficient oxidative removal of a carbon template in a porous SiCN material was recently shown by our group.¹⁰ A thin layer of Ir@SiCN was deposited on the modified porous SiCN support in order to adress a high metal accessibility.

7.2 Results and Discussion

We synthesized a structured SiCN material (PS₆₀SiCN₁₀₀₀) following the polystyrene based synthesis protocol recently developed by our group.^{8a} A calcination study in a fixed bed reactor with coupled online GC was established in order to find suitable conditions for the SSA

increase. The temperature depending carbon dioxide release (**Figure 1A**) verified a very good removal of carbon as carbon dioxide at 500 °C. Hence, the structured SiCN material was heated to 500 °C under nitrogen atmosphere, calcinated for 45 min (carbon dioxide release reduced to 50 % conversion), and cooled down under nitrogen atmosphere in order to rise the SSA (**Figure 1B**).

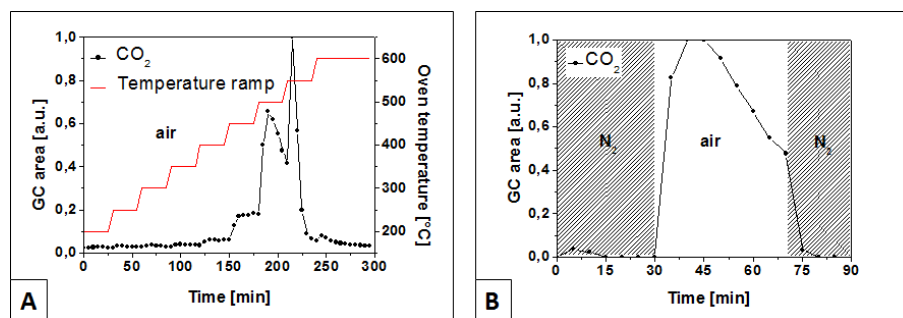


Figure 2. Online GC studies. (A) Temperature dependent CO₂ release up to 700 °C. (B) Calcination program with heating to 500 °C and cooling down under nitrogen flow obtaining a short calcination window at 500 °C.

The enhancement of the SSA by the oxidative partial carbon removal was investigated using nitrogen sorption measurements. The isotherms (**Figure 2A**) of PS₆₀SiCN₁₀₀₀ and the calcinated material indicate a hierarchical micro- and mesoporous materials.¹¹ We observed an increase of the SSA from 37 m²/g to 220 m²/g after the calcination procedure, which is an enhancement of 595 %. As seen in **Figure 2B**, the calcinated material exhibits an increased mesopore amount of 89 % (untreated material: 78 %). After calcination, homogenously distributed pores in the range of 35 nm were observed by SEM measurements (**Figure 2C**).

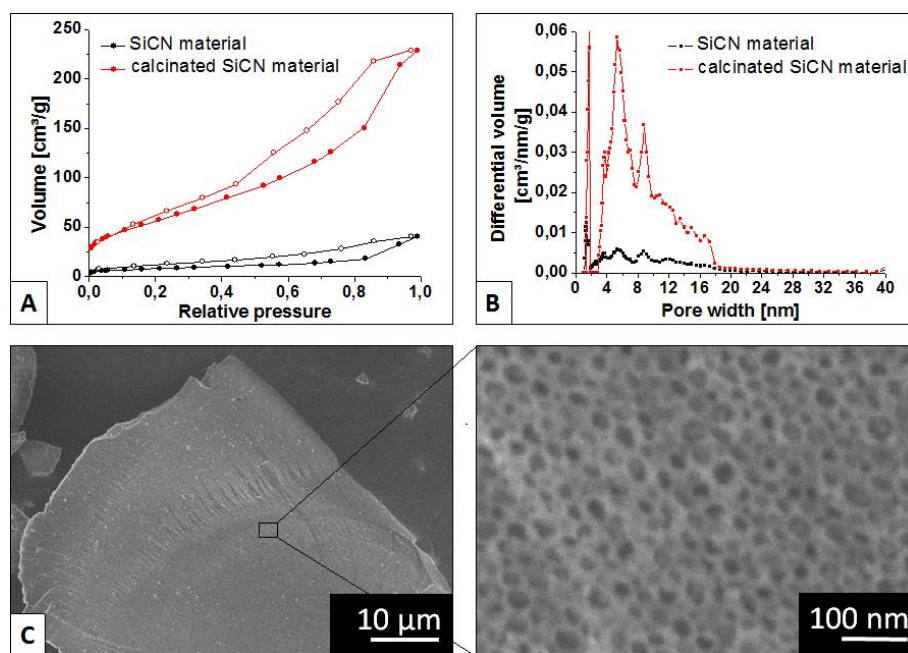


Figure 2. Nitrogen sorption measurement with isotherms (A) and the calculated pore size distribution (B) of the calcinated SiCN material and the SiCN material as well as SEM images (C) of the calcinated SiCN material.

After the enlargement of the SSA, we coated the calcinated SiCN material with Ir@SiCN. Therefore, the calcinated SiCN material was suspended in hexane and mixed with the ceramic precursor HTT-1800, the cross-linker dicumylperoxide (DCP), and an iridium aminopyridinato complex. The Ir@SiCN layer was cross-linked at 110 °C during the continuously vaporization of hexane. The Ir@SiCN-SiCN core-shell material was obtained after pyrolysis at 1000 °C. The surface structure of the Ir@SiCN coated material was analyzed by SEM measurements (**Figure 3A**). An open porosity in the macro scale range was observed. TEM measurements (**Figure 3B**) show homogenously distributed nanoparticles with a particle size distribution in the range of 0.6 nm and 1.6 nm. The presence of iridium in the SiCN support was indicated by the characteristic elemental signals by EDX measurements (**Figure 3C**). The SSA was reduced to 110 m²/g, which was determined by nitrogen sorption measurements. This goes along with the reduction of the pore amount evidenced by the pore size distribution (**Figure 3D**).

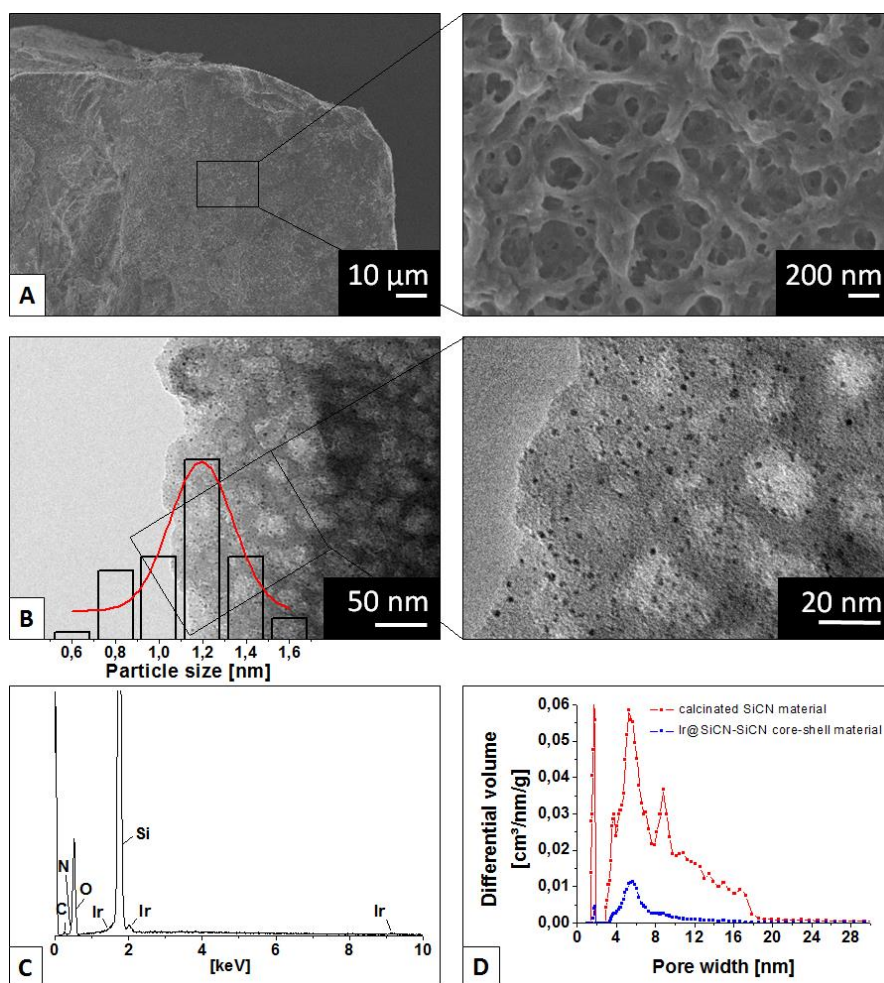


Figure 3. SEM measurement (A), TEM measurement with particle size distribution (B) and EDX measurement (C) of the Ir@SiCN-SiCN core-shell material as well as calculated pore size distribution from nitrogen sorption measurements (D) of the Ir@SiCN-SiCN core-shell material compared to the calcinated SiCN material.

7.3 Conclusion

We introduced an Ir@SiCN-SiCN core-shell system mediated by an Ir@SiCN coating. A hierarchically micro- and mesoporous SiCN material was utilized as support. We used a calcination process to partially remove the incorporated carbon of the SiCN material and increased the SSA and the mesopore amount. The modified SiCN support was coated with a thin Ir@SiCN layer. Thereby, iridium nanoparticles with an average particle size of 1.2 nm were generated on the surface in order to enable a better metal accessibility.

7.4 Experimental Section

Materials

All reactions were carried out in a dry argon atmosphere using standard Schlenk techniques. Nonhalogenated solvents were dried over sodium benzophenone ketyl. (1-Hexadecyl)-trimethylammonium bromide (CTAB) (98% purity, abcr, Karlsruhe, Germany), 2,2'-azobis(2-methylpropionamidine)dihydrochloride (97% purity, Aldrich Chemistry, Steinheim, Germany), KiON HTT-1800 (Clariant Advanced Materials GmbH, Frankfurt, Germany) and dicumylperoxide (97% purity, Aldrich Chemistry, Steinheim, Germany) were purchased from commercial sources and used without further purification. Styrene (>99% purity, Sigma Aldrich, Steinheim, Germany) and divinylbenzene (technical grade, 55%, Aldrich Chemistry, Steinheim, Germany) were destabilized over an alumina B column (ICN Biomedicals GmbH, Eschwege, Germany).

Methods

Ceramisation was performed in a high temperature furnace (GERO, Berlin, Germany) under nitrogen atmosphere. The pyrolysed ceramic was milled in a ball mill “Pulverisette 0” (Fritsch, Idar-Oberstein, Germany) for 20 min. *Scanning electron microscopy (SEM)* and *energy dispersive X-ray spectroscopy (EDX)* measurements were performed using a Zeiss Field-Emission-Scanning-Electron-Microscope (FESEM) “LEO 1530 GEMINI”. The acceleration voltage was 1-5 kV. The samples were sputter-coated with a 1.3 nm layer of platinum. *Transmission electron microscopy (TEM)* measurements were performed using a Varian LEO 9220 (Carl Zeiss, 120 kV, Oberkochen, Germany) instrument. The samples were suspended in chloroform and sonicated for 5 min. Two microliters of the suspension were placed on a CF200-Cu-grid (Electron Microscopy Sciences, Hatfield, USA) and allowed to dry. *Nitrogen sorption analysis* were carried out using a Nova2000e (Quantachrome, Odelzhausen, Germany) instrument. The specific surface areas were calculated using p/p_0 -values from 0.05–0.31 (BET). The pore width and average pore volume was calculated by DFT calculations (N_2 at 77 K on carbon (slit/cylindric pore, NLDFT equilibrium model)).

Preparation of the structured SiCN material

In a round bottom Schenk flask 1 g degassed PS₆₀-particles^{8a} were dispersed in 40 mL toluene under stirring. 500 mg of HTT1800 (7.77 mmol) and 50 mg DCP (1.85 mmol) were added. Without stirring, the suspension was heated to 110 °C for 24 h. After removal of the solvent the

cross-linking process of the *in situ* structured green body was completed at 110 °C (24 h). The green body was pyrolysed under nitrogen atmosphere according to the following program:

$RT \xrightarrow{1\text{ K min}^{-1}, 3\text{ h}} 300\text{ °C} \xrightarrow{1\text{ K min}^{-1}, 3\text{ h}} 400\text{ °C} \xrightarrow{0.5\text{ K min}^{-1}, 3\text{ h}} 500\text{ °C} \xrightarrow{1\text{ K min}^{-1}, 4\text{ h}} 600\text{ °C} \xrightarrow{0.5\text{ K min}^{-1}, 0\text{ h}} 700\text{ °C} \xrightarrow{1\text{ K min}^{-1}, 0.5\text{ h}} 1000\text{ °C}$

Calcination of the PS₆₀SiCN₁₀₀₀ material

The calcination of the PS₆₀SiCN₁₀₀₀ material was carried out in a fixed bed reactor under controlled conditions. 50 mg of the SiCN material was given into the reactor tube and treated with the following program:

$RT \xrightarrow{10\text{ °C min}^{-1}} 500\text{ °C (N}_2) \xrightarrow{0.5\text{ h}} 500\text{ °C (air)} \xrightarrow{10\text{ °C min}^{-1}} RT\text{ (N}_2)$

The reactor feed consisting of air (filtered compressed air) and nitrogen (5.0, Rießner-Gase) was mixed by mass flow controllers (SMART6 GSC, Vögtlin). The outgoing flow was analysed by online gas chromatography in order to observe the calcination process.

Ir@SiCN coating

35 mg of the calcinated material was suspended in 5 mL hexane in a lever lid glass in a Schlenk tube. 15 µL HTT-1800, 1 mg DCP, and 1 mg iridium[(4-methyl-pyridin-2-yl)-(2,4,6-trimethyl-phenyl)-amine(cyclooctadiene)]^{3c} were solved in 5 mL hexane and subsequently added under stirring. Under evaporation of the solvent the coated Ir@SiCN layer was cross-linked at 110 °C on the matrix surface. The coated material was pyrolysed under nitrogen flow according to the following program:

$RT \xrightarrow{1\text{ K min}^{-1}, 1\text{ h}} 300\text{ °C} \xrightarrow{5\text{ K min}^{-1}, 1\text{ h}} 1000\text{ °C}$

7.5 Acknowledgements

We thank the SFB 840 and the Elitenetzwerk Bayern e.V. for financial support.

7.6 References

- 1 a) R. Riedel, H.-J. Kleebe, H. Schönfelder, F. Aldinger, *Nature* **1995**, *374*, 526-528; b) W. Weibelzahl, G. Motz, D. Suttor, G. Ziegler, *Key Eng. Mater.* **1999**, *161-163*, 111-114; c) E. Kroke, Y.-L. Li, C. Konetschny, E. Lecomte, C. Fasel, R. Riedel, *Mater. Sci. Eng. R* **2000**, *26*, 97-199; d) P. Greil, *Adv. Eng. Mat.* **2000**, *2*, 339-348; e) H. J. Kleebe, H. Störmer, S. Trassl, G. Ziegler, *Appl. Organomet. Chem.* **2001**, *15*, 858-866; f) R.

- Riedel, G. Mera, R. Hauser, A. Klonczynski, *J. Ceram. Soc. Jpn.* **2006**, *114*, 425-444;
- g) A. R. Studart, U. T. Gonzenbach, E. Tervoort, L. J. Gauckler, *J. Am. Ceram. Soc.* **2006**, *89*, 1771-1789; h) P. Colombo, G. Mera, R. Riedel, G. D. Sorarù, *J. Am. Ceram. Soc.* **2010**, *93*, 1805-1837; i) P. Colombo, R. Riedel, G. D. Soraru, H.-J. Kleebe, *Polymer Derived Ceramics - From Nanostructure to Applications*, DEStech Publications, Inc. Pennsylvania, **2010**; j) E. Ionescu, H. J. Kleebe, R. Riedel, *Chem. Soc. Rev.* **2012**, *41*, 5032-5052; k) G. Mera, A. Navrotsky, S. Sen, H.-J. Kleebe, R. Riedel, *J. Mat. Chem. A* **2013**, *1*, 3826; l) *Ceramics Science and Technology: Volume 4: Applications*, (Eds: Ralf Riedel and I-Wei Chen), Wiley-VCH Verlag GmbH & Co. KGaA, **2013**; m). E. Bernardo, L. Fiocco, G. Parcianello, E. Storti, P. Colombo, *Materials* **2014**, *7*, 1927-1956.
- 2 M. Zaheer, T. Schmalz, G. Motz, R. Kempe, *Chem. Soc. Rev.* **2012**, *41*, 5102-5116.
- 3 a) G. Glatz, T. Schmalz, T. Kraus, F. Haarmann, G. Motz, R. Kempe, *Chem. Eur. J.* **2010**, *16*, 4231-4238; b) M. Zaheer, G. Motz, R. Kempe, *J. Mater. Chem.* **2011**, *21*, 18825; c) D. Forberg, J. Obenauf, M. Friedrich, S.-M. Hühne, W. Mader, G. Motz, R. Kempe, *Catal. Sci. Technol.* **2014**, *4*, 4188-4192.
- 4 Y. Shi, Y. Wan, D. Zhao, *Chem. Soc. Rev.* **2011**, *40*, 3854-3878.
- 5 a) M. Kamperman, C. B. Garcia, P. Du, H. Ow, U. Wiesner, *J. Am. Chem. Soc.* **2004**, *126*, 14708-14709; b) J. Wan, A. Alizadeh, S. T. Taylor, P. R. L. Malenfant, M. Manoharan, S. M. Loureiro, *Chem. Mater.* **2005**, *17*, 5613-5617; c) J. Wan, P. R. L. Malenfant, S. T. Taylor, S. M. Loureiro, M. Manoharan, *Mater. Sci. Eng. A* **2007**, *463*, 78-88; d) M. Kamperman, A. Burns, R. Weissgraeber, N. van Vegten, S. C. Warren, S. M. Gruner, A. Baiker, U. Wiesner, *Nano Lett.* **2009**, *9*, 2756-2762.
- 6 a) C. T. Nguyen, P. H. Hoang, J. Perumal, D. P. Kim, *Chem. Commun.* **2011**, *47*, 3484-3486; b) S. K. Pillai, W. P. Kretschmer, C. Denner, G. Motz, M. Hund, A. Fery, M. Trebbin, S. Forster, R. Kempe, *Small* **2013**, *9*, 984-989.
- 7 B. H. Jones, T. P. Lodge, *J. Am. Chem. Soc.* **2009**, *131*, 1676-1677.
- 8 a) J.-K. Ewert, C. Denner, M. Friedrich, G. Motz, R. Kempe, *Nanomaterials* **2015**, *5*, 425-435; b) J.-K. Ewert, D. Weingarh, C. Denner, M. Friedrich, M. Zeiger, A. Schreiber, N. Jackel, V. Presser, R. Kempe, *J. Mater. Chem. A*, **2015**, *3*, 18906-18912.
- 9 M. Zaheer, C. D. Keenan, J. Hermannsdörfer, E. Roessler, G. Motz, J. Senker, R. Kempe, *Chem. Mater.* **2012**, *24*, 3952-3963.

- 10 S. Schwarz, M. Friedrich, G. Motz, R. Kempe, *ZAAC* **2015**, *641*, 2266-2271.
- 11 K. S. W. Sing, D. H. Everett, R. A. W. Haul, L. Moscou, R. A. Pierotti, J. Rouquerol, T. Siemieniewska, *Pure & Appl. Chem.* **1984**, *57*, 603-619.

8 List of Publications

The following publications haven been published or are to be submitted during the work on this thesis:

1. J.-K. Ewert, C. Denner, M. Friedrich, G. Motz, R. Kempe, *Nanomaterials* **2015**, 5, 425-435.
“Meso-Structuring of SiCN Ceramics by Polystyrene Templates”
2. J.-K. Ewert, D. Weingarth, C. Denner, M. Friedrich, M. Zeiger, A. Schreiber, N. Jäckel, V. Presser, R. Kempe, *J. Mater. Chem. A* **2015**, 3, 18906-18912.
„Enhanced Capacitance of Nitrogen-Doped Hierarchical Porous Carbide-Derived Carbon in Matched Ionic Liquids”
3. J.-K. Ewert, C. Denner, M. Friedrich, R. Kempe, to be submitted.
“A Hierarchical Structured Reusable Iridium Catalyst for the Sustainable Synthesis of Pyrroles, Pyridines, and Quinolines”
4. J.-K. Ewert, S. Schwarz, C. Denner, M. Friedrich, R. Kempe, to be submitted.
“Coating of an Ir@SiCN Nanocomposite on a Hierarchically Porous (Micro/Meso) SiCN Support”

9 Acknowledgements / Danksagung

9.1 Acknowledgements

I would like to express my gratitude for my academic supervisor

Prof. Dr. Rhett Kempe

for giving me the opportunity to work on this extremely interesting topic in his working group. Moreover, I would like to thank him for granting me great scientific independence, wonderful working conditions, and endless scientific discussions.

I am truly thankful to Dr. Christine Denner for her supervision in the “SiCN group”, her endless support, the SEM measurements, and for her friendship.

Special thanks to my students Tobias Schwob, Gabriela Wietzel, Annabelle Weinmüller, Ferdinand Seibold, Christoph Bäumler and Marco Schwarz for their assistance in the.

A special thanks goes to Prof. Dr. Volker Presser, Dr. Daniel Weingarth, and their colleges for the great cooperation project we have performed. Thank you, for the endless scientific discussions and the extensive electrochemical measurements.

A great thanks goes to Heidi Maisel, Simone Hoch, Sandra Keller, Walter Kremnitz, Anna-Maria Dietel and especially to Marlies Schilling for their assistance and support regarding administration matters and their work in the lab.

A special thanks goes to Martin Friedrich for TEM and TGA measurements and his IT support, to Dr. Wolfgang Milius and Florian Puchter for XRD measurements as well as to the BayCeer institute for ICP-OES measurements.

I would like to thank the Elitenetzwerk Bayern e.V. for financially support with a dissertation scholarship.

A warm thanks goes to my lab colleges Daniel Forberg, Sonja Fehn, Stefan Schwarz, Dr. Muhammad Zaheer, Dr. Saravana Pillai, Gabriela Wietzel, and Tobias Schwob for the great time in the lab, their support and the wonderful working atmosphere. Moreover, I would like to thank my colleagues Sina Rösler, Dr. Johannes Obenauf, Thomas Dietel, Andreas Gollwitzer, Dr.

Susanne Ruch, Dr. Justus Herrmannsdörfer, Nicklas Deibl, Toni Hille, Dr. Torsten Irrgang, Dr. Winfried Kretschmer, Dr. Sadaf Qayyum and Dr. Awal Noor for the nice time in the last years.

My sincere thanks goes to my mum, my brother Dirk, and Hans for their support in every possible way, their love and motivation.

Last but not least, I would like to truly thank my Domi for his motivation, his never ending support, his patience, and for his love.

9.2 Danksagung

Mein besonderer Dank gilt meinem akademischen Lehrer

Prof. Dr. Rhett Kempe

für die Möglichkeit, diese Arbeit auf einem sehr interessanten Gebiet in seiner Arbeitsgruppe zu bearbeiten. Außerdem möchte ich ihm für die gewährte große wissenschaftliche Freiheit, die wunderbare Arbeitsatmosphäre und die unendlich große Diskussionsbereitschaft danken.

Ich danke Dr. Christine Denner für ihre Betreuung in der „SiCN Gruppe“, ihre stete Unterstützung, für die REM Messungen und für ihre Freundschaft.

Besonderer Dank gilt meinen Studenten Tobias Schwob, Gabriela Wietzel, Annabelle Weinmüller, Ferdinand Seibold, Christoph Bäumler und Marco Schwarz für ihre unterstützende Arbeit im Labor.

Ein besonderer Dank gilt Prof. Dr. Volker Presser, Dr. Daniel Weingarth und ihren Kollegen für die großartige Kooperationsarbeit. Vielen Dank für die vielen wissenschaftlichen Diskussionen und die aufwendigen elektrochemischen Messungen.

Ein großer Dank gilt Heidi Maisel, Simone Hoch, Sandra Keller, Walter Kremnitz, Anna-Maria Dietel und besonders Marlies Schilling für ihre Unterstützung hinsichtlich administrativer Angelegenheiten und ihrer unterstützenden Arbeiten im Labor.

Besonderer Dank gilt Martin Friedrich für TEM und TGA Messungen, sowie seiner Unterstützung bezüglich IT-Fragen, Dr. Wolfgang Milius und Florian Puchter für XRD Messungen und dem BayCeer Institut für ICP-OES Messungen.

Ich möchte mich bei dem Elitenetzwerk Bayern e.V. für die finanzielle Unterstützung in Form eines Graduiertenstipendiums bedanken.

Ein großes Dankeschön geht an meine Laborkollegen Daniel Forberg, Sonja Fehn, Stefan Schwarz, Dr. Muhammad Zaheer, Dr. Saravana Pillai, Gabriela Wietzel und Tobias Schwob für die großartige Zeit im Labor, ihre Unterstützung und die wunderbare Arbeitsatmosphäre. Des Weiteren möchte ich mich bei meinen Kollegen Sina Rösler, Thomas Dietel, Dr. Johannes Obenauf, Andreas Gollwitzer, Dr. Susanne Ruch, Dr. Justus Herrmannsdörfer, Nicklas Deibl, Toni Hille, Dr. Torten Irrgang, Dr. Winfried Kretschmer, Dr. Sadaf Qayyum and Dr. Awal Noor für die tolle Zeit in den letzten Jahren bedanken.

Mein aufrichtiger Dank gilt meiner Mama, meinem Bruder Dirk und Hans für ihre Unterstützung in jedweder Weise, für ihre Liebe und Motivation.

Zuletzt möchte ich mich bei meinem Domi für seine Motivation, seine unendliche Unterstützung, seine Geduld und seine Liebe aus tiefstem Herzen bedanken.

10 Declaration / Erklärung

(§ 8 S. 2 Nr. 6 PromO)

Hiermit erkläre ich mich damit einverstanden, dass die elektronische Fassung meiner Dissertation unter Wahrung meiner Urheberrechte und des Datenschutzes einer gesonderten Überprüfung hinsichtlich der eigenständigen Anfertigung der Dissertation unterzogen werden kann.

(§ 8 S. 2 Nr. 8 PromO)

Hiermit erkläre ich eidesstattlich, dass ich die Dissertation selbständig verfasst und keine anderen als die von mir angegebenen Quellen und Hilfsmittel benutzt habe.

(§ 8 S. 2 Nr. 9 PromO)

Ich habe die Dissertation nicht bereits zur Erlangung eines akademischen Grades anderweitig eingereicht und habe auch nicht bereits diese oder eine gleichartige Doktorprüfung endgültig nicht bestanden.

(§ 8 S. 2 Nr. 10 PromO)

Hiermit erkläre ich, dass ich keine Hilfe von gewerblichen Promotionsberatern bzw. -vermittlern in Anspruch genommen habe und auch künftig nicht nehmen werde.

Bayreuth, den 24.11.2015

Julia-Katharina Ewert